# Alternative Metrics of Green Roof Hydrologic Performance: Evapotranspiration and Peak Flow Reduction

Daniel E. Marasco

Submitted in partial fulfillment of the
requirements for the degree of
Doctor of Philosophy
in the Graduate School of Arts and Sciences

COLUMBIA UNIVERSITY

2014

# ABSTRACT

## ALTERNATIVE METRICS OF GREEN ROOF HYDROLOGIC PERFORMANCE: EVAPOTRANSPIRATION AND PEAK FLOW REDUCTION

Daniel E. Marasco

Stormwater runoff presents an issue for many urban areas, triggering sewer overflows and water body pollution. Green roofs, engineered vegetative systems that replicate the stormwater absorption properties of natural landscapes, have become an attractive strategy for attenuating stormwater runoff. Historically, green roof hydrologic research has been focused on stormwater volume retention with less emphasis on evapotranspiration (ET) and stormwater detention. ET is associated with green roof environmental benefits, including stormwater runoff attenuation and urban heat island mitigation, and is an important parameter in hydrologic and energy models. Stormwater detention limits flow rate of stormwater into sewer systems, reducing the chance of sewer overflow. The aim of this research is to investigate green roof ET and stormwater detention behavior and develop methods to predict these performance metrics based on readily available environmental data.

In order to study green roof ET and stormwater detention, a series of four New York City green roofs were instrumented with sensors to measure rainfall, runoff, ET, and other environmental data. The green roofs span several extensive green roof installation types, specifically the

vegetated mat, built-in-place, and modular tray systems. Environmental monitoring for this analysis began in January 2009 and concluded in October 2013.

In the first study, a dynamic chamber method was developed to conduct high-resolution measurements of green roof ET. Results showed monthly ET depths ranging from 2.2 to 153.6 mm. Chamber results were compared to two ET estimation methods, specifically the Penman-Monteith equation and an energy balance model. Dynamic chamber results were similar to Penman-Monteith estimates; however, the Penman-Monteith equation over-predicted bottommost green roof ET fluxes during the winter, and under-predicted peak summer fluxes.

In the second study, the dynamic chamber measurements were analyzed to reveal green roof ET behavior and evaluate various predictive models, particularly in water-limited conditions. Comparison of Hargreaves, Priestley-Taylor, Penman, and Penman-Monteith equation results to chamber measurements revealed that the Priestley-Taylor equation best estimated ET. However, the Priestley-Taylor equation still overestimated observations of lower ET fluxes and underestimated high fluxes. Application of a storage model, antecedent precipitation index, and advection-aridity model indicated that the antecedent precipitation index best estimated ET in water-stressed conditions.

In the third study, 501 rainfall events were used to characterize green roof stormwater detention behavior, through analysis of event peak rainfall rate reductions. Empirical models relating event peak runoff rate to rainfall depth and peak rainfall rate were developed. Roof-specific models allow for the comparison of peak reduction behavior among roofs, while a combined model allows for designers to estimate green roof event peak rainfall reduction performance. The models indicated that the modular tray system was most effective at reducing peak rainfall rate.

Overall, this research provides valuable insight into green roof hydrologic performance. Analysis of environmental data revealed not only the ET and peak rainfall rate reduction performance of green roofs, but also the environmental factors that affected performance. Additionally, predictive models for ET and peak runoff rate developed as part of the research described in this dissertation can be valuable tools for researchers, practitioners, and policymakers to estimate green roof hydrologic performance.

# TABLE OF CONTENTS

# LIST OF FIGURES

# LIST OF TABLES

# ACKNOWLEDGEMENTS

In completing this dissertation, I have faced many obstacles. I would never have been able overcome these challenges to complete this dissertation without the care, support, and guidance of faculty advisors, family, and friends. I would like to thank my advisor, Professor Patricia Culligan for admitting me into the National Science Foundation (NSF) Integrative Graduate Education and Research Training (IGERT) graduate program, and for her continued guidance and mentorship throughout my PhD research. I would also like to thank Professor Wade McGillis for offering me an undergraduate internship and cultivating my interest in green infrastructure as well as environmental science. Additionally, I would like to express my gratitude to the faculty and staff of Department of Civil Engineering and Engineering Mechanics, who have mentored and supported me for the past six years. For their input and commentary on my dissertation, I would like to thank my dissertation committee: Professor George Deodatis, Professor Steve Sun, Professor Pierre Gentine, and Professor Stuart Gaffin.

I want to extend my gratitude to the friends and colleagues I have met and worked with as part of the *IGERT: Solving Urbanization Challenges by Design* program and the *Columbia Green Roof Consortium.* Your feedback and support have made this research possible. Specifically, I would like to thank: Tyler Carson for sharing the responsibility for maintaining the green roof monitoring network in addition to sharing ideas, an office, and an apartment; and Robert Elliott for his support and unique insight. I would also like to thank my friend Evan Bauer for providing an outside perspective on my research.

This dissertation could not have been completed without the love, support, and encouragement of my family. I would like to thank my father, Daniel Marasco, for always believing in me and developing my interest in engineering; and my mother, Maria Codina, for providing the life experiences that have made me a better person and for motivating me during difficult times. I would also like to thank my girlfriend, Rebecca Guiterman. Over the past four and a half years you have provided me with an unprecedented level of love, laughter, and support, and have made me a better researcher, writer, and above all, person.

Finally, the research presented in this dissertation would have not been possible without the support of the NSF and Environmental Protection Agency (EPA). I would like to acknowledge the support of the NSF grants CMMI-0928604 and DEB-0949387, as well as the EPA grant AE-83481601-1. Additionally, I want to acknowledge the NSF IGERT Fellowship DGE-0903597, which supported my graduate studies and provided me with a unique interdisciplinary experience.

*To my parents, who have always supported me*

# Chapter 1

## INTRODUCTION

Pollution from stormwater runoff significantly impacts water quality in the United States, and results in urban flooding as well as the impairment of coastal waters, rivers, lakes, and estuaries (Berghage *et al* 2009, Bricker *et al* 2007). In municipalities with combined sewer systems (CSSs), which transport both surface water and sanitary waste, these issues are magnified. Common rainfall events, with rainfall rates as low as 3 mm $hr^{-1}$, can cause combined sewer overflows (CSOs) (Montalto et al 2007). CSO events discharge sewer water containing various pollutants, including floatables, pathogenic microorganisms, oxygen-demanding substances, suspended solids, nutrients, toxicants, and other chemicals into local water bodies (US EPA 2004). In the United States alone, CSOs impact 746 communities in 32 states, resulting in the discharge of 850 billion gallons of polluted water each year (US EPA 2004). In New York City (NYC), 433 CSS outfalls discharge over 20 billion gallons per year (Mayor's Office of Long-Term Planning and Sustainability 2008). This pollution undermines the productivity of urban water bodies and limits natural resource availability, recreation, and commercial activity.

Mitigation of stormwater related pollution is a major focus of many US government agencies and municipalities. Traditional "gray" stormwater infrastructure solutions, such as storage tanks and other end of pipe solutions, face significant cost and design issues. These problems are magnified in dense urban areas like New York City (NYC), where available land is limited and subsurface development can be prohibitively expensive. In response, many governments have implemented policies and stormwater control measures (SCMs) designed to retain, detain, and treat water on-

site (Fassman-Beck *et al* 2013). One increasingly popular, low cost, and effective tool to attenuate stormwater runoff is low impact development (LID). LID incorporates a distributed network of micro-scale engineered systems in the urban environment to encourage temporary storage, infiltration, and evapotranspiration (ET) of stormwater before it enters the sewer system. LID techniques, including green roofs, green streets, street trees, rain gardens, and bio-swales, can be implemented incrementally with limited impact on existing infrastructure (NYC DEP 2010).

Green roofs, also known as vegetated roofs, are a LID alternative to traditional rooftops and have the ability to attenuate stormwater. Green roofs are normally constructed by installing a drainage course, growing substrate, and vegetation on top of a roof's waterproof membrane. Green roofs have been historically used for stormwater management in Germany (Köhler and Keeley 2005) and according to April 2014 records from the Green Roof and Wall Projects Database (GreenRoofs.com 2014), over 1,400 green roofs have been install within the United States.

Green roofs can be classified as either extensive or intensive based on substrate depth and maintenance requirements. Extensive roofs typically have less than 150 mm of substrate and are planted with shallow-rooted and drought resistant plants. Intensive roofs normally have at least 150 mm of substrate and may be planted with deep-rooted vegetation, including shrubs and trees. In practice, extensive green roofs are cheaper, require less maintenance, and are lighter than intensive systems. Thus, extensive systems are more prominent than intensive systems, particularly on existing buildings where rooftop load capacity is limited.

Extensive green roofs can be categorized into three major types: the vegetated mat system, the built-in-place system, and the modular tray system (Oberndorfer *et al* 2007). The vegetated mat

and built-in-place systems are both comprised of continuous substrate layers and drainage courses, but are installed differently. The vegetated mat system is assembled and planted off-site, while the built-in-place layers are placed on the roof individually. For the modular tray system, the substrate is placed in plastic trays, which are then positioned on the rooftop waterproof membrane. The different systems impose unique set of boundary conditions on the substrate layer, which affect drainage behavior and runoff characteristics. Construction of the green roof system also determines the composition and location of non-vegetated areas required for maintenance activities, which can affect overall hydrologic performance (Carson *et al* 2013).

Compared to typical impervious roofs, green roofs have been shown to provide a range of environmental benefits (Yang *et al* 2008, Berndtsson *et al* 2009, Getter *et al* 2009, Sailor and Hagos 2011). However, research on hydrologic performance has generally been focused on understanding green roof stormwater volume retention (Mentens *et al* 2006, Spolek 2008, Berndtsson 2010, Gregoire and Clausen 2011, Stovin *et al* 2012, Carson *et al* 2013, Fassman-Beck *et al* 2013), with less study of green roof evapotranspiration (ET) and detention behavior.

ET behavior is important in determining vitality and performance of urban green roofs. Research has shown that ET is directly related to environmental benefits in stormwater management (Stovin *et al* 2013, Wadzuk *et al* 2013), urban heat island mitigation (Taha 1997), carbon sequestration (Pataki *et al* 2006), building energy usage (Ouldboukhitine *et al* 2011), and air pollution (Christen and Vogt 2004, Jim and Chen 2009). Furthermore, ET measurements or predictions are required for many green roof hydrologic models (Sherrard and Jacobs 2012, Stovin *et al* 2013) and energy models (Lazzarin *et al* 2005, Ouldboukhitine *et al* 2011).

Stormwater detention is also an important measure of green roof performance. Detention reduces the flow rate of stormwater into sewer systems, allowing extended time for delivery and treatment. Because sewer overflows are triggered by flow rate in the sewer system (Mayor's Office of Long-Term Planning and Sustainability 2008), detention of this flow is important for mitigating water body pollution.

Through my research I aim to fill a gap in the understanding of green roof behavior by exploring two aspects of green roof hydrologic performance, namely the ET and peak hourly rainfall rate reduction. For each of these hydrologic performance metrics, I ask the following questions: (1) *How can the metric be measured?* (2) *How do green roofs perform?* (3) *What factors influence the metric?* (4) *How can the metric be predicted?*

## 1.1 Background

### *1.1.1 Green roof evapotranspiration*

ET, the combined water vapor surface flux that results from evaporation and plant respiration, is an important factor affecting the vitality and performance of urban green roofs. ET from green roofs has historically received limited attention (DiGiovanni *et al* 2013, Voyde *et al* 2010b). Since ET is invisible and difficult to measure directly, other techniques have been employed to determine ET. Elevated lysimeters have been used to measure ET through mass balance of precipitation, runoff, and test box weight (to estimate moisture storage) (Liu *et al* 2002, Tyagi *et al* 2000, Howell *et al* 1991, Jordan 1968, Voyde *et al* 2010b, DiGiovanni *et al* 2013). ET has also been estimated through water balances of precipitation and runoff measurements on full-scale green roofs (Bengtsson *et al* 2005, Moran *et al* 2005, Carson *et al* 2013). However, these studies have had difficulty capturing continuous data. Based on the limited study of green roof

ET, I ask the following questions: (1) *How can high-resolution measurements of green roof ET be conducted?* (2) *What are the diurnal and seasonal variations in green roof ET?*

Models, such as the Hargreaves (Hargreaves and Allen 2003), Priestley-Taylor (1972), Penman (1948), and Penman-Monteith (Monteith 1965) equations, have been developed to predict ET from environmental data (Zhao *et al* 2013). However, these models neglect factors that affect actual ET, including substrate moisture availability, surface conditions, crop coefficients, plant vitality, and weather (Allen *et al* 1996, 2005a, Zhao *et al* 2013).

Differences between modeled and actual ET primarily result from limited substrate water availability (Brutsaert 2005). In response, various soil moisture extraction functions (SMEFs) have been employed to relate the degree of substrate saturation to the difference between modeled and actual ET (Sherrard and Jacobs 2012, Zhao *et al* 2013, DiGiovanni *et al* 2013). In the absence of soil moisture data, other methods have been used to estimate actual ET, such as accumulated precipitation and ET deficit models (Grindley 1970, Priestley and Taylor 1972, Calder *et al* 1983, Arora 2002), antecedent precipitation indices (Choudhury and Blanchard 1983, Ali and Mawdsley 1987), the advection-aridity model (Brutsaert and Stricker 1979), water stress - surface temperature relationships (Moran *et al* 1994, Boulet *et al* 2007), and relative humidity profiles (Berthier *et al* 2006, Salvucci and Gentine 2013).

As the environmental processes and conditions on green roofs vary from those of agricultural and natural environments (Graham *et al* 2004), these models might inaccurately portray ET behavior. Studies of ET models applied to green roofs are limited. DiGiovanni *et al* (2013) showed that Penman-Monteith equation was able to predict ET on non-water-limited days and a soil moisture reduction factor improved results when water was limited. Sherrard and Jacobs

(2012) developed a green roof hydrologic model which reduced Penman-Monteith ET estimates based on substrate moisture storage, but the model showed limited correlation in the with ET. The unique environmental conditions and the limited ET model evaluation related to green roofs have prompted me to ask the following questions: (1) *What factors influence green roof ET?* (2) *What models provide the best predictions of green roof ET?*

### *1.1.2 Green roof peak rainfall rate reduction*

While volume retention performance of extensive green roofs has been documented (Mentens *et al* 2006, Spolek 2008, Berndtsson 2010, Gregoire and Clausen 2011, Stovin *et al* 2012, Carson *et al* 2013, Fassman-Beck *et al* 2013), there has been less focus on green roof detention. Green roof peak rainfall rate reduction is a function of antecedent rainfall, vegetation and drainage configuration, in addition to other environmental, site, and moisture conditions (Bliss *et al* 2009, Berndtsson 2010). Some green roof hydrologic studies have reported measurements of peak rainfall rate reduction on green roofs (Bliss *et al* 2009, Fassman-Beck *et al* 2013, Hutchinson *et al* 2003, Berghage *et al* 2009, Moran *et al* 2005, Kurtz 2008, Carpenter and Kaluvakolanu 2011). However, the limited attempts at modeling peak runoff have resulted in either limited correlation with observed data (Stovin *et al* 2012) or complicated models requiring input of difficult to quantify variables (Villarreal and Bengtsson 2005, Villarreal 2007). In response, I ask the following: (1) *How can green roof peak rainfall rate reduction be measured?* (2) *What is the peak rainfall reduction performance of green roofs?* (3) *What factors affect green roof peak rainfall rate reduction?* (4) *How can green roof peak rainfall rate reduction be predicted?*

## 1.2 Research questions and dissertation format

This dissertation has a three-paper structure. The overarching question, which prompted the research presented in this paper, is: *How can alternative metrics of green roof hydrologic performance be quantified?* The structure of this dissertation and the sub-questions that correspond to each chapter are outlined in Figure 1. In contrast to many studies, which explore green roof volume retention, my research aims to quantify and predict two alternative aspects of green roof hydrology, namely the ET and peak rainfall rate reduction.

The subsequent sections of this manuscript explore the research I have performed and its importance for engineers, practitioners, and policymakers. In Chapter 2, I present a methodology for high-resolution measurements of ET and compare results to commonly used predictive methods. In Chapter 3, I apply results from dynamic chamber deployment on two green roofs to evaluate ET behavior and determine the effectiveness of multiple predictive models for estimating green roof ET. Chapter 4 explores measured rainfall event characteristics and how they relate to stormwater peak rainfall rate reduction on green roofs. Data were used in the development of a predictive model to estimate event peak rainfall rate reduction. In Chapter 5, I discuss the practical and theoretical contributions of my research, while in Chapter 6 I discuss possible avenues of future research to enhance understanding of green roof ET and stormwater detention. The manuscript closes with a list of referenced sources and two appendices: Appendix A, which presents more details about the green roof sites studied; and Appendix B, which describes the design, construction, and calibration of the runoff flow meters discussed in Chapter 4.

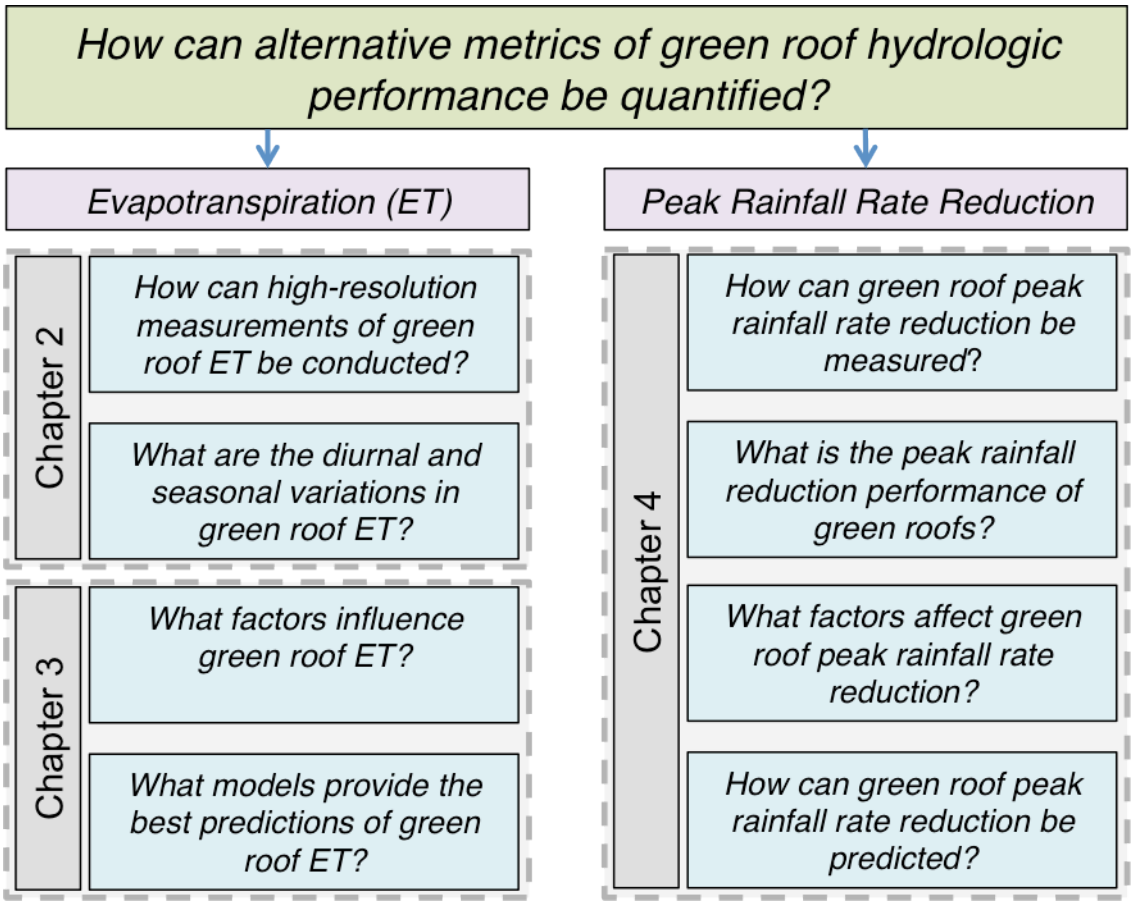


Figure 1: Dissertation format and research questions

# Chapter 2

# QUANTIFYING EVAPOTRANSPIRATION FROM URBAN GREEN ROOFS: A COMPARISON OF CHAMBER MEASUREMENTS WITH COMMONLY USED PREDICTIVE METHODS


## Abstract

Quantifying green roof evapotranspiration (ET) in urban climates is important for assessing environmental benefits, including stormwater runoff attenuation and urban heat island mitigation. In this study, a dynamic chamber method was developed to quantify ET on two extensive green roofs located in New York City. Hourly chamber measurements taken from July 2009 to December 2009 and April 2012 to October 2013 illustrate both diurnal and seasonal variations in ET. Observed monthly total ET depth ranged from 0.22 cm in winter to 15.36 cm in summer. Chamber results were compared to two predictive methods for estimating ET; namely the Penman-based ASCE standardized reference evapotranspiration (ASCE RET) equation, and an energy balance model, both parameterized using on-site environmental conditions. Dynamic chamber ET results were similar to ASCE RET estimates; however, the ASCE RET equation overestimated bottommost ET values during the winter months and underestimated peak ET values during the summer months. The energy balance method was shown to underestimate ET compared the ASCE RET equation. The work highlights the utility of the chamber method for quantifying green roof ET and indicates green roof ET might be better estimated by Penman-based ET equations than energy balance methods.

## 2.1 Introduction

Green infrastructure is a means of re-introducing vegetation and perviousness into city landscapes in an attempt to restore the urban hydrological cycle to pre-development conditions. Green roofs are a component of urban green infrastructure that have proven to be a successful and minimally invasive means of increasing the vegetated area in cities. Replacing traditional black roofs with green roofs can enhance evapotranspiration (ET), the combined water vapor surface fluxes that result from evaporation and plant respiration (Oke 1987), thereby reducing building energy costs, lowering local air temperatures and decreasing stormwater runoff (Taha *et al* 1989, 1991). Quantification of green roof ET can help enumerate the thermal and hydrological benefits of these vegetated systems, enabling informed design and implementation decisions as well as improved understanding of the impact of green roofs on urban micro-climates (Berghage *et al* 2010, Gregoire and Clausen 2011, Hathaway *et al* 2008, Kurtz 2008, Liu and Minor 2005, Moran *et al* 2005, Palla *et al* 2011, Toronto and Region Conservation Authority 2006, Taha *et al* 1989, 1991, Berndtsson 2010, NYC DEP 2010, Stovin *et al* 2012).

Traditional ET estimation techniques are based on water or energy balance methods that evolved from agricultural research (Hillel 1998, Liu *et al* 2002, Tyagi *et al* 2000) and have not been widely validated against direct measurements of green roof ET. Water balance methods estimate ET from observed differences between incoming and outgoing water fluxes. Observations are often made with a lysimeter, a confined tank system designed to simulate a full-scale green roof and instrumented to provide continuous data on precipitation, runoff, and change in water storage (through weight) (Liu *et al* 2002, Tyagi *et al* 2000, Howell *et al* 1991, Jordan 1968, Voyde *et al* 2010b, DiGiovanni *et al* 2013). Water balance studies of full-scale green roofs have

also been used to estimate green roof ET (Bengtsson *et al* 2005, Moran *et al* 2005, Carson *et al* 2013). However, capturing reliable continuous data on precipitation, runoff, and water storage has proven to be more challenging for full-scale systems than lysimeters due to rooftop drainage configurations and the difficulty of developing measurement equipment capable of quantifying changes in rooftop water storage as well as the full range of roof runoff rates (Carson *et al* 2013, Fassman-Beck *et al* 2013).

Energy based methods, originally developed to predict ET from open water bodies, have been employed for agricultural applications. These methods include the Bowen ratio as well as energy transfer equations including Priestley-Taylor and Hargreaves (Brutsaert 2005, Hargreaves and Allen 2003). The Bowen ratio describes the inverse relationship between sensible and latent heat (ET), via estimation of the heat flux term in an energy balance equation (Oke 1987, Bowen 1926, Hillel 1998, Fuchs and Tanner 1970, Fritschen 1965, Perez *et al* 1999, Olejnik *et al* 2001). Energy transfer equations parameterize ET based on air temperature and radiation data. However, most transfer methods do not consider many of the factors affecting green roof ET including advection(Rosenberg 1969, Blad and Rosenberg 1974, Bertela 1989), water limitations, and increased surface resistance during drought (Martens *et al* 2008, Gaffin *et al* 2005, Fuchs and Tanner 1970, Voyde *et al* 2010b).

The Penman-Monteith equation estimates reference ET from vegetation based on daily mean temperature, wind speed, relative humidity, solar radiation, advective transfer and surface resistance (Monteith 1965, Allen *et al* 1998). Several variations of the Penman-Monteith equation have been found to overestimate ET for the *Sedum* species common on green roof systems, especially under water-limited conditions (Oke 1987, Ouldboukhitine *et al* 2011,

DiGiovanni *et al* 2013). A recent lysimeter study conducted at a green roof located in Bronx, NY concluded that the use of on-site, versus regional, climatic data considerably improved agreement between Penman-Monteith ET estimates and lysimeter measurements (DiGiovanni *et al* 2013).

In this study, a dynamic chamber technique for high-resolution field measurement of green roof ET is presented together with results obtained from two deployments of the chamber on *Sedum* green roof systems in Manhattan, NY. In one deployment, measurements of ET were obtained at 30-minute intervals from July 2009 to December 2009 on a vegetated mat system (referred to as W118). In the second deployment, measurements of ET were obtained at 60-minute intervals from April 2012 to October 2013 on a built-in-place system (referred to as USPS). Chamber measurements at the green roof sites are compared with estimates of reference ET obtained from the Penman-based American Society of Engineers Standardized Reference Evapotranspiration (ASCE RET) equation, parameterized with on-site climatic data. ASCE RET estimates are also compared to ET estimates obtained from an energy balance model parameterized with data obtained on a *Sedum* green roof tray system (referred to as ConEd) located in Queens, NY. Comparisons between the dynamic chamber measurements, ASCE RET estimates, and estimates from the energy balance model enable an initial evaluation of the performance of these commonly used predictive ET methods against a unique field data set.

## 2.2 Sites and Methods

### *2.2.1 Green Roof Characteristics and Instrumentation*

Dynamic chamber deployment and environmental monitoring took place on a Columbia University residence (termed W118) at 423 West 118$^{th}$ St, Manhattan, NY. The 600 m$^2$ roof was

outfitted with a vegetated Xero Flor America XF301 + 2FL extensive green roof system in 2007 (Carson *et al* 2013). The 3.2 cm thick green roof substrate was planted with a variety of *Sedum* species. The roof is approximately 65 m above mean sea level, and located at 40°48' North. Chamber measurements were collected for at least 11 days each month between July 2009 and December 2009 with the exception of September 2009; the roof was not irrigated during the study period. Measurements of environmental data were recorded at 5-minute intervals from January 2009 to October 2013 by a Campbell Scientific CR1000 weather station with attached Kipp and Zonen CMP3 pyranometer, CS215 air temperature/relative humidity (RH) sensor, RM Young 05103 wind monitor, and Met One 385 tipping bucket rain gage.

The second dynamic chamber deployment and environmental monitoring took place on the 10,000 $m^2$ USPS Morgan Processing and Distribution Center green roof (termed USPS) in Manhattan, NY. TectaGreen of Tecta America installed the extensive green roof in 2009. 10 cm of roof substrate was planted with *Sedum* and native species (Carson *et al* 2013). The roof is approximately 45 m above mean sea level, and located at 40°45' North. The dynamic chamber was deployed between April 2012 and October 2013; the roof was not irrigated during this period. Measurements were continuous except from July 8 to July 29, 2012 when the rooftop lost power. Environmental conditions were monitored from May 2012 to October 2013 with an Onset Hobo U30 weather station with attached S-THB-M002 2-bit air temperature/relative humidity (RH) sensor, LIB-M003 solar radiation sensor, S-WCA-M003 wind speed sensor, S-SMC-M005 EC-5 Soil Moisture sensor, and S-RGB-M002 tipping bucket rain gage. The solar radiation sensor malfunctioned from July 8, 2012 until September 14, 2012. Due to similar daily solar radiation between W118 and USPS, missing radiation data were acquired from W118.

Data for parameterizing the ASCE RET equation and energy balance calculations were recorded on the ConEdison Learning Center green roof (termed ConEd) in Long Island City, NY. The roof is approximately 10 m above mean sea level and located at 40°45' North. The 2,700 $m^2$ GreenGrid-G2 extensive green roof was constructed in 2008. *Sedum* pre-germinated modular trays, containing 10 cm of substrate were placed on the roof (Carson *et al* 2013). Measurements were recorded at 5-minute intervals from January 2009 to December 2013 by a Campbell Scientific CR3000 weather station with attached CNR 4L allwave radiometer, 107 temperature probes, CS215 temperature/relative humidity sensor, Apogee IR roof surface temperature radiometer, Nova Lynx rain gage, and RM Young 05103 wind monitor (Gaffin *et al* 2010). The roof was not irrigated during the study period.

*2.2.2 Dynamic Chamber Measurements*

ET proliferates the quantity of water vapor in the air. Establishing a fixed measurement volume with closed boundaries, excepting the boundary at the evaporative surface, provides a system where observations of the rise in water vapor concentration with time in the fixed volume can be related to the rate of water loss, or ET, from the surface (Arnone and Obrist 2003).

The Licor Biosciences LI-8100 automated soil $CO_2$ flux system (LI-8100) was used to conduct dynamic chamber measurements of green roof ET (Figure 2). While unattended, the system was programmed to undertake the following protocol for a 5-minute measurement period: Prior to each period, the system's air intake and outlet lines were purged with atmospheric air. The system's measurement chamber (volume, $V = 6850$ $cm^3$ on W118, $V = 7005$ $cm^3$ on USPS) then enclosed an area of the green roof surface (surface area, $S = 323.6$ $cm^2$) and an infrared sensor detected $CO_2$ and water vapor changes within the chamber every second, while a thermistor

within the chamber recorded the ambient air temperature. At the end of every 5-minute period, the chamber was raised. The chamber was not lowered again for a further 25 minutes on W118 or 55 minutes on USPS, which helped to minimize disruption to the gas transfer processes.

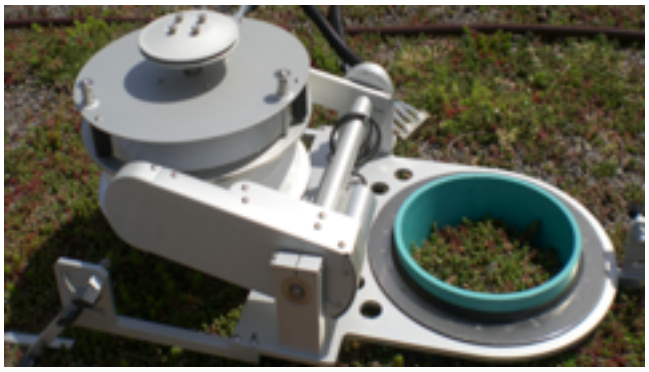

Figure 2: Image of Licor Biosciences LI-8100 automated soil $CO_2$ flux system on W118 roof.

The LI-8100 outputs chamber water vapor concentration, $w_c$, in mmol mol$^{-1}$ (ppt), with a range of 0 to 60 mmol mol$^{-1}$ and an accuracy of 1.5% (Rada 2006). The flux of water into the chamber, $f_w$, from the sealed surface (mol cm$^{-2}$ s$^{-1}$) is a measure of ET from the surface. At constant chamber pressure, the rate at which water evaporates into the chamber, $Sf_w$ (mol s$^{-1}$), is balanced by a small flow rate of air out of the chamber, $u$ (mol s$^{-1}$), leading to a water mass balance within the chamber of

$$V \frac{\partial p_c^w}{\partial t} = Sf_w - w_c u \qquad (1)$$

where $p_c^w$, the number density of water vapor in the chamber (mol cm$^{-3}$), is equal to $p_c w_c$, with $p_c$ representing the total number density of air in the chamber (Rada 2006).

The total number density of air in the chamber is given by the ideal gas law, $p_c = P\,(RT)^{-1}$, where $P$ is the pressure in the chamber (kPa), $R$ is the gas constant (8.314 x 10$^3$ cm$^3$ kPa K$^{-1}$ mol$^{-1}$) and

$T$ is the absolute temperate in the chamber (K). If $P$ and $T$ are constant, and taking into account that $Sf_w = u$ with constant $P$, Equation (1) can be re-organized to give

$$f_w = \frac{V}{S}\frac{P}{RT}\frac{1}{\left(1-\frac{w_c}{1000}\right)}\frac{\partial\left(\frac{w_c}{1000}\right)}{\partial t} \quad (2)$$

The rate of increase of $w_c$ within the chamber can be described by the following equation (Rada 2006, Liss 1973)

$$\frac{\partial w_c}{\partial t} = K\frac{S}{V}(w_s - w_c) \quad (3)$$

where $w_s$ is the saturation concentration of water vapor at the evaporative surface (mmol mol$^{-1}$) and $K$ is the water vapor transfer velocity (cm s$^{-1}$). If $K$, $S$, $V$, and $w_s$ are constant, then integration of Equation (3) with respect to time yields

$$w_c(t) = w_s + (w_c(0) - w_s)e^{-K\frac{S}{V}t} \quad (4)$$

where $w_c(0)$ is the water vapor concentration in the chamber at time $t = 0$ (mmol mol$^{-1}$).

In practice, there is a delay between the instant the LI-8100 chamber closes and the time required to establish steady mixing of gases in the chamber. Thus, $w_c(0)$ is estimated from the intercept of a linear regression of $w_c$ versus $t$ using the first five measurement points after chamber closure. This value is then used as a parameter in a modified version of Equation (4), viz

$$w_c(t) = w_s + (w_c(0) - w_s)e^{-K\frac{S}{V}(t-t_0)} \quad (5)$$

where $t_0$ is the time when $w_c(t)$ is equal to $w_c(0)$ (s).

A nonlinear regression of $w_c(t)$ versus time data with an exponential function of the form given in Equation (5) returns values for $K$, $w_s$, and $t_0$. ET is then obtained from the water vapor flux at $t$=0, yielding

$$\mathrm{ET} = \frac{P(0)}{RT(0)} \frac{1}{\left(1-\frac{w_C(0)}{1000}\right)} K\left(\frac{w_S - w_C(0)}{1000}\right) \quad (6)$$

where the initial pressure, $P(0)$, and initial temperature, $T(0)$, in the chamber are obtained from a linear regression of the first five measurement points of chamber pressure and temperature, respectively, after the chamber closes. ET obtained from Equation (6) was converted to units of (cm $s^{-1}$) by assuming 18 grams of water per mol and a water density of 1 g $cm^{-3}$.

To ensure that the LI-8100 provided accurate measurements of ET, the equipment was calibrated in the laboratory against a controlled series of pan evaporation experiments(Liss 1973, Sumner and Jacobs 2005) involving three trials of open water pan evaporation and three trials using a wet sample of the Xero Flor green roof system. For each trial, a pan was placed in the enclosure and a mass of water was evaporated over 12 hours. The evaporative surface area ($S$ = 324.3 $cm^2$) and average chamber volume ($V$ = 4968.1 $cm^3$) across trials were comparable to field conditions. The pan was weighed every 30 minutes. Chamber measurement cycles occurred midway between each weight measurement. A lamp, to raise temperature, and a small fan, to pull air across the pan surface, were utilized to induce ET fluxes between 0.006 – 0.036 cm $hr^{-1}$. For each 5-minute measurement period, the initial 10 seconds of measurements, termed the deadband, were excluded to allow time to establish steady mixing. Thus, only measurements for the 50 seconds that followed were fit using Equation (5) to obtain $K$, $w_s$ and $t_0$. The identification of these

parameters for the chamber system involved minimization of the error in the regression of $w_c(t)$ across all six pan evaporation trials.

Results of the calibration demonstrate a systematic error, where the chamber records lower ET than determined from the weight measurements. This error is believed to be caused by polar water vapor molecules sticking to the surfaces of the air-lines between the system's chamber and infrared measurement sensor. A linear regression of the weight-measured evapotranspiration ($ET_{Actual}$) versus chamber estimates ($ET_{Chamber}$) was used to create a calibration equation of the following form

$$ET_{corrected} = C(1)(ET_{Chamber}) + C(2) \quad (7)$$

Where $ET_{corrected}$ is the corrected (i.e., actual) ET value, $C(1)$ represents the non-dimensional correction factor (found to be 3.1) and $C(2)$ is the equation intercept (given by -0.0062 cm $hr^{-1}$).

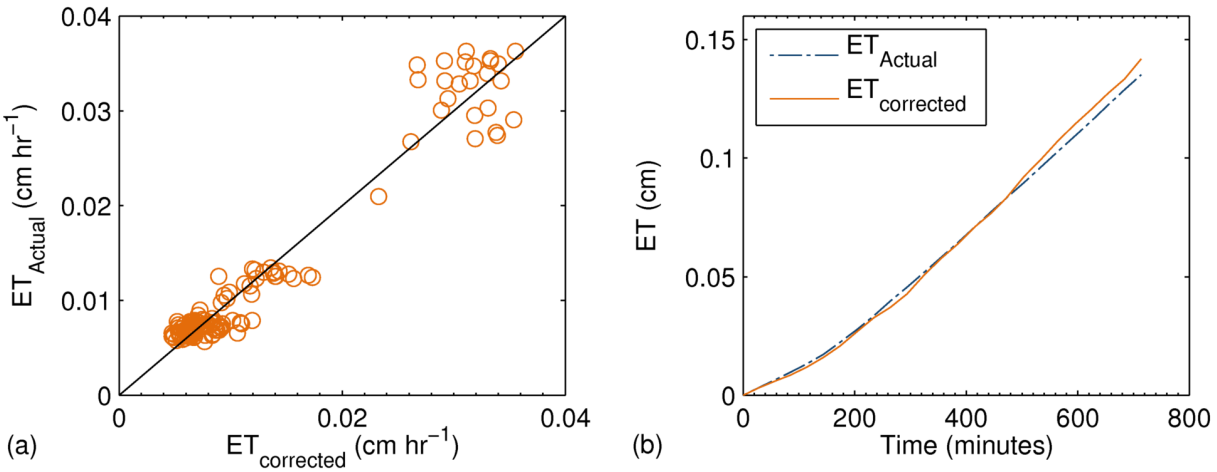


Figure 3: $ET_{Actual}$ (cm $hr^{-1}$) from weight measurement compared to $ET_{corrected}$ (cm $hr^{-1}$) from chamber measurement through (a) scatterplot comparison and (b) cumulative ET during one pan evaporation trial, conducted using green roof substrate.

A comparison of corrected ET values determined from chamber measurements during all pan trials versus those obtained from weight measurements (Figure 3(a)) has an r-squared value of 0.95, while the r-squared values for prediction of the cumulative ET from each trial lies above 0.99 (Figure 3 (b)). Equation (7) is valid for ET fluxes above 0.003 cm $hr^{-1}$, below this rate, it is assumed that $ET_{corrected} = ET_{Chamber.}$

*2.2.3 ASCE Standardized Reference Evapotranspiration Calculation*

The Penman Monteith-based ASCE Standardized Reference Evapotranspiration (ASCE RET) equation for the short reference surface (e.g. cut grasses) was employed to predict daily reference evapotranspiration (RET) on each roof. The ASCE RET equation was developed to predict ET from a standard vegetative surface based on available weather data and specified surface and aerodynamic resistance constants. The ASCE recommends this equation as the standard method for predicting or comparing ET results (DiGiovanni *et al* 2013, Allen *et al* 2005b). The ASCE equation for RET (mm $d^{-1}$), is given by

$$\mathrm{RET} = \frac{0.408\Delta(R_n - G) + \gamma\left(\frac{C_n}{T+273}\right)u_2(e_s - e_a)}{\Delta + \gamma(1 + C_d u_2)} \qquad (8)$$

where Δ is the slope of the saturation vapor pressure-temperature curve (kPa $°C^{-1}$); $R_n$ is the calculated net radiation (MJ $m^{-2}$ $d^{-1}$); $G$ is the soil heat flux density at the soil surface (MJ $m^{-2}$ $d^{-1}$); γ is the psychrometric constant (kPa $°C^{-1}$); $C_n$ is the numerator constant for the short reference type (900 K mm $s^3$ $Mg^{-1}$ $d^{-1}$ for the daily time step); $T$ is the mean daily air temperature at 1.5 to 2.5 m height (°C); $u_2$ is the mean daily wind speed at 2 m height (m $s^{-1}$); $e_s$ is the mean saturation vapor pressure at 1.5 to 2.5 m height (kPa); $e_a$ is the mean actual vapor pressure at 1.5 to 2.5 m height (kPa); and $C_d$ is the denominator constant for short reference type (0.34 s $m^{-1}$). The

inverse of latent heat of vaporization (2.45 MJ $kg^{-1}$) multiplied by the density of water (1.0 Mg $m^{-3}$) is 0.408, the coefficient in the numerator of Equation (8) (Allen *et al* 2005b).

Variables for Equation (8) for each green roof were defined from measurements of solar radiation, wind speed, air temperature and relative humidity, as well as information on date, site elevation, and latitude according to the ASCE specified daily RET methodology. The measurements were obtained at the ASCE specified elevations above the rooftop surface. Net shortwave radiation for the calculation of net total radiation ($R_n$) was measured directly on ConEd. W118 and USPS weather stations only monitored downward solar (shortwave) radiation during chamber deployment and consequently net shortwave was estimated from albedo and solar radiation based on the ASCE specified calculation. An albedo of 0.28, similar to the ASCE RET suggested value of 0.23, was determined from linear regression of 5-minute upward and downward shortwave radiation measurements from the USPS roof collected between March 2011 and June 2012 (r-squared = 0.997). Mean daily air temperatures ($T$), and subsequently saturation vapor pressure ($e_s$), were defined as the mean of the minimum and maximum hourly values. The actual vapor pressure ($e_a$) was calculated hourly and averaged daily, as preferred by the ASCE methodology (Allen *et al* 2005b).

*2.2.4 Energy Balance Model*

ET, or the latent heat flux, can be calculated from an energy balance. The residuals of the other components of the energy balance; net shortwave radiation $R_{SW}$ (W $m^{-2}$), net longwave radiation $R_{LW}$ (W $m^{-2}$), sensible heat flux $Q_{sensible}$ (between the air and rooftop, W $m^{-2}$), and conductive heat flux $Q_{conduction}$ (between the rooftop and building, W $m^{-2}$) are the sum of the latent heat flux $Q_{latent}$ (W $m^{-2}$) and changes to the internal energy IE of the rooftop (W $m^{-2}$). Over extended

periods, changes in internal energy are nominal and the latent heat flux can be described by (Gaffin *et al* 2005)

$$Q_{latent} = R_{sw} + R_{Lw} - Q_{sensible} - Q_{conduction} \quad (9)$$

Data from ConEd were used to parameterize the terms of the energy balance equation for this roof. Net shortwave and longwave radiation were measured directly through the radiometer while sensible heat flux was calculated based on the temperature and wind speed relationship developed by Gaffin *et al* (2010).

$$\text{if } u_2 > 1.75,\ Q_{sensible} = 6.6{u_2}^{0.8}\left(T_{roof} - T_{air}\right)$$

$$\text{else},\ Q_{sensible} = 10.3\left(T_{roof} - T_{air}\right) \quad (10)$$

Where $u_2$ is the wind speed (m $s^{-1}$), $T_{roof}$ is the temperature in the green roof substrate (K), and $T_{air}$ is the ambient air temperature (K).

Conductive heat flux (W $m^{-2}$) was determined from the difference in temperature between the rooftop and ceiling, viz

$$Q_{conduction} = \kappa\left(T_{roof} - T_{ceiling}\right) \quad (11)$$

Where $\kappa$ is the thermal conductivity of the roof layer (W $m^{-2}$ $K^{-1}$), and $T_{ceiling}$ is the temperature below the roof (K). For ConEd, $\kappa$ was determined to be to 0.3 W $m^{-2}$ $K^{-1}$ (Gaffin *et al* 2005).

Direct measurements of $R_{LW}$ together with values obtained from Equations (10) and (11) were input into Equation (9) to obtain $Q_{latent}$. ET (kg $m^{-2}$ $s^{-1}$) was then estimated from

$$ET = \frac{Q_{latent}}{\lambda} = \frac{Q_{latent}}{1918.46(\frac{T_{air}}{T_{air}-33.91})^2} \quad (12)$$

where λ is the latent heat of vaporization (kJ $kg^{-1}$), calculated from the equation developed by Henderson-Sellers (1984). ET values obtained from Equation (12) were converted to units of cm $s^{-1}$ assuming a water density of 1 g $cm^{-3}$.

## 2.3 Results and Discussion

### *2.3.1 ET Chamber Measurement Results*

The dynamic chamber collected approximately 14,000 hours of usable ET measurements. Seven percent of the collected data were removed due to physical interference preventing the chamber from sealing (recorded in chamber data files), or high variance in regression of Equation (5) (r-squared < 0.6) resulting from improper mixing of chamber air. Figure 4(a) displays example ET measurements from July 2009 on W118. The measurements show clear diurnal trends with ET increasing after sunrise and peaking just after noon. During the 2009 chamber deployment on W118, the highest daily ET was recorded in July, with an average daily peak of 0.064 cm $hr^{-1}$ (408.0 W $m^{-2}$), while ET in December was the lowest, only reaching 0.002 cm $hr^{-1}$ (14.48 W $m^{-2}$). Results from USPS show similar trends with the highest average daily peak of 0.065 cm $hr^{-1}$ (439.3 W $m^{-2}$) in August 2012, and the lowest value of 0.001 cm $hr^{-1}$ (6.98 W $m^{-2}$) in January 2013. ET values were used to calculate average hourly ET values for each month (Figure 4(b)), as well as monthly total ET. The average hourly results from the USPS deployment illustrate a decrease in the number of hours over which ET occurs as the month moves from August (~ 12 hrs) to January (~ 3 hrs), as well as a decrease in the strength of the diurnal signal. With respect to monthly total ET on W118 in 2009; July had the maximum ET depth of 14.85 cm (average

0.0200 cm $hr^{-1}$) while December had the minimum depth of 0.755 cm (average 0.0010 cm $hr^{-1}$). For USPS, July 2013 had the maximum monthly ET depth of 15.36 cm (average 0.0206 cm $hr^{-1}$), while January 2013 had the minimum depth of 0.224 cm (average 0.0003 cm $hr^{-1}$). Total yearly ET on USPS from April 2012 to March 2013 was 62.53 cm. This represents 58% of the rainfall over this period, indicating an average annual rooftop rainfall retention of the same amount. This value compares well with the predicted annual retention of 53% for USPS based on roof runoff measurements (Carson *et al* 2013).

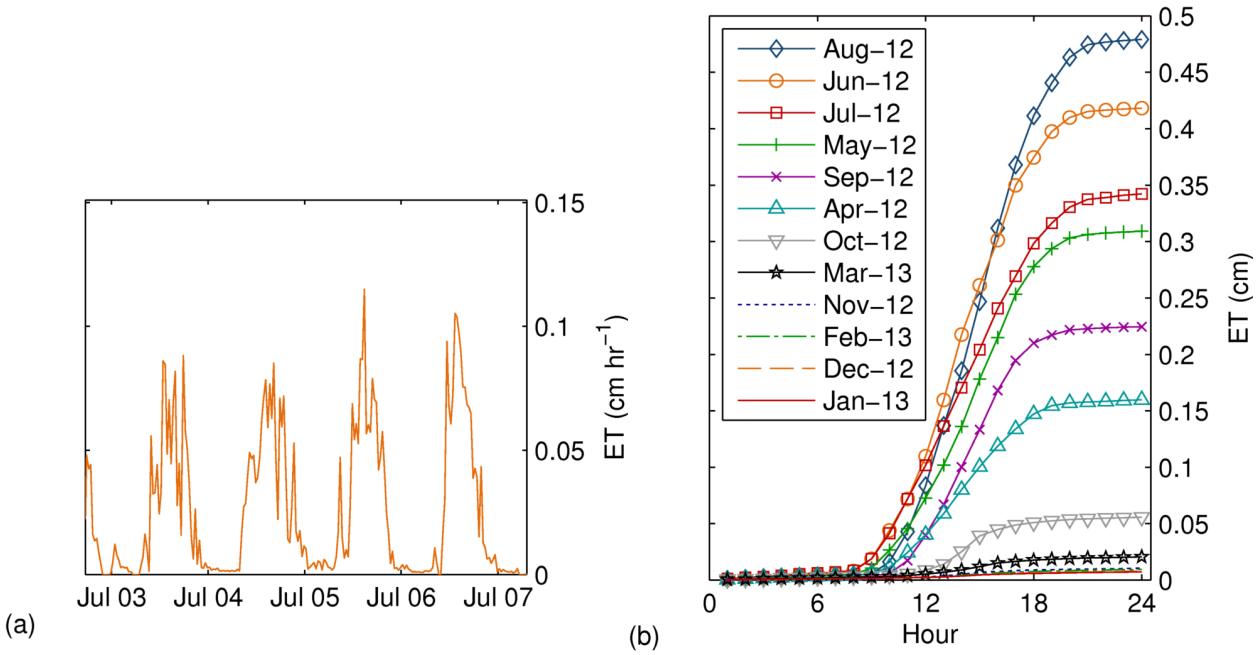


Figure 4: (a) Example of 30-minute ET results (cm $hr^{-1}$) from the dynamic chamber during W118 deployment in 2009. The peak ET recorded (0.115 cm $hr^{-1}$) is shown on July 05. (b) Cumulative average hourly ET (cm) from the USPS dynamic chamber deployment from April 2012 to March 2013.

Chamber ET results from this study fall within the range of results reported from other green roof ET studies in the United States and temperate regions in France and New Zealand (Table 1) (DiGiovanni *et al* 2013, Feller 2011, Ouldboukhitine *et al* 2012, Sherrard and Jacobs 2012,

Tabares-Velasco and Srebric 2011, Voyde *et al* 2010b). In particular, lysimeter measurements from a green roof located in Bronx, NY from July – December 2009 are similar to the dynamic chamber results measured on W118 during the same period (DiGiovanni *et al* 2013).

Table 1: Summary of green roof ET studies and average measured ET rates.

| Publication | Location | Setup Type | Measurement Method | Study Period | ET (cm day$^{-1}$) |
|---|---|---|---|---|---|
| This Study | W118 | Full-Scale | Dynamic Chamber | Jul 09 - Dec 09 | 0.197 |
| | | | ASCE RET | Jul 09 - Dec 09 | 0.240 |
| | | | ASCE RET | Apr 12 - Oct 13 | 0.293 |
| | | | Surface Model | Apr 12 - Oct 13 | 0.213 |
| | USPS | Full-Scale | Dynamic Chamber | May 12 - Oct 13 | 0.212 |
| | | | ASCE RET | Apr 12 - Oct 13 | 0.250 |
| | ConEd | Full-Scale | ASCE RET | Apr 12 - Oct 13 | 0.269 |
| | | | Energy Balance | Apr 12 - Oct 13 | 0.085 |
| DiGiovanni *et al* (2013) | Bronx, NY | Test-Box | Lysimeter | Jun 09 - Jun 10 | 0.190 |
| | | | ASCE RET | Jun 09 - Jun 10 | 0.284 |
| Feller (2011) | Villanova, PA | Test-Box | Lysimeter | Apr 09 - Nov 09 | 0.240 |
| Ouldboukhitine *et al* (2012) | Rochelle, FR | Test-Box | Lysimeter | 1 week Oct 10 | 0.142 |
| Sherrard & Jacobs (2012) | Seacoast, NH | Test-Box | Lysimeter | Aug 09 - Nov 09 | 0.090 |
| Tabares-Velasco & Srebric (2012) | University Park, PA | Lab Setup | Lysimeter | 43 days | 0.300 |
| Voyde *et al* (2010b) | Auckland, NZ | Greenhouse | Lysimeter | May 08 | 0.103 |

The chamber measurements were used to explore how *Sedum* green roof ET varies with air temperature and relative humidity (RH) observations. Figure 5 provides a surface model of ET measurements versus air temperature and RH for W118 (Figure 5(a)) and USPS (Figure 5(b)) generated using the gridfit MATLAB software package for least-squares surface reconstruction (D'Errico 2005). Overall, and as reported by others (Liss 1973, DiGiovanni *et al* 2013), for a constant RH, ET increases exponentially with temperature, whereas for a constant temperature ET decreases with RH. The surface models for W118 and USPS show similar trends (Figure 5 (c)). However, W118 displays higher ET near 30 °C and 40% relative humidity. This difference

primarily results from low ET values observed on USPS over the period July 4 – 7, 2012 (0.07 – 0.16 cm day$^{-1}$), caused by a span of limited rainfall and low soil moisture. Figure 5(d) provides a surface model of ET based on the data from both roofs. Although other factors, including wind speed, solar radiation, and soil moisture are known to influence ET (Monteith 1965, DiGiovanni *et al* 2013), Figure 5(d) can be used to provide an initial empirical estimate of ET for *Sedum* roofs based on two common environmental measurements. This approach is explored in section 2.3.4 below.

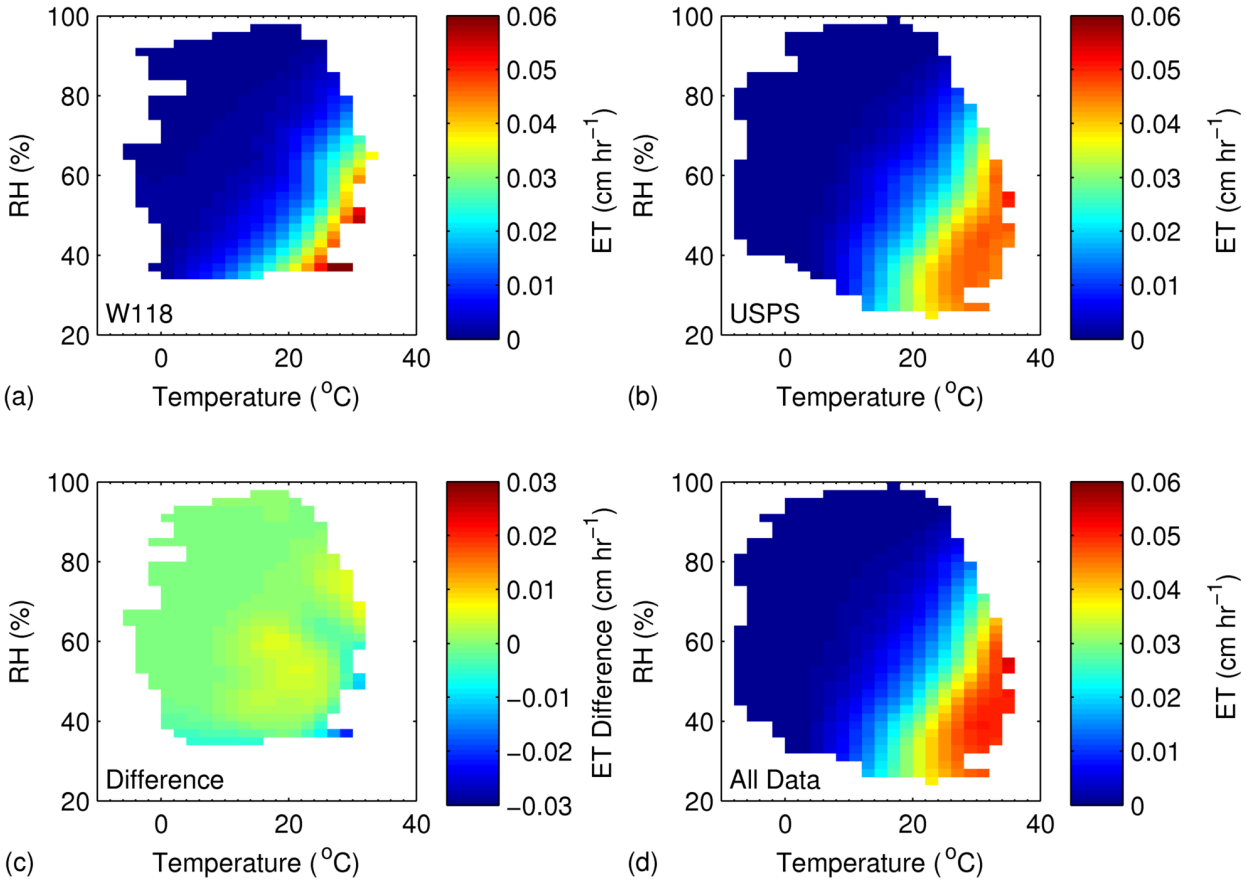


Figure 5: Least squares estimated surface model of ET(cm hr$^{-1}$) compared to air temperature (°C) and relative humidity (RH) (%) for (a) W118 and (b) USPS. (c) is the ET on USPS minus the ET on W118. (d) is the combined surface model from data collected both roofs. Blank space on the figures indicates no available data.

*2.3.2 ET Estimates from the ASCE Standardized Reference Evapotranspiration Equation*

Figure 6 shows the estimated monthly RET depths for each roof based on the ASCE RET equation. The similarity of RET depths is attributed to close rooftop proximity (less than 6.3 km apart), similar environmental conditions, and the standardized ASCE RET model. Peak ASCE RET estimates occurred in July 2012 for all rooftops, with a total depth of 15.66 cm (average 0.021 cm $hr^{-1}$), 12.79 cm (average 0.017 cm $hr^{-1}$), and 14.36 cm (average 0.019 cm $hr^{-1}$) for W118, USPS, and ConEd, respectively. Minimum ET estimates occurred in December 2012, with a total depth of 2.40 cm (average 0.003 cm $hr^{-1}$), 1.87 cm (average 0.003 cm $hr^{-1}$), and 2.33 cm (average 0.003 cm $hr^{-1}$) for W118, USPS, and ConEd, respectively. Over the period from April 2012 (May for USPS) to March 2013, the ASCE RET was 92.3 cm for W118, 72.3 cm for USPS, and 86.4 cm for ConEd. This represents an annual green roof water retention of 81.0%, 72.8%, and 72.5% of the rainfall for W118, USPS and ConEd, respectively. According to Carson *et al* (2013), predicted average annual water retention for W118, USPS and ConEd are 45%, 53% and 58%, respectively. Thus, the ASCE RET method returns higher values for annual green roof water retention than a water balance study.

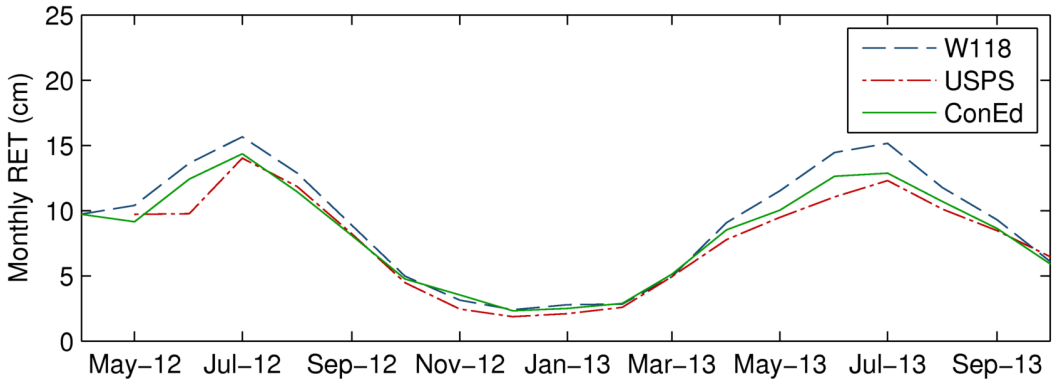


Figure 6: Monthly reference evapotranspiration (RET) from the ASCE standardized RET equation for W118, USPS, and ConEd from April 2012 – October 2013.

*2.3.3 ET Estimates from the Energy Balance Model*

Figure 7 shows the monthly average latent heat flux (upward; i.e., from the roof to the atmosphere) on ConEd, estimated from the energy balance model, compared to sensible heat flux (upward), net radiation (downward), and conductive heat flux (upward). Sensible heat flux peaked in April 2013 with a monthly average of 37.50 W $m^{-2}$. Average monthly sensible heat flux was downward for the winter months, reaching a maximum downward flux of 31.46 W $m^{-2}$ in November 2012. Average latent heat followed a different trend, reaching a peak of 50.08 W $m^{-2}$ (0.0074 cm $hr^{-1}$) in June 2013, becoming slightly negative in the winter with a peak downward flux of 11.48 W $m^{-2}$ (0.0016 cm $hr^{-1}$) in January 2013. Conductive heat flux was generally minimal. Variation in latent and sensible heat trends confirms that energy models employing a constant linear conversion factor like Bowen's Ratio ($\beta = Q_{sensible}\ Q_{latent}^{-1}$), are not likely sufficient for estimating latent heat from sensible heat on a green roof (Oke 1987).

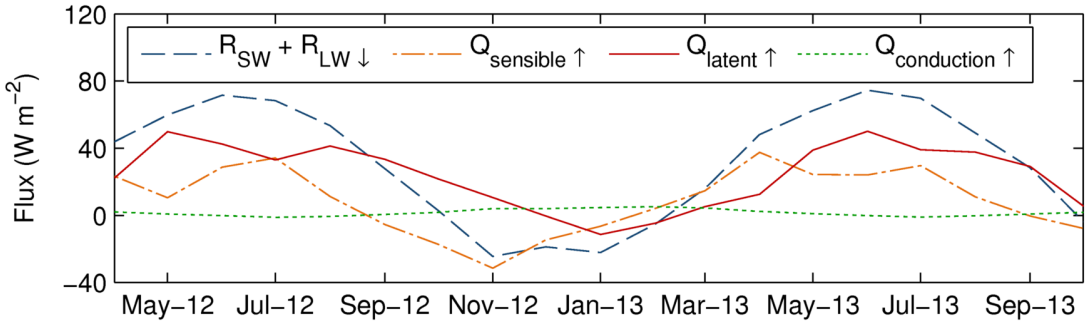


Figure 7: Monthly averages for net radiation ($R_{SW} + R_{LW}$), sensible heat ($Q_{sensible}$), latent heat ($Q_{latent}$), and conductive heat ($Q_{conduction}$) on the ConEd rooftop between April 2012 and October 2013. Arrows indicate direction of flux, with upward indicating a flux from the rooftop to the atmosphere.

*2.3.4 Comparison of Methods*

Monthly ET depths are net positive with the exception of energy balance winter results, indicating water was leaving the rooftop (Figure 8). Seasonal variation was generally consistent across methods, with maximum ET in summer months and minimum ET in winter months. This trend agrees with both green roof and agricultural studies that state conditions in warm seasons support higher ET (Gaffin *et al* 2010, DiGiovanni *et al* 2013, Mentens *et al* 2006, Villarreal *et al* 2004, Sumner and Jacobs 2005, Wever *et al* 2002).

Through observation of seasonal and daily measurements (Figure 8), a systematic error is seen where the ASCE RET equation overestimates ET at lower fluxes and underestimates at higher values compared to dynamic chamber measurements. The ASCE RET equation does not consider reductions in ET caused by water limitations or limited *Sedum* productivity in winter. ET measurements from a lysimeter located on a green roof in Bronx, NY between 2009 and 2010 and a forest in central Massachusetts between 1992 and 2000 show winter ET rates similar to the dynamic chamber (DiGiovanni *et al* 2013, Czikowsky and Fitzjarrald 2004). Particularly high ET values from ASCE RET estimates compared to the chamber ET measurements (e.g. DC ET = 0.09 cm $day^{-1}$, ASCE RET = 0.60 cm $day^{-1}$ on July 7, 2012) occur on dry summer days, as observed through onsite soil moisture and rainfall measurements (Figure 9).

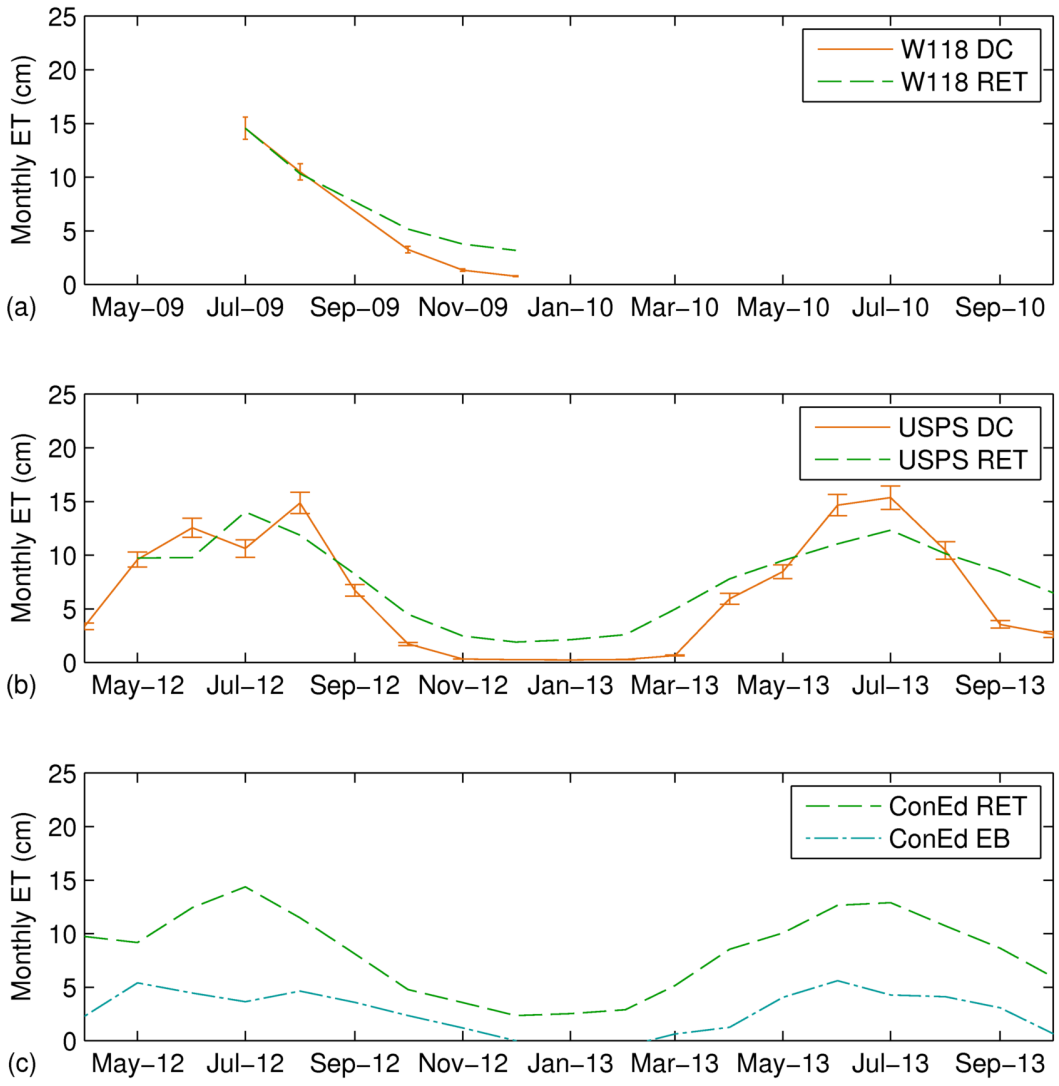


Figure 8: Comparison of monthly dynamic chamber (DC) ET, ASCE RET, and energy balance (EB) ET depth (cm) for (a) W118; (b) USPS; and (c) ConEd. Error bars represent 95% confidence intervals of calibration coefficients for dynamic chamber.

While the monthly trends of the energy balance method are similar to the dynamic chamber and ASCE RET equation, the depths of ET, especially in warmer months, vary significantly. The energy balance, as with other energy methods, shows a comparative underestimation of ET (Rosenberg 1969, Blad and Rosenberg 1974, Bertela 1989).

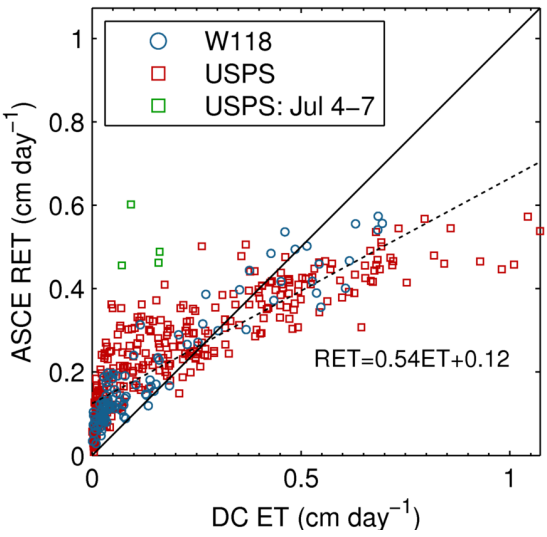


Figure 9: Comparison of daily ET from dynamic chamber (DC) with ASCE RET estimates. Dotted line represents linear regression of RET vs ET for both roofs.The points labeled "USPS: Jul 4 – 7" represent the Jul 4 – 7 , 2012 drought period on USPS.

The data in Figure 5(d) were used to predict ET on USPS from May 2012 to October 2013 based on site air temperature and RH. Because Figure 5(d) displays a surface of ET in RH-temperature space, this method is termed the "surface model". The results of the surface model show similar average daily ET (0.213 cm day$^{-1}$) compared to the dynamic chamber (0.212 cm day$^{-1}$) and ASCE RET (0.250 cm day$^{-1}$) results. The surface model shows a comparatively higher ET peak in July 2012 (0.71 cm day$^{-1}$), where soil moisture and rainfall results show limited available water in the first part of this month, and lower fluxes in May and June 2013 (0.26 cm day$^{-1}$), which had increased rainfall (17.22 and 25.32 cm, respectively) compared to average annual trends (Figure 10).

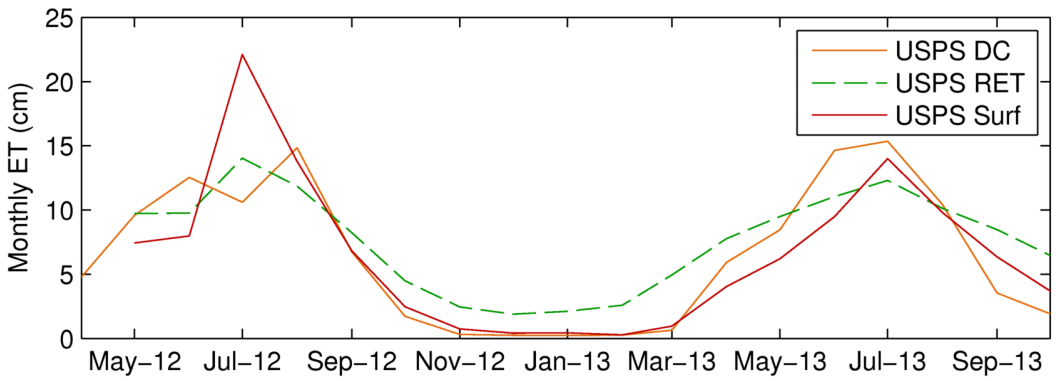


Figure 10: Comparison of monthly total dynamic chamber (DC) ET,ASCE RET, and Surface model (Surf) ET depth (cm) for USPS for April 2012 – October 2013.

### *2.3.5 Benefits and Limitations*

This study has shown that the LI-8100 system can be used to measure green roof ET. The LI-8100 can be quickly deployed on an existing roof, is minimally invasive, and operates unattended. Chamber ET measurements can be taken every 30 minutes, providing an extensive field data set useful for discerning diurnal and seasonal green roof ET trends and improving understanding of the thermal and hydrological behavior of green roofs. The data set is also advantageous for examining the influence of environmental factors such as relative humidity and temperature on ET, as demonstrated by the surface model. Nonetheless, chamber methods only record ET at a particular location. Because full-scale green roofs contain vegetated and non-vegetated areas, measurements made at a single vegetated location might not capture the overall performance.

Comparison of the chamber ET measurements to the ASCE RET equation and energy balance model results indicates that the ASCE RET equation might provide a more accurate estimate of ET than widely used energy balance methods. Parameterization of the ASCE RET method

requires less monitoring equipment, and thus capital, to implement than the energy balance model. However, the equation does not account for variations in soil moisture availability and plant vitality, leading to ET overestimations, as seen during the dry period on USPS from July 4 – 7, 2012. Low ET estimates from the energy balance method show the need for further calibration and refinement of this approach for adoption on green roofs.

# Chapter 3

## APPLICABILITY OF COMMON PREDICTIVE MODELS FOR ESTIMATION OF EVAPOTRANSPIRATION ON URBAN GREEN ROOFS


### Abstract

Although the ET process has historically received limited attention, it is an important factor for assessing both the health and performance of urban green spaces. In this study, common models for potential evapotranspiration (PET) and actual evapotranspiration (AET), parameterized by on-site climate conditions, are compared to ET measurements from a dynamic chamber system deployed on two extensive green roofs (termed W118 and USPS) in Manhattan, NY. Dynamic chamber ET was measured from July 2009 to December 2009 on W118 and from April 2012 to October 2013 on USPS. Comparison of PET estimates from the Hargreaves, Priestley-Taylor, Penman, and Penman-Monteith equations to dynamic chamber measurements reveal that the Priestley-Taylor equation best predicts measured ET (r-squared = 0.96 for W118, 0.82 for USPS). However, a systematic error is seen whereby the Priestley-Taylor equation overestimates lower ET fluxes during the winter months and underestimates high summer ET fluxes. A storage model, antecedent precipitation index, and advection-aridity equation are applied to calculate AET in water-stressed conditions. Results indicate that AET may be better estimated through antecedent precipitation index (r-squared = 0.96 on W118, 0.85 on USPS), based solely on rainfall data, than through a storage model. Results inform the understanding of green roof ET

behavior and applicability of ET models for quantifying ET and parameterizing hydrological and energy models.

## 3.1 Introduction

The expansion of urban green spaces, specifically green roofs, urban forests, bio-swales, and green streets, is an increasingly popular decentralized strategy to counter urban land development impacts. These green spaces are engineered vegetative systems primarily designed to re-introduce pre-development hydrological conditions and enhance natural processes. Urban green spaces have the potential to detain and retain stormwater, offset carbon emissions, improve air quality, reduce energy usage, and increase public space (Taha *et al* 1991, Jim and Chen 2009, NYC DEP 2010, Voyde *et al* 2010a, Ouldboukhitine *et al* 2011, Wadzuk *et al* 2013, Marasco *et al* 2014).

Evapotranspiration (ET) is the combined water vapor surface flux that results from evaporation and plant respiration. ET is an important factor affecting the vitality and performance of urban green spaces; however, the quantification of ET from these spaces has historically received limited attention (Grimmond and Oke 2002, DiGiovanni *et al* 2013, Voyde *et al* 2010b). Studies have shown that the ET process is directly correlated with environmental benefits related to stormwater management (Stovin *et al* 2013, Wadzuk *et al* 2013), urban heat island mitigation (Taha 1997), building energy usage (Ouldboukhitine *et al* 2011), carbon sequestration (Pataki *et al* 2006), and air pollution (Christen and Vogt 2004, Jim and Chen 2009). Additionally, ET is an important parameter in many urban hydrologic (Sherrard and Jacobs 2012, Zhao *et al* 2013, Stovin *et al* 2013) and energy transfer models (Lazzarin *et al* 2005, Ouldboukhitine *et al* 2011, Wang *et al* 2013).

ET primarily results from solar energy, but is affected by various environmental conditions, including the stomatal resistance of vegetation, surface albedo, aerodynamic roughness, boundary layer humidity profile, and available substrate moisture (Allen *et al* 1996, Salvucci and Gentine 2013, Mawdsley and Ali 1985). Because the ET process is invisible and difficult to measure directly, equations and models have been developed to predict ET from environmental data (Zhao *et al* 2013). Equations developed to estimate ET, such as Hargreaves (Hargreaves and Allen 2003), Priestley-Taylor (1972), Penman (1948), and Penman-Monteith (Monteith 1965) generally estimate the "potential evapotranspiration" (PET) (i.e. the energy-limited ET) over a static underlying surface, such as water, bare soil, or specified vegetation. The Hargreaves and Priestley-Taylor equations are based on a composite of energy and temperature data, while the Penman and Penman-Monteith models also incorporate wind and humidity measurements to estimate advective ET.

PET models neglect factors that affect the actual evapotranspiration (AET), including substrate moisture availability, surface conditions, crop coefficients, plant vitality, and weather (Allen *et al* 1996, 2005a, Zhao *et al* 2013). When transpiration is minimal (e.g. during the winter and early spring), ET consists primarily of evaporation and is significantly correlated with substrate moisture at the surface level (Allen *et al* 2005a). Evaporation from bare soil can be considered "energy-limited" or "water-limited" based on the moisture availability. When evaporation is energy-limited, sufficient surface moisture is available to supply the PET demand. As surface moisture evaporates and insufficient moisture is available to supply the PET demand, evaporation becomes "water-limited", and is affected by soil heat density, soil properties, and remaining moisture availability (Allen *et al* 2005a). Transpiration is a more complex process

than evaporation. Even in energy-limited, or potential, conditions, transpiration is affected by sub-surface moisture, as well as the structure and vitality of substrate vegetation (Allen *et al* 1996, Brutsaert 2005). Additionally, PET is often estimated from non-potential environmental conditions. When ET drops below potential, excess energy becomes available, altering air temperature, humidity, and turbulence near the surface (Brutsaert and Stricker 1979). PET calculated under these conditions is referred to as "apparent" PET (Brutsaert 2005).

The environmental processes and conditions affecting the hydrologic cycle in urban green spaces vary from those of homogeneous, well-watered, agricultural and natural settings. Consequently, assumptions made in conventional hydrologic models may inaccurately portray the behavior and benefits of urban green spaces (Graham *et al* 2004). ET in urban environments is generally lower than the surrounding natural environment and is often neglected or simplified in hydrologic models (Grimmond and Oke 2002, Berthier *et al* 2006). However, urban ET can still be a major component of the water balance, especially when urban trees and green spaces are present (Grimmond and Oke 1991, 2002). ET from urban green spaces is affected by their unique properties, including small scale, vegetation heterogeneity, shallow substrate depths, underlying surfaces, and uncertain moisture availability (Spronken-Smith *et al* 2000, Grimmond and Oke 2002, Jim and Peng 2012, DiGiovanni *et al* 2013). The increased air temperature and lower humidity of the surrounding built-up environment can enhance local and micro-scale moisture advection of urban green spaces (Spronken-Smith *et al* 2000) and alter transport of heat and momentum (Taha 1997). In addition, as described by Jim and Peng (2012), shallow extensive roof substrates can have elevated temperatures in water-limited conditions, enhancing ET.

In this study, predictive models parameterized by on-site climate conditions are employed to calculate PET and AET on two extensive green roof systems in Manhattan, NY. The predicted daily ET fluxes (collectively referred to as $ET_p$) from these models are compared to ET measurements from a dynamic chamber system ($ET_{DC}$). Concurrent $ET_{DC}$ and on-site climate measurements were conducted from July 2009 to December 2009 on a vegetated mat system (referred to as W118) and from April 2012 to October 2013 on a built-in-place system (referred to as USPS). Comparisons between ET models and dynamic chamber measurements inform the applicability of PET and AET models for quantification of green roof benefits and calculation of ET for input in urban hydrologic and energy transfer models.

## 3.2 Summary of AET models and Green Roof ET studies

### *3.2.1 Actual Evapotranspiration Models*

AET estimation procedures generally calculate flux from PET results based on existent non-potential conditions (Brutsaert 2005). The variation between PET and AET is primarily a function of water availability in the soil. At substrate field capacity, AET is equal to PET; as soil moisture decreases, so does AET. Various soil moisture extraction functions (SMEFs) based on a combination of actual soil moisture, field capacity, and wilting point have been employed to relate the degree of substrate saturation to AET (Zhao *et al* 2013, DiGiovanni *et al* 2013).

In the absence of soil moisture data, other moisture indices and PET reduction procedures have been employed to estimate AET, including accumulated precipitation and ET deficit models (Grindley 1970, Priestley and Taylor 1972, Calder *et al* 1983, Arora 2002), antecedent precipitation indices (Choudhury and Blanchard 1983, Mawdsley and Ali 1985, Ali and Mawdsley 1987, Westenbroek *et al* 2010), the advection-aridity model (Brutsaert and Stricker

1979, Ali and Mawdsley 1987, Kahler and Brutsaert 2006), water stress - surface temperature relationships (Moran *et al* 1994, Boulet *et al* 2007), and relative humidity profiles (Berthier *et al* 2006, Salvucci and Gentine 2013).

### *3.2.2 Studies of Green Roof ET*

Green roof ET has been measured in a variety of studies in order to quantify rooftop behavior. ET is most often measured with a lysimeter (Voyde *et al* 2010b, Ouldboukhitine *et al* 2012, Sherrard and Jacobs 2012, DiGiovanni *et al* 2013, Wadzuk *et al* 2013). Results from these studies show average ET rates between 1 and 3 mm $day^{-1}$. DiGiovanni *et al* (2013) compared AET measurements to Penman-Monteith equations, showing that the equations performed well on non-water-limited days. A variation of the Thornthwaite-Mather (1955) attenuating factor was employed to estimate AET from PET, improving predictions when water was limited. Lazzarin *et al* (2005) employed a empirical version of the Penman equation and a reduction factor based on relative humidity to predict AET. The formulation worked well in well-watered conditions, but the reduction factor was unable to account for moisture limitations.

Jim and Peng (2012) investigated the influence of substrate moisture on green roof ET by dividing monitored days into 9 categories defined from 3 weather (sunny, cloudy, and rainy) and substrate moisture (wet, moist, and dry) types. Results show that substrate moisture had a limited influence on ET, and the primary factors correlated with ET were those included in PET equations. Dry substrates on sunny days demonstrated higher ET, explained by shallow substrate allowing solar energy to heat up the entire substrate layer, increasing temperature and enhancing ET.

ET estimation techniques have been employed in a variety of studies to predict behavior and supplement green roof hydrologic and energy models. Berthier *et al* (2011) and Sherrard and Jacobs (2012) developed and calibrated reservoir storage models to predict runoff, incorporating daily calculations of Penman-Monteith PET. Berthier *et al* used PET, while Sherrard and Jacobs incorporated a soil moisture extraction function to modify PET in water limited conditions. Sherrard and Jacobs' calibrated model was compared to data measured from a lysimeter setup and was shown to accurately predict daily storage and runoff (r-squared equal to 0.94 and 0.98, respectively) but showed reduced correlation in the prediction of ET (r-squared equal to 0.59). Stovin *et al* (2013) applied average monthly estimations of PET and a soil moisture extraction function (SMEF) to better predict green roof storage and runoff. The model was used to evaluate the performance of green roofs in four different climate regions based on variations in precipitation and PET. Results show that climate variations affect rooftop hydrological performance and drought susceptibility.

## 3.3 Site Descriptions and Methodology

### *3.3.1 Site Descriptions and Instrumentation*

Dynamic chamber measurements and environmental monitoring were conducted on two *Sedum* extensive green roofs in Manhattan, NY between January 2009 and October 2013. A more detailed description of the site characteristics, instrumentation, and data collection is provided in Chapter 2 and Appendix A. Initial dynamic chamber measurements were collected on a Columbia University residential building (termed W118), located at 423 West 118$^{th}$ St, Manhattan, NY (Table 2) for a minimum 11-days each month between July 2009 and December 2009, with the exception of September 2009. Solar radiation, air temperature, relative humidity,

wind speed, and precipitation data were recorded at five-minute intervals by a Campbell Scientific CR1000 weather station from January 2009 to October 2013. A second dynamic chamber deployment and collection of environmental data took place on the US Post Office Morgan Processing and Distribution Center green roof (termed USPS) in Manhattan, NY (Table 2) between April 2012 and October 2013. Measurements were continuous with the exception of July 8 – July 29, 2012 when the rooftop lost power. An Onset Hobo U30 weather station recorded air temperature, relative humidity, solar radiation, wind speed, and precipitation were recorded at five-minute intervals from January 2012 to October 2013. Measurements were continuous except in April 2012 and from July to September 2012, when sensors malfunctioned. The substrate field capacity was measured by Carson *et al* (2014) and shown to match manufacturer specifications.

Table 2: Monitored green roof site characteristics

| **Roof Name** | **W118** | **USPS** |
|---|---|---|
| Construction Type | Vegetated mat | Built-in-place |
| Year Built | 2007 | 2009 |
| Latitude | 40°48’ | 40°45’ |
| Roof Height (m) | 65 | 45 |
| Roof Area ($m^2$) | 600 | 10,000 |
| Sub. Depth (mm) | 32 | 100 |
| Field Capacity (mm) | 12 | 49 |
| Irrigation | None | None |

*3.3.2 Dynamic chamber Measurements*

Dynamic chamber measurements of green roof ET were conducted using the Licor Biosciences LI-8100 automated soil $CO_2$ flux system. Measurements occurred every 30 minutes on W118 and 60 minutes on USPS. For each measurement, the system’s chamber (volume, $V = 6850$ $cm^3$ for W118, $V = 7005$ $cm^3$ for USPS) encloses a section of the green roof (surface area, $S = 323.6$

$cm^2$) for 5 minutes and records chamber water vapor concentration, $w_c$, in mmol $mol^{-1}$ (ppt). The flux of water from the sealed green roof surface into the chamber (mol $cm^{-2}$ $s^{-1}$) is a measure of ET. A nonlinear regression of water vapor concentration versus time data, $t$(s), with an exponential function of the form

$$w_c(t) = w_s + (w_c(0) - w_s)e^{-K\frac{S}{V}(t-t_0)} \quad (1)$$

is performed for the first minute of measurement, excluding the first 10 seconds to allow for the system to establish steady mixing. Fitting of Equation (1) to measured values of $w_c(t)$ returns values for $w_s$, the saturation concentration of water vapor at the evaporative surface (mmol $mol^{-1}$), $K$, the water vapor transfer velocity (cm $s^{-1}$), and $t_0$, when $w_c(t)$ is equal *to* $w_c(0)$ (s). ET is then obtained from the water vapor flux at $t = 0$, yielding

$$\mathrm{ET} = \frac{P(0)}{RT(0)} \frac{1}{\left(1-\frac{w_c(0)}{1000}\right)} K\left(\frac{w_s-w_c(0)}{1000}\right) \quad (2)$$

where $P(0)$ is the initial pressure (kPa), $T(0)$ is the initial temperature (K), and $R$ is the gas constant (8.314 x $10^3$ $cm^3$ kPa $K^{-1}$ $mol^{-1}$). ET values from Equation (2) were converted to mm $day^{-1}$ by assuming 18 grams of water per mol and a water density of 1 g $cm^{-3}$.

The dynamic chamber was calibrated with a series of 6 pan evaporation experiments conducted in Columbia University's Carleton Laboratory. During each 12-hour trial, a pan of open water or wet substrate was placed in the chamber. The pan was weighed every 30 minutes to measure cumulative evaporation. Chamber estimates of ET were obtained during each 5-minute automated chamber closure, programed to occur halfway between each weight measurement. A comparison of chamber and weight measurements reveals a systematic error, where the chamber

records lower ET than measured by weight. The error is believed to be the result of polar water vapor molecules adhering to the surfaces of the air-lines between chamber and infrared sensor. A linear regression of the weight-measured ET versus the chamber estimate is able to correct this error (r-squared = 0.95). A more detailed description of the dynamic chamber methodology and calibration is provided in Chapter 2.

*3.3.3 Potential Evapotranspiration Estimates*

The four equations for estimating PET (i.e. the maximum amount of water that would evaporate a well-watered and healthy vegetated surface) employed in this study are the Hargreaves, Priestley-Taylor, Penman, and Penman-Monteith equations.

The empirical 1985 Hargreaves equation estimates $PET_H$ (mm $day^{-1}$) using air temperature and location data, and is generally accurate for periods of a week or longer (Hargreaves and Allen 2003). The equation is as follows

$$PET_H = 0.408(0.0023R_a\ (T_{mean} + 17.8)(T_{max} - T_{min})^{0.5}) \quad (3)$$

where $T_{max}$ and $T_{min}$ are the daily maximum and minimum temperature, respectively.

The Priestley-Taylor (1972) equation is a refinement of the Slatyer-McIlroy (1961) equation for baseline PET from a moist surface. The Priestley-Taylor equation predicts $PET_{PT}$ (mm $day^{-1}$) considering a wet vegetated surface with minimal advection. The equation for $PET_{PT}$ is given by

$$PET_{PT} = 0.408\left[\alpha \frac{\Delta}{\Delta+\gamma}(R_n - G)\right] \quad (4)$$

The coefficient, $\alpha$, is equal to 1.26 and represents the ratio between the equilibrium evapotranspiration and observed ET from moist, advection-free land and water surfaces (Priestley and Taylor 1972).

The Penman (1948) equation is similar to the Priestley-Taylor equation, but has an added advection term. The equation for $PET_p$ (mm $day^{-1}$) is described by

$$PET_P = 0.408\left[\frac{\Delta}{\Delta+\gamma}(R_n - G)\right] + \left[\frac{\gamma}{\Delta+\gamma}E_A\right] \quad (5)$$

$$\text{where, } E_A = 2.6(1 + 0.54u_2)\,(e_s - e_a) \quad (6)$$

The ASCE Standardized Reference Evapotranspiration (ASCE PM) equation for the short reference surface (e.g. cut grasses) was the analyzed version of the Penman-Monteith equation (Allen *et al* 2005b). This form of the equation reduces the surface and aerodynamic resistance variables in the Penman-Monteith (Monteith 1965) equation to standard values for reference vegetation types. The ASCE equation for $PET_{PM}$ (mm $day^{-1}$), is given by

$$PET_{PM} = \frac{0.408\Delta(R_n-G)+\gamma\left(\frac{C_n}{T_{mean}+273}\right)u_2(e_s-e_a)}{\Delta+\gamma(1+C_d u_2)} \quad (7)$$

where $C_n$ is the numerator constant (900 K mm $s^3$ $Mg^{-1}$ $d^{-1}$ for the daily time step) and $C_d$ is the denominator constant (0.34 s $m^{-1}$) for the short reference type.

Variables used in equations (3-7), including mean temperature, $T_{mean}$ (°C), extraterrestrial radiation, $R_a$ (MJ $m^{-2}$ $d^{-1}$), net radiation, $R_n$ (MJ $m^{-2}$ $d^{-1}$), soil heat flux density, $G$ (MJ $m^{-2}$ $d^{-1}$), the psychrometric constant, $\gamma$ (kPa $°C^{-1}$), slope of the saturation vapor pressure-temperature curve, $\Delta$ (kPa $°C^{-1}$), wind speed, $u_2$ (m $s^{-1}$), saturation vapor pressure, $e_s$ (kPa), and vapor pressure, $e_a$

(kPa), were calculated on the daily timescale according to ASCE standardized reference evapotranspiration (ASCE PM) specifications (Allen *et al* 2005b), described in Chapter 2. An albedo of 0.28 was calculated from linear regression of upward and downward shortwave radiation measurements from USPS roof between March 2011 and June 2012 (r-squared = 0.997). The density of water (1.0 Mg $m^{-3}$) divided by the approximate latent heat of vaporization (2.45 MJ $kg^{-1}$) is 0.408, the coefficient in equations (3-7).

### *3.3.4 Actual Evapotranspiration Estimates*

Three methods were employed to calculate AET from PET estimates, a soil moisture extraction function (SMEF) based on data calculated from a green roof storage model, an antecedent precipitation index (API) based on monitored precipitation data, and an advection-aridity (A-A) model parameterized by PET equations.

A SMEF, similar to those employed by Sherrard and Jacobs (2012), DiGiovanni *et al* (2013), and Stovin *et al* (2013), was incorporated as a coefficient to calculate AET from PET estimates. The dimensionless SMEF coefficient, $\beta$, is a function of soil moisture storage depth at the specified interval, $S$ (mm), and the field capacity of the substrate, $S_{fc}$ (mm) (Table 2), and is calculated on the $d^{th}$ day as follows

$$\beta_{(d)} = \frac{S_{(d-1)}}{S_{fc}} \tag{8}$$

AET is then calculated as the following function of $\beta$ and PET

$$\mathrm{AET}_{\mathrm{SM}(d)} = \beta_{(d)}\mathrm{PET}_{(d)} \tag{9}$$

Because soil moisture data is not often readily available, a continuous storage model on a daily time step, similar to those developed by Berthier *et al* (2011) and Stovin *et al* (2013), was applied to predict soil moisture at each interval. The model calculates storage on the $d^{th}$ day as

$$S_{(d)} = min\{S_{fc},\ S_{(d-1)} + P_{(d)} - \mathrm{AET}_{\mathrm{SM}(d)}\} \quad (10)$$

where $P$ is precipitation (mm). Because $\mathrm{AET}_{\mathrm{SM}}$ decreases with $S$, specification of a substrate wilting point or lower boundary on storage is redundant.

The antecedent precipitation index (API) model is a modification of the Priestley-Taylor (1972) PET equation. The model modifies predicted PET based on a function of antecedent precipitation in the previous 28 days to account for variations in soil moisture content and predict AET in drought conditions (Ali and Mawdsley 1987, Mawdsley and Ali 1985).

The equation is as follows

$$\mathrm{AET}_{\mathrm{API}} = 0.408\alpha\left[\frac{\Delta}{\Delta+\gamma}(R_n - G)\right] \quad (11)$$

where the dimensionless coefficient, $\alpha$, is expressed as

$$\alpha = 0.123(\mathrm{API}) - 0.0029(\mathrm{API})^2 - 0.0000056(\mathrm{API})^3, for\ \mathrm{API} \leq 20$$

$$\alpha = 1.26, for\ \mathrm{API} > 20 \quad (12)$$

with the function for API (mm) for each day ($d$) given by Kohler and Lindsey (1951), limited to each of the previous 28 days ($t$ = 1, 2, 3, … 28)

$$\mathrm{API}(d) = \sum_{t=1}^{28} K^{(t-1)} P_{(d-t)} \quad (13)$$

where is the dimensionless recession constant, $K$, is set to 0.9 (Kohler and Linsley 1951, Ali and Mawdsley 1987).

The advection-aridity model (A-A), developed by Brutsaert and Stricker (1979) to predict AET, is based on a hypothesis developed by Bouchet (1963). Bouchet postulates that when AET is less than PET due to limited water availability, the excess energy is transferred to other components of the energy balance, which increases PET even though AET has declined (Ali and Mawdsley 1987, Brutsaert 2005). The A-A model assumes that the increase in PET is exactly equal to the reduction in the AET, leading to the following equation

$$\mathrm{AET_{A-A}} = 2\mathrm{PET_{PT}} - \mathrm{PET_P} \tag{14}$$

where Brutsaert and Stricker suggested using the Priestley-Taylor model for "apparent" PET ($\mathrm{PET_{PT}}$) in non-potential conditions, and the Penman equation for the PET given non-water-limiting conditions ($\mathrm{PET_p}$). Substituting in Equations (4) and (5) into Equation (14) gives

$$\mathrm{AET_{A-A}} = (2\alpha - 1)0.408\left[\frac{\Delta}{\Delta+\gamma}(R_n - G)\right] - \left[\frac{\gamma}{\Delta+\gamma}E_A\right] \tag{15}$$

for $\mathrm{AET_{A\text{-}A}}$ on each day, where $E_A$ is calculated from Equation (6).

### *3.3.5 Daily data assimilation and comparison*

All recorded environmental data, including 30-minute W118 dynamic chamber measurements, were averaged over each hour. For the purpose of calculating daily values, missing hourly dynamic chamber ET fluxes were estimated from a linear regression of the prior and following ET measurements, as long as they were within 2 hours. Lower ET fluxes during nighttime resulted in increased errors (10 %) compared to daytime data (7 %), which would result in an

overestimation of daily ET. Days with remaining missing data were eliminated from the analysis. Additionally, while statistics are based on all concurrent PET estimates and $ET_{DC}$ measurements; due to sensor malfunctions in 2012, the focus of the USPS trend analysis is period between October 2012 and September 2013, where measurements were continuous.

Daily ET fluxes from the dynamic chamber ($ET_{DC}$) were compared to $ET_P$ estimates from Equations (3-15). For each $ET_P$ calculation, a dimensionless crop coefficient (i.e. the ratio of actual ET to a potential or reference ET), $K_c$, in the following equation

$$\mathrm{ET_{DC}} = K_c \mathrm{ET_P} \tag{16}$$

was determined from a least-squares linear regression of daily results for each roof (Allen 2000).

For visualization of daily time series data, a quadratic Savitzky-Golay (S-G) filter, commonly used to eliminate noise in lysimeter studies (Vaughan and Ayars 2009, Peters *et al* 2014), was applied with a span of 11-days to more clearly illustrate ET trends. The S-G method uses local least squares polynomial approximation to filter measurement results.

## 3.4 Analysis and Results

### *3.4.1 Precipitation and Environmental Conditions*

Precipitation totals measured on W118 during July, August, and October (147, 116, and 125 mm) are similar to records from the NOAA Belvedere Castle weather station in Central Park, New York, NY between 1970 -2012 (Figure 11(a)). Growing season (April – October) precipitation totals during chamber deployment on USPS are less similar. In May 2012, May 2013, and June 2013, USPS received a particularly high amount of precipitation compared to the

historic average (180, 203, and 265 mm, respectively). In April and August 2013 USPS received limited precipitation (43 and 71 mm, respectively) compared to historic data. Snowfall events occurred during dynamic chamber deployment in December 2009, and between November 2012 and March 2013, as recorded by the NOAA Central Park, NY weather station. Average monthly temperatures were similar to historic data with exception of November 2009 (12.2 °C) and March 2012 (10.8 °C), which were considerably warmer compared to historic data (Figure 11(b)).

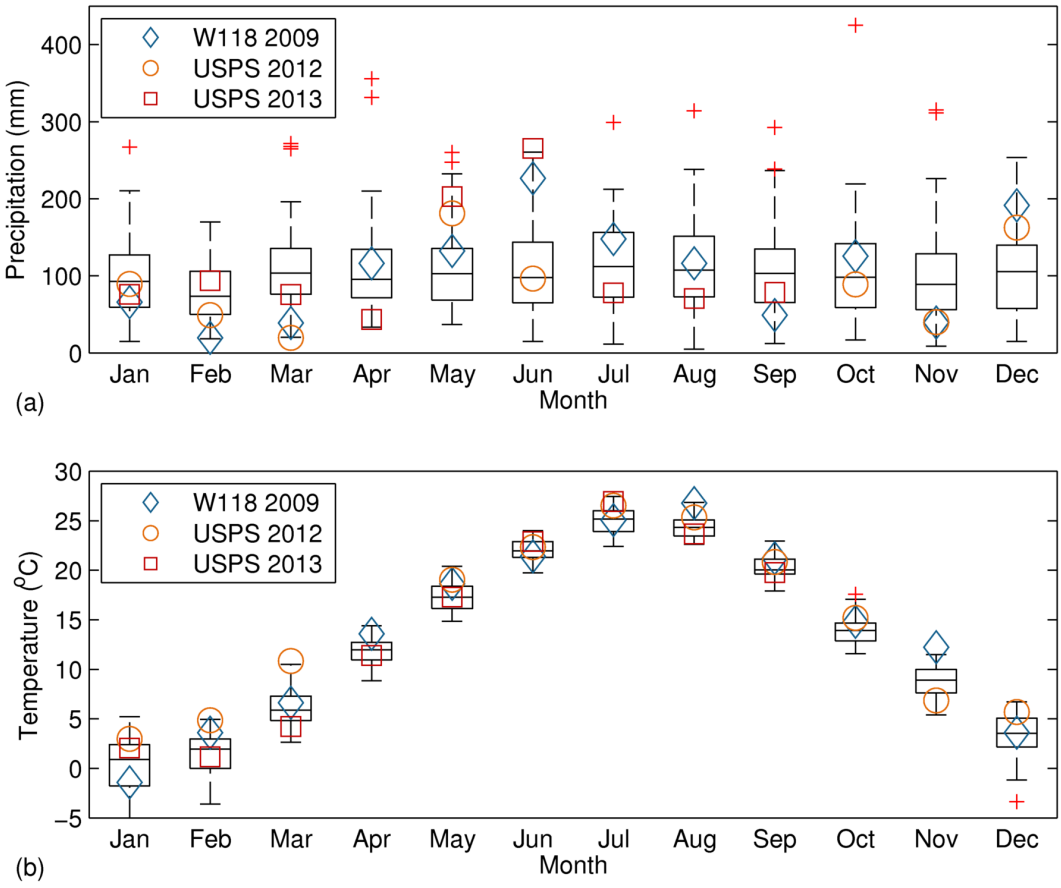


Figure 11: Monthly precipitation (a) and average temperature (b) from W118 in 2009, and USPS in 2012 and 2013 compared to box plots of historic data from 1970 – 2012. Rooftop data displayed for months with at least 24 days of measurements.

*3.4.2 Measured Evapotranspiration*

The two dynamic chamber deployments resulted in 12,000 hours of ET measurements. The seasonal variation in average ET flux was similar for W118 in 2009, USPS in 2012, and USPS in 2013 (Figure 12). Daily ET flux ranged from 0.022 to 6.94 mm $day^{-1}$ on W118 and 0.003 to 11.38 mm $day^{-1}$ on USPS. Average daily ET flux for the extent of the monitoring period was 1.55 mm $day^{-1}$ for W118 and 1.93 for USPS. As expected, the average daily ET flux between April 2013 and September 2013 on USPS was higher (3.15 mm $day^{-1}$) compared to October 2012 – March 2013 (0.22 mm $day^{-1}$), due to increased available energy for ET. A more detailed description of the dynamic chamber results is provided in Chapter 2.

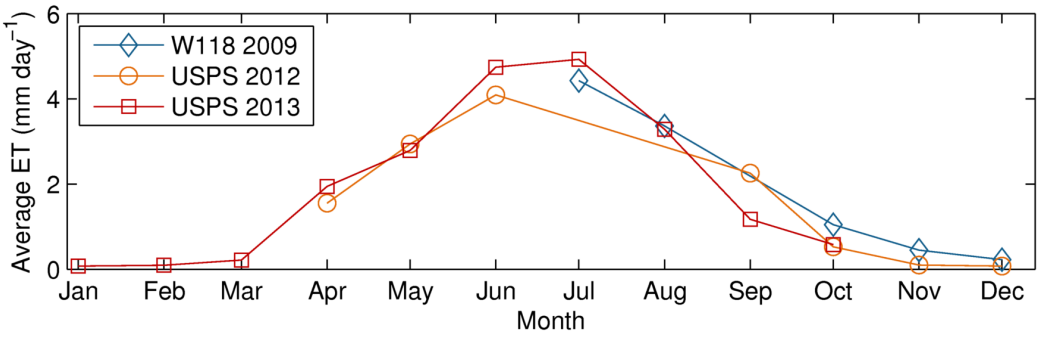


Figure 12: Monthly average ET from W118 in 2009, and USPS in 2012 and 2013 from dynamic chamber measurements.

*3.4.3 Potential Evapotranspiration Estimates*

Daily PET estimates were compared with $ET_{DC}$ measurements from the dynamic chamber (Table 3). Monitoring resulted in 472 days of concurrent PET and dynamic chamber data. As expected, PET equations show higher average ET values than the dynamic chamber, as they do not account water availability. The Priestley-Taylor equation resulted in the lowest root mean square errors (RMSE) between PET estimates and $ET_{DC}$ measurements on both W118 (0.49 mm $day^{-1}$) and

USPS (1.27 mm day$^{-1}$). Crop coefficients for the Priestley-Taylor and ASCE PM estimates are approximately one (0.98 - 1.02) for both roofs, while the Hargreaves and Penman equations result in lower crop coefficients (0.84 - 0.96). Inclusion of the crop coefficient only appreciably improved results of the Penman equation (RMSE for $K_c PET_P$ equal to 0.83 mm day$^{-1}$ for W118, and 1.42 mm day$^{-1}$ for USPS); however, the dynamic chamber results were still most correlated with Priestley-Taylor estimates.

Table 3: Average ET (mm day$^{-1}$), RMSE (mm day$^{-1}$), and crop coefficients of PET estimates compared to dynamic chamber results.

| ET Method | Average ET (mm day$^{-1}$) | | RMSE (mm day$^{-1}$) | | Crop Coefficient ($K_c$) | |
|---|---|---|---|---|---|---|
| | W118 | USPS | W118 | USPS | W118 | USPS |
| **Dynamic Chamber** | 1.55 | 1.93 | - | - | - | - |
| **Hargreaves** | 1.90 | 2.60 | 0.90 | 1.58 | 0.96 | 0.87 |
| **Priestley-Taylor** | 1.61 | 2.28 | 0.49 | 1.27 | 1.02 | 0.98 |
| **Penman** | 2.27 | 2.72 | 0.95 | 1.49 | 0.84 | 0.85 |
| **ASCE PM** | 1.91 | 2.27 | 0.81 | 1.38 | 0.98 | 1.02 |

Figure 13 displays S-G filtered daily PET and $ET_{DC}$ for W118 in 2009 and USPS between October 2012 and September 2013. Estimates from the PET equations generally follow similar trends. PET peaks in summer, with a maximum flux of 7.16 mm day$^{-1}$ on USPS on June 21, 2012 (from the Penman equation), and is lowest in the winter, with a minimum flux of 0.0048 mm day$^{-1}$ on USPS on December 10, 2012 (from the Penman equation). However, there are some particular differences in the behavior of PET estimates. In winter months, the addition of the advective term in the Penman and ASCE PM equations results in overestimation of ET compared to dynamic chamber and Priestley-Taylor fluxes. The empirical Hargreaves equation is generally comparable to the radiation based transfer equations (4-7), with the exception of a few periods where it overestimates PET (e.g. May 17 to May 27, 2013 on USPS).

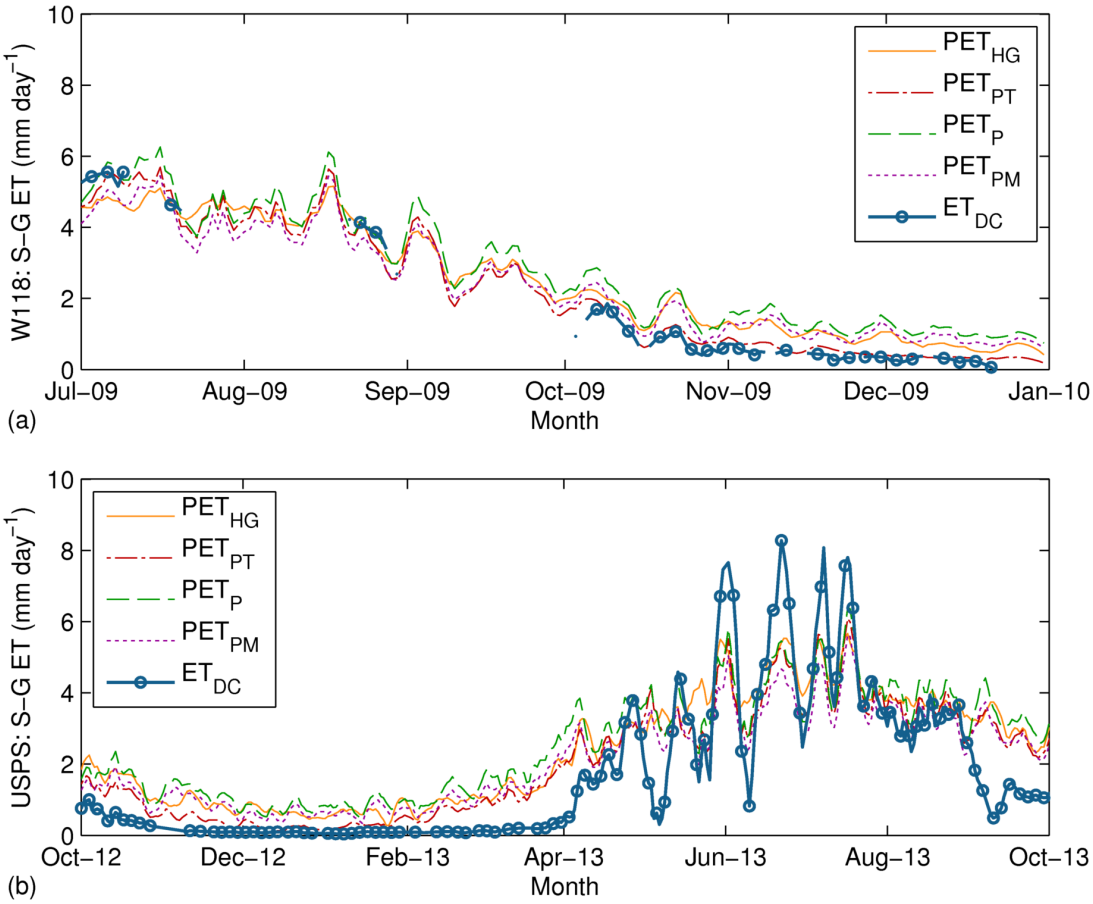


Figure 13: 11-day S-G filtered daily dynamic chamber ET ($ET_{DC}$) results from (a) W118 in 2009 and (b) USPS between October 2012 and September 2013 compared to PET estimates.

While PET patterns generally mimic those of the measured dynamic chamber ET, the PET equations tend to over-predict ET during drought and under-predict during periods of heavy precipitation. PET fluxes are considerably higher than dynamic chamber measurements in April, May, and September 2013. For each of these periods, limited precipitation was recorded in the preceding month, leading to limited substrate moisture and increased substrate surface resistance, and consequently reduced dynamic chamber ET. Conversely, the PET equations under predict the magnitude of ET throughout June and July 2013, where both antecedent precipitation and

available energy were elevated. This behavior is supported by the findings of Spronken-Smith *et al* (2000) and Jim and Peng (2012) who demonstrate the unique conditions of green spaces in urban environments can increase the actual ET in relation to estimated potential.

### *3.4.4 Actual Evapotranspiration Equations*

AET was calculated for each method and compared to dynamic chamber measurements (Table 4). The Priestley-Taylor equation was used to calculate PET for input in the storage model as it had the strongest correlation with dynamic chamber ET measurements and was used for the API and A-A models. As expected, all AET models show reduced ET compared to the Priestley-Taylor equation; however, only the API model shows an improvement in RMSE. Average ET estimates from the storage and the A-A model were lower than dynamic chamber results for both W118 and USPS. The API model resulted in the lowest root mean square errors (RMSE) between $ET_p$ (PET or AET) estimates and chamber ET measurements on both W118 (0.48 mm $day^{-1}$) and USPS (1.19 mm $day^{-1}$). Crop coefficients for the AET models all exceed one; however, coefficients for API model were near unity with $K_c$ values of 1.03 and 1.04 for W118 and USPS, respectively.

Table 4: Average ET (mm $day^{-1}$), RMSE (mm $day^{-1}$), and crop coefficients of AET estimates compared to dynamic chamber results during dynamic chamber deployment.

| ET Method | Average ET (mm $day^{-1}$) | | RMSE (mm $day^{-1}$) | | Crop Coefficient ($K_c$) | |
|---|---|---|---|---|---|---|
| | W118 | USPS | W118 | USPS | W118 | USPS |
| **Dynamic Chamber** | 1.55 | 1.93 | - | - | - | - |
| **Storage Model** | 0.97 | 1.66 | 1.50 | 1.62 | 1.45 | 1.28 |
| **API** | 1.59 | 2.17 | 0.48 | 1.19 | 1.03 | 1.04 |
| **Advection-Aridity** | 0.93 | 1.82 | 0.88 | 1.32 | 1.09 | 1.10 |

Figure 14 displays S-G filtered daily AET estimates and dynamic chamber measurements from W118 in 2009 and USPS between October 2012 and September 2013. The AET equations display dissimilar trends. The storage model shows proper ET reductions in the spring and fall; however, high fluxes in the summer result in a loss of moisture storage, and consequently a decline in subsequent AET. API results on W118 are very similar to Priestley-Taylor estimates. During chamber deployment on W118, precipitation was fairly regular (Figure 11(a)) and $\alpha$ hardly deviates from 1.26. Reductions in $\alpha$ mainly occur in cooler months where energy available for ET is minimal (minimum $\alpha = 0.89$ on November 30, 2009). The API estimates show more significant deviations from Priestley-Taylor results on USPS (minimum $\alpha = 0.41$ on May 8, 2013). Reduced values of $\alpha$ correspond with periods where precipitation in the preceding month was limited, including April, May, and September 2013. The A-A equation does not predict any of the reductions in ET corresponding with water-stressed conditions demonstrated by storage model, API method, or dynamic chamber results. However, on USPS, the A-A formulation of the transfer equations better reflects the seasonal variation of dynamic chamber ET.

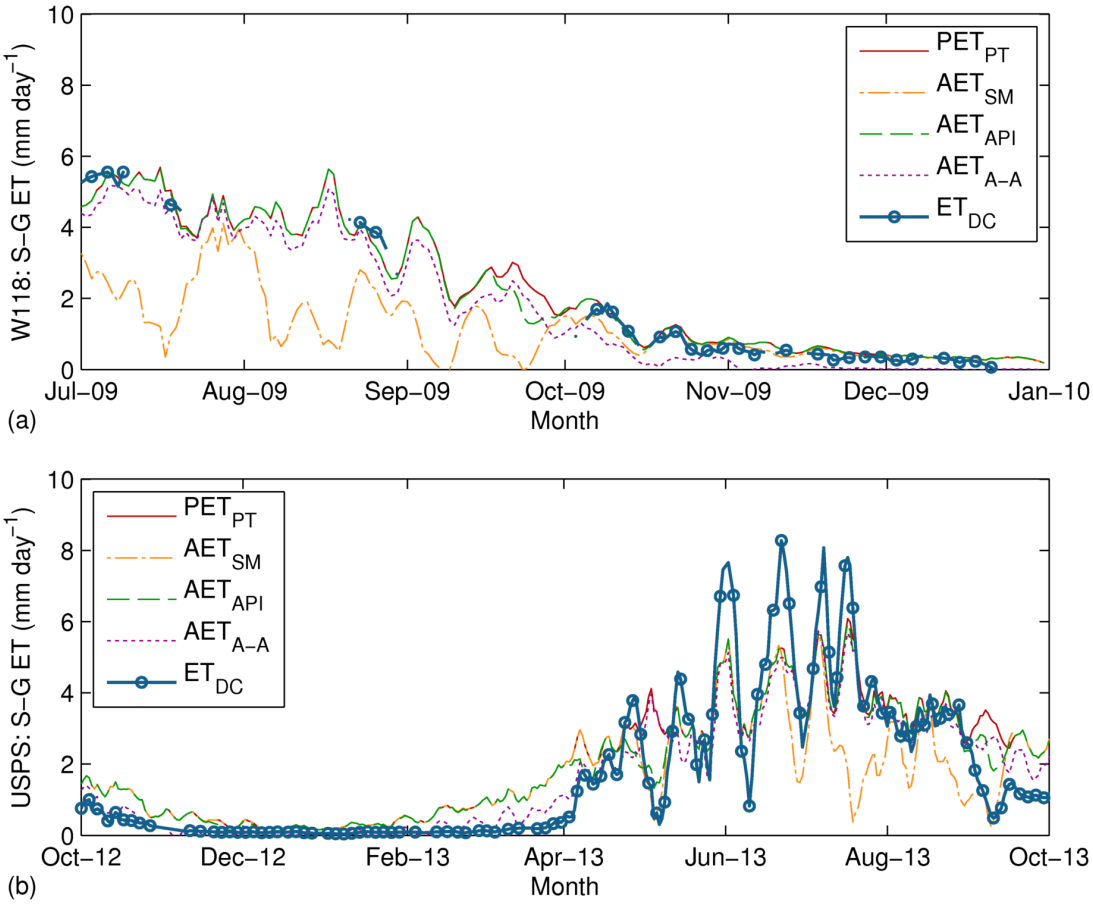


Figure 14: 11-day S-G filtered daily dynamic chamber ET ($ET_{DC}$) results from (a) W118 in 2009 and (b) USPS between October 2012 and September 2013 compared to AET estimates.

## 3.5 Discussion and concluding remarks

### *3.5.1 Evapotranspiration behavior*

The evaluation of four PET estimation equations calculated from on-site environmental data against ET measurements from a dynamic chamber system reveals that the Priestley-Taylor equation is most effective for predicting ET on the studied green roofs (RMSE = 0.49 on W118, 1.27 on USPS). Although there are variations in the magnitude of ET, fluctuations in PET estimates mimic those of the dynamic chamber measurements (Figure 13). While the crop

coefficients based on linear regression of Priestley-Taylor and dynamic chamber fluxes are approximately one ($K_C$ = 1.02 for W118, 0.98 for USPS), a systematic error is seen on USPS where the Priestley-Taylor equation over predicts ET at lower fluxes and under predicts ET at higher fluxes (Figure 15(a)). The PET equations overestimate ET in the winter on both rooftops, as the equations do not consider factors which limit winter PET, including decreased vegetation productivity, higher albedo of snow-covered surfaces (0.40 – 0.90), or increased ET resistance of frozen substrates (Allen *et al* 1998).

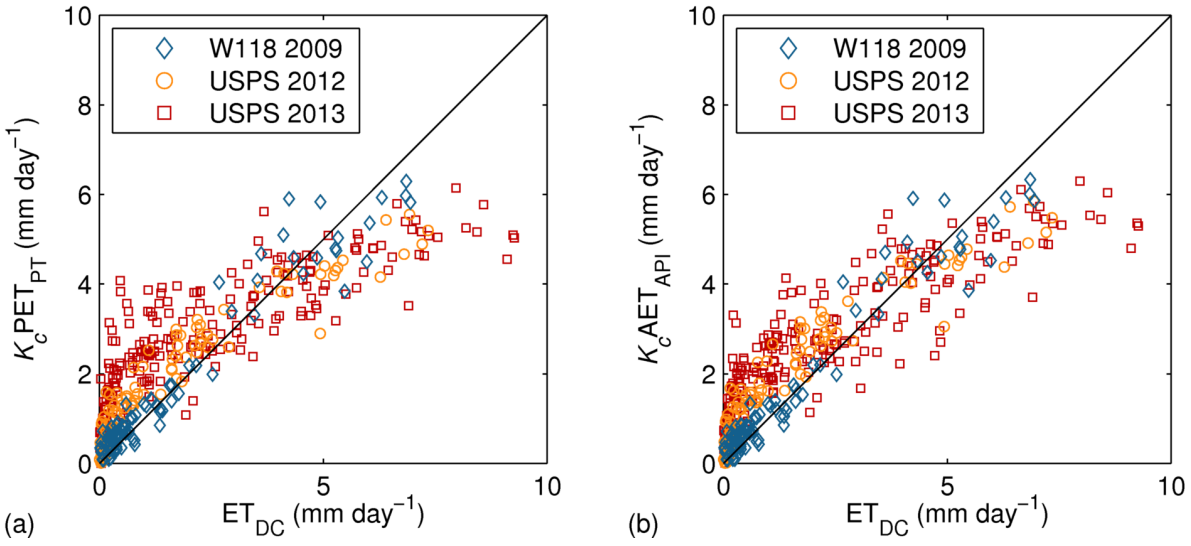


Figure 15: Scatter plot of dynamic chamber ET ($ET_{DC}$) results from W118 and USPS compared to (a) Priestley-Taylor ($PET_{PT}$) and (b) APT ($AET_{API}$) estimates, corrected with crop coefficients, $K_c$.

As expected, the PET equations over predict ET during periods of limited water availability, observed through precipitation data, predicted storage, and API calculations (Figure 13(b)). In June and July 2013 dynamic chamber ET measurements exceeded PET estimates, thought to be the result of elevated surface temperature and more frequent precipitation during this period. Maximum daily surface temperatures, measured by the dynamic chamber exceed maximum daily

air temperatures in the summer, resulting in increased energy availability for ET (Jim and Peng 2012). Application of the Hargreaves equation (Equation (3)) with surface temperature values shows maximum PET fluxes similar to dynamic chamber measurements in June and July 2013 (Figure 16). Additionally, frequent precipitation in May and June 2013 is believed to have enhanced *Sedum* productivity and transpiration, as well as replenish surface moisture, reducing surface resistance for evaporation (Allen *et al* 2005a).

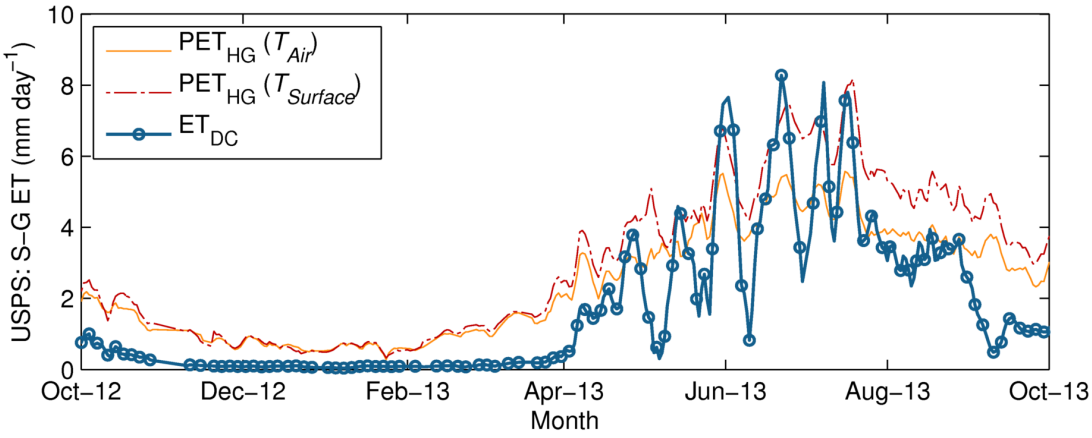


Figure 16: 11-day S-G filtered daily dynamic chamber ET ($ET_{DC}$) results from USPS in 2013 compared to Hargreaves estimates ($PET_{HG}$) based on air temperature ($T_{Air}$) and surface temperature ($T_{Surface}$).

Analysis of the storage, API, and A-A model reveals that only the API model improves the prediction of measured ET (RMSE = 0.48 on W118, 1.19 on USPS) compared to the Priestley-Taylor equation. The API model corrects many overestimations visible in Priestley-Taylor results (Figure 15(b)). For W118 in 2009 and USPS in 2012, precipitation was frequent enough that API AET estimates are nearly equal to Priestley-Taylor PET estimates. However, on USPS in May and September 2013, API AET results are comparatively lower, which corresponds to the behavior of measured ET. During drought periods, the day where the API coefficient, α, first decreases varies with respect to when dynamic chamber ET begins to deviate from PET;

however, the overall behavior is similar (Figure 14(b)). As expected, when a significant precipitation event occurs both the API and dynamic chamber fluxes return to potential.

The SMEF used in the storage model reduces PET in periods of dry weather, however the magnitude of these reductions is overestimated. The storage model does not account for processes that increase water availability, including, interception, vegetation storage, temporary detention, and ponding water or factors that alter ET fluxes, including the location of moisture in the substrate, non-potential environmental conditions, and transpiration. It is also important to note that reductions in dynamic chamber ET compared to PET estimates are delayed with respect to the storage model, which supports the idea that there is a range of storage depths where ET is still energy limited, and only when storage crosses that threshold, does AET decline in comparison to PET (Allen *et al* 2005a).

*3.5.2 Model Sensitivity*

The crop coefficients determined for the Priestley-Taylor, ASCE PM, and API models are between 0.98 and 1.04, indicating that calibration of these models based on the scalar crop coefficient, $K_c$, does not considerably improve the model. The remaining variance is sensitive to other conditions on the roof or the relationship between PET equation variables.

The storage model was shown to underestimate ET in summer months when ET fluxes were elevated. Increased ET fluxes deplete water storage and consequentially the coefficient $\beta$ used to predict AET in Equation (9) is reduced. Modification of Equation (8) for $\beta$ or specifying a storage depth threshold where ET becomes water-limited does not considerably improve the model, as higher PET values will deplete storage depth faster. As discussed by DiGiovanni *et al*

(2013), the model is sensitive to storage depth; however, increasing storage depth in this analysis results in ET overestimation during the water-limited period on USPS in May 2013.

The coefficients for the cubic α function (Equation (12)) and variables in the API formulation (Equation (13)) were analyzed to determine $AET_{API}$ sensitivity. The following variables were analyzed within the given ranges: (1) the decay coefficient, $K$ (0.80-0.95), (2) input antecedent precipitation days (5-50 days), (3) maximum daily precipitation input (5-104 mm), and (4) the maximum API for α calculation (5-50 mm), The standard API formulation results ($K_c AET_{API}$) along with two variations of the method are displayed in Figure 17. In the first modification ($AET_{API}$ – Fitted α), a cubic regression of α and $ET_{DC}$ $(K_c PET_{PT})^{-1}$ was performed to determine coefficients for Equation (12), where all $ET_{DC}$ $(K_c PET_{PT})^{-1}$ ratios associated with API greater than the maximum API (i.e. 20 mm) were set to unity. In the second model ($AET_{API}$ – Modified, Fitted α), in addition to regression of α, $K$ was set to 0.95, max API was set to 10 mm, and 15 antecedent precipitation days were used in the analysis. The modified API formulation showed increased significance between the API and $ET_{DC}$ $(K_c PET_{PT})^{-1}$ ($p = 2.8\times10^{-68}$), compared to the original API ($p = 7.4\times10^{-23}$). However, the analysis reveals that $AET_{API}$ results are particularly insensitive to these adjustments, with adjusted models having nominal effects on $AET_{API}$ behavior and RMSE (Figure 17).

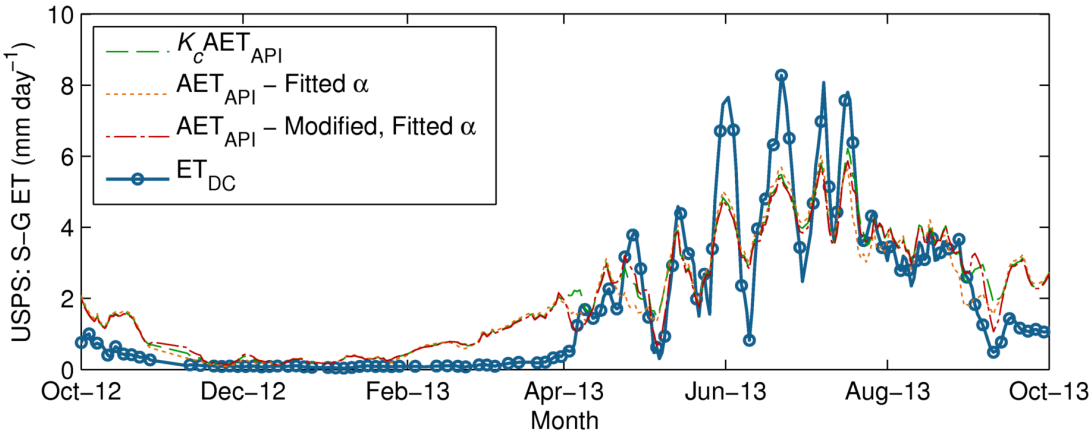


Figure 17: 11-day S-G filtered daily dynamic chamber ET ($ET_{DC}$) results from USPS in 2013 compared to the original API values ($AET_{API}$), an API model with modified α ($AET_{API}$ – Fitted α), and an API model with fitted α, *K* of 0.95, and a max API of 10, calculated from 15 antecedent precipitation days ($AET_{API}$ – Modified, Fitted α).

The A-A equation (15) can be considered a form of the Penman equation (5) with differing coefficients for the radiation and advective term. The major distinction between models is that for the A-A model, Brutsaert and Stricker (1979) assumed that advective term was negatively correlated with actual ET. Multi-variate linear regression of the separated terms of Equation (5) in the following form

$$\mathrm{ET_{DC}} = C(1)0.408\left[\frac{\Delta}{\Delta+\gamma}(R_n - G)\right] + C(2)\left[\frac{\gamma}{\Delta+\gamma}E_A\right] \qquad (17)$$

reveals coefficients of a similar form to the A-A model, with *C*(1) = 1.34 and *C*(2) = -0.09 on W118, and *C*(1) = 1.47 and *C*(2) = -0.50 on USPS. This approach improves correlation slightly (RMSE = 0.48 on W118, 1.26 on USPS) compared to the Priestley-Taylor equation with crop coefficient (RMSE = 0.49 on W118, 1.28 on USPS) and shows that a form of the A-A model may be useful for quantifying seasonal differences between potential and measured ET.

*3.5.3 Evapotranspiration behavior compared to other studies*

Studies of certain agricultural (Ali and Mawdsley 1987, Salvucci and Gentine 2013), natural (Kahler and Brutsaert 2006), and green roof (Sherrard and Jacobs 2012, Wadzuk *et al* 2013) sites show a systematic error where predictive algorithms overestimate lower ET fluxes and underestimate higher ET fluxes, as seen on USPS, especially in 2013. In many studies (Ali and Mawdsley 1987, Kahler and Brutsaert 2006, Sherrard and Jacobs 2012, Salvucci and Gentine 2013), a water availability algorithm was included, but did not account for this error.

Water limitations affect actual ET and alter PET estimates. Studies of green roof ET have reported that estimates from predictive equations are more correlated with measured ET during years with frequent precipitation (Lazzarin *et al* 2005, Wadzuk *et al* 2013) or when considering only non-water-limited days in the analysis (DiGiovanni *et al* 2013). In this study, W118 and USPS in 2012 (Figure 15(a)) more closely match Priestley-Taylor results than USPS in 2013, which received irregular precipitation.

*3.5.4 Application of ET models for green roof hydrologic and energy models*

ET estimation techniques are important for quantifying green roof benefits and supplementing green roof hydrologic and energy models. PET equations provide an acceptable prediction of overall ET behavior. The Priestley-Taylor equation showed the strongest correlation with measured ET on both W118 and USPS, with the crop coefficient, $K_c$, approximately equal to one. The PET equations overestimated ET in winter months on both roofs where limited plant productivity, snow reflectance, and the resistance of ET from frozen surfaces is thought to limit ET (Allen *et al* 1998). Advection estimates in the winter further increased Penman and ASCE PM estimates; however, empirical analysis of the Penman equation showed a negative

correlation between actual ET and advection, similar to the theory of the A-A model. Additionally, since the equations cannot account for water availability or non-potential conditions affecting PET estimates, correlation is reduced in during water-limited conditions.

The AET models attempt to account for differences between the apparent PET and AET. The API model proves to be a straightforward and practical method to account for water availability when calculating AET. Although the method is empirical, it is insensitive to changes to its formulation and unaffected by preceding ET fluxes, water storage, or site conditions. The method is able to predict AET during significant dry periods such as during May and September 2013, where AET is most limited. During normal precipitation conditions, such as most of the chamber deployment on W118, the $AET_{API}$ is simply equal to $PET_{PT}$. Although the storage model has a more physical basis than the other AET calculation procedures, it is highly sensitive to the rooftop water storage and environmental conditions that can affect ET. This behavior resulted in significant underestimations of ET during the summer, when ET fluxes were high and storage was depleted quickly. However, if a designer is only interested in estimating runoff for a precipitation event, a storage model may be sufficient, as seen by results from Berthier *et al* (2011) and Sherrard and Jacobs (2012).

# Chapter 4

## PEAK RAINFALL REDUCTION PERFORMANCE OF FOUR EXTENSIVE GREEN ROOFS IN NEW YORK CITY: HYDROLOGIC OBSERVATIONS AND ANALYSIS


### Abstract

Green roofs are an alternative to traditional impervious rooftops that aim to replicate the stormwater absorption properties of natural landscapes. A green roof temporarily detains stormwater, restricting flow into the sewer, and subsequently lessening the risk of flooding and sewerage overflows into local water bodies. In this study, event rainfall and runoff characteristics from 501 storm events recorded between June 2011 and April 2013 are analyzed to determine the peak rainfall rate reduction behavior of four extensive *Sedum* green roofs. The roofs studied include three systems with continuous vegetation, specifically two vegetated mat systems (termed W115 and W118) and a built-in-place system (termed USPS), in addition to a modular tray system (termed ConEd). Results show that event peak hourly runoff rate is correlated to event rainfall depth and peak rainfall rate. From monitored data, empirical models relating event peak runoff per unit area of monitored green roof to rainfall depth and peak rainfall were created. Individual roof models were developed to compare peak reduction behavior among roofs, defined as the ratio of event peak runoff rate per unit monitored rooftop area to peak rainfall, while a combined model for the three continuous systems was generated to predict average peak rainfall reduction. Application of roof-specific models to historic rainfall data from Central Park, NY shows that the ConEd modular tray system has the highest average peak rainfall reduction,

77%, compared to 70.8, 74.3, and 75.1% for W115, W118, and USPS, respectively. Although, unable to predict the variations between roofs, the combined model for the continuous systems (r-squared = 0.88) can be a valuable tool for designers to estimate green roof event peak rainfall reduction performance.

## 4.1 Introduction

Wet-weather triggered stormwater discharges are the predominant cause of non-point source pollution in urban areas (US EPA 2004). These discharges, which consist of stormwater runoff, combined sewer overflow (CSO), and sanitary sewer overflow (SSO), occur when sewer system or wastewater treatment plant (WWTP) capacity is exceeded, leading to urban flooding and water body impairment (Berghage *et al* 2009). In New York City (NYC) most wastewater treatment plants are designed to treat twice the dry weather sewer flow (NYC DEP 2010). However, this capacity is often exceeded, resulting in CSOs during storm events with as little as 3 mm of rainfall in 1 hour (Montalto *et al* 2007). The relationship between precipitation and CSO discharge is not universal, and depends on many factors, including rainfall, catchment, and sewer system characteristics (Mayor's Office of Long-Term Planning and Sustainability 2008).

To mitigate CSO discharges, many governments and municipalities in the United States and abroad have implemented policies and stormwater control measures (SCMs) to detain water onsite (Fassman-Beck *et al* 2013). One increasingly popular, low cost, and effective SCM is low impact development (LID), also referred to as "green stormwater infrastructure". For LID, micro-scale engineered systems are designed to replicate pre-development hydrology in the urban environment, in order to attenuate stormwater runoff (Coffman 2000). LID techniques can be implemented incrementally with limited modification to existing infrastructure, making them

ideal for urban areas (NYC DEP 2010). The temporary storage of stormwater on-site by LID reduces the flow rate into sewer systems, allowing extended time for delivery and treatment, and thereby lessening the chance of both flooding and sewer overflow (Mayor's Office of Long-Term Planning and Sustainability 2008).

Vegetated roofs, or green roofs, are a type of LID alternative to traditional impervious rooftops that have the capability to both retain and detain stormwater (Carson *et al* 2013). Green roofs are engineered systems comprising of vegetation, substrate, and drainage layers placed on a roof's waterproof membrane. Lightweight, low cost, and low maintenance types of green roofs, referred to as extensive systems, can be implemented on many existing structures without modification. The extensive roof consists of engineered lightweight substrate layer, typically less than 150 mm deep, cultivated with shallow rooted and drought tolerant plants such as *Sedum* (Berndtsson 2010). At present, the three major categories of extensive green roofs are the vegetated mat, built-in-place, and modular tray systems (Oberndorfer *et al* 2007). The vegetated mat and built-in-place systems both consist of continuous substrate layers and drainage courses, but differ in installation method. The vegetated mat system is assembled and planted offsite, while the built-in-place layers are placed on the roof individually. The modular tray differs in that the substrate is contained in plastic trays, which are then placed on the rooftop membrane.

To understand rainfall detention behavior, it is important to understand how water is stored and transported within a green roof. At the start of a storm event, plants capture a portion of rainfall on vegetated areas. After the initial abstractions, water then begins to saturate the substrate or infiltrate and flow towards the drainage layer. The rainfall rate attenuation performance of the vegetated portion of the green roof will be stronger during this time, as both permanent and

temporary storage, as well as suction forces, reduce the flow rate on the roof (Bliss *et al* 2009). Any moisture present at the start of the event will reduce the rainfall volume required to saturate the substrate (Berndtsson 2010). When the substrate becomes fully saturated, the flow through the media is limited by the hydraulic conductivity and excess water accumulates on the surface (She and Pang 2010).

Saturated substrates will continue to drain until the field capacity is reached (Berndtsson 2010). On the continuous systems, water can enter the drainage course from any part of the substrate. However, on the modular ConEd roof, water must exit the substrate through holes on the underside of each tray (Carson *et al* 2013). Once water enters the drainage layer, it will flow horizontally towards the drain, this flow can be affected by drainage layer construction, as well as rooftop configuration (Berghage *et al* 2009).

The behavior of rainfall that lands on non-vegetated areas, required for rooftop access and maintenance, varies from the behavior of vegetated portions. A small quantity of the rainfall on non-vegetated areas is held through depression storage; however, the majority of water will flow towards the drain (Carson *et al* 2013). The reduction in flow rate is dependent on construction (e.g. gravel or asphalt) and configuration (e.g. flow path lengths and interaction with vegetated portions of roof).

To date, much emphasis has been placed on understanding stormwater volume retention performance of extensive green roofs (Mentens *et al* 2006, Spolek 2008, Berndtsson 2010, Gregoire and Clausen 2011, Stovin *et al* 2012, Carson *et al* 2013, Fassman-Beck *et al* 2013), with less focus on the factors influencing green roof detention. The attenuation of peak rainfall rate by a green roof is highly variable and does not depend solely on substrate properties and

peak rainfall rate. Green roof peak runoff rate is a function of antecedent rainfall, vegetation and drainage configuration, as well as other environmental, site, and moisture conditions (Bliss *et al* 2009, Berndtsson 2010). A number of studies, both in the United States and abroad, have reported the peak rainfall rate reduction on green roofs (Bliss *et al* 2009, Fassman-Beck *et al* 2013, Hutchinson *et al* 2003, Berghage *et al* 2009, Moran *et al* 2005, Kurtz 2008, Carpenter and Kaluvakolanu 2011). However, attempts to model reduction have either resulted in limited correlation (Stovin *et al* 2012), applicability to only a handful of storms, or complex models requiring input of initial runoff delay, total runoff depth, or other variables considered difficult to quantify (Villarreal and Bengtsson 2005, Villarreal 2007).

This study aims to advance understanding of the factors controlling green roof stormwater detention by quantifying, analyzing, and modeling green roof peak stormwater reduction from for three extensive systems with continuous vegetation as well as one modular tray system, all located in New York City. Environmental data gathered from the roofs between June 2011 and April 2013 are used to summarize green roof stormwater detention performance, analyze factors affecting detention behavior, and develop a model to predict peak hourly runoff rate from continuous and modular green roof systems.

## 4.2 Summary of previous green roof detention studies

While stormwater volume retention has been widely studied as a green roof hydrologic performance metric (Mentens *et al* 2006, Spolek 2008, Berndtsson 2010, Gregoire and Clausen 2011, Stovin *et al* 2012, Carson *et al* 2013, Fassman-Beck *et al* 2013), green roof capacity to reduce the peak rate of stormwater runoff is significantly less documented. Studies have been performed on full-scale roofs; however, many studies were performed on small, 0.37 to 12 $m^2$,

pilot-scale roofs or elevated test boxes (Carson *et al* 2013). As opposed to full-scale roofs, pilot-scale roofs and test boxes generally do not include non-vegetated regions and have significantly shorter flow path lengths. Most often, studies report this hydrologic performance metric as the reduction in peak rainfall rate for a given storm event, as defined by the ratio of event peak runoff rate per unit monitored rooftop area to peak rainfall. However, many studies report green roof reduction in of event peak runoff rate per unit monitored rooftop area to measurements from an asphalt control rooftop. Moran *et al* (2005) observed an average 5-minute peak rainfall rate reduction of 87 and 57% for two full-scale green roof systems in North Carolina, respectively. Carpenter and Kaluvakolanu (2011) measured runoff at 5-minute intervals on full-scale green, stone, and asphalt roofs. Average peak flow reduction compared to the asphalt roof for the green and stone roofs for this study were 89 and 69%, respectively. Berghage *et al* (2009) measured runoff at 5-minute intervals on pilot-scale green and asphalt rooftops in University Park, PA. Results showed an 88% maximum (44% average) peak 5-min rainfall rate reduction for storms greater than 0.5 in (12.7 mm) for the green roof, compared to a maximum of 50% (4% average) for the asphalt control roof. Bliss *et al* (2009) recorded runoff every second from a green roof test-box, as well as a control roof in Pittsburgh, PA. Reported green roof peak runoff rate reduction compared to the control roof ranged from 5 to 70%. In addition, results from the Bliss *et al* (2009) study showed that as storms progressed and the substrate saturation increased, green roof peak runoff reduction compared to the control roof diminished.

Fassman-Beck *et al* (2013) analyzed peak rainfall rate reduction on 2 full-scale roofs and 4 pilot-scale roofs. Monitored results demonstrate that the 2 full-scale roofs were more effective at reducing peak rainfall rate, with median reductions of 90 and 84%, respectively. The pilot-scale

roofs, while showing reduced performance compared to the full-scale system, revealed that deeper substrates can more effectively dampen peak runoff flow, with median reduction of 74% for the 150 mm thick substrate compared to 62% for the 100 mm thick substrate.

Stovin *et al* (2012) provided a thorough analysis of peak 5-minute runoff rate from an extensive green roof test box located in Sheffield, UK. A 5-minute peak rainfall rate reduction of 20-100% (average 59.22%) was observed for 21 storms between 8.8-99.6 mm in depth. A regression analysis was performed to relate peak runoff rate to storm and weather characteristics, resulting in a final model based on event rainfall duration. However, the peak runoff rate model showed poor predictive performance (r-squared = 0.478).

Villareal and Bengtsson (2005) analyzed 1-minute rainfall data collected on an extensive green roof test box for 4 simulated rainfall events repeated with the test box at 2°, 5°, and 8° slopes. Their data indicate that while roof slope can influence overall retention, it does not affect the shape of the hydrograph or the peak rainfall rate reduction. Results from a unit hydrograph model (Singh 1976) demonstrate that the model can accurately simulate the runoff response and peak rainfall rate for the series of events in this study; however, the model creation requires input of accumulated rainfall before the onset of runoff and total runoff depth in addition to rainfall data.

Models to predict peak runoff rate have been applied to larger watersheds and show varying levels of success (Jones and Grant 1996, Tasker and Stedinger 1989). However, there are differences between the functions of green roofs, compared to larger watersheds. Loague and Freeze (1985) employed a regression model, a unit hydrograph model, and a physically based model to predict event based runoff in three U.S. catchment basins. The unit hydrograph method

assumed a constant infiltration rate, which is not appropriate for modeling green roof hydrology. Results from the regression show that the 2-min peak rainfall rate was not able to accurately predict peak runoff rate. For prediction of event depth and time of peak, regression analysis showed similar or improved predictive performance compared to more data intensive, physically based models.

## 4.3 Monitoring Sites and Systems

### *4.3.1 Site Descriptions*

Four extensive *Sedum* green rooftops were monitored for this study. For roofs with multiple drains (W118, USPS, and ConEd) a watershed typical of the roof configuration was chosen for environmental monitoring. A summary of the rooftop sites is provided in Table 5. Further description of the monitored green roofs is provided in Appendix A.

Table 5: Monitored green roof site and storm event characteristics

| **Roof Name** | | **W115** | **W118** | **USPS** | **ConEd** |
|---|---|---|---|---|---|
| System Type | | Vegetated mat | Vegetated mat | Built-in-place | Modular Tray |
| Drainage Layer | | Drainage Course | Drainage Course | Drainage Course | Corrugated Plastic |
| Year Built | | 2007 | 2007 | 2009 | 2008 |
| Roof Area ($m^2$) | | 99 | 600 | 10,000 | 2,700 |
| Substrate Depth (mm) | | 32 | 32 | 100-200 | 100 |
| Monitored Watershed | Area ($m^2$) | 99 | 310 | 390 | 940 |
| | % Vegetated | 58 | 53 | 67 | 52 |
| Monitoring | Start | 11-Jul | 11-Jun | 11-Jun | 11-Jul |
| | End | 12-Oct | 13-Apr | 13-Mar | 13-Apr |
| # Events | Total | 130 | 161 | 199 | 141 |
| | Suitable | 103 | 128 | 170 | 100 |

The Columbia University owned 635 West 115$^{th}$ Street (W115) and 423 West 118th Street (W118) buildings in Manhattan, NY were retrofitted with a *Sedum* vegetated mat, specifically

the Xero Flor America's XF301+2FL green roof system. This system consists of a 32 mm thick pre-vegetated mat, layered above two 6 mm thick water retention fleeces developed from recycled synthetic fibers, a 19 mm non-woven polymer drainage mat, and a 0.5 mm polyethylene root barrier. The roof substrate has a water-saturated density of 1.37 g $cm^{-3}$, water storage capacity of 37.1%, and a saturated hydraulic conductivity of 0.021 cm $s^{-1}$, as measured by Hummel and Co. Inc. in April 2007. Gravel borders, angled parapets, and bare roof comprise the non-vegetated areas on these rooftops.

The US Post Office Morgan Processing and Distribution Center green roof (USPS) in Manhattan, NY was installed by TectaGreen of Tecta America. The roof was built-in-place by installing drainage layers and substrate in areas bounded by metal brackets. Most of the vegetated area consists of 100 mm of substrate and was planted with various *Sedum* types, however a selection of 200mm thick, 2 m wide berms created on the roof have different plant species. The substrate has a water-saturated density between 1.15-1.35 g $cm^{-3}$, water storage capacity between 35-65%, and a saturated hydraulic conductivity between 0.001-0.120 cm $s^{-1}$, as measured by Skyland USA LLC in March 2011. Non-vegetated areas in the monitored watershed consist of gravel ballast.

The ConEdison Learning Center (ConEd) green roof in Queens, NY consists of 61 cm × 122 cm × 10 cm GreenGrid-G2 modular trays. Trays were packed with substrate and placed in adjacent rows on the roof. 15 *Sedum* varieties were established on the roof with plugs and cuttings. The substrate has a water-saturated density of 1.18 g $cm^{-3}$, water storage capacity of 31.8%, and a saturated hydraulic conductivity of 0.326 cm $s^{-1}$, as measured by Penn State University's

Agricultural Analytical Services Laboratory in July 2008. The non-vegetated portions of this roof consist of rubber mat walkways, gravel ballast borders, and raised skylights.

*4.3.2 Instrumentation*

An Onset Hobo U30 weather station was installed on each green roof to record rainfall, runoff, and environmental conditions in the monitored watershed. An Onset tipping bucket rain gauge measured rainfall and a custom designed flow meter measured runoff. The Onset tipping bucket is accurate to ± 1.0% at up to 20 mm $h^{-1}$ and temperatures between 0 and 50 °C.

The runoff flow meters consist of a runoff chamber with an outlet weir and a Senix TSPC-30S1 ultrasonic distance sensor. The distance sensor measures the depth of water behind the weir face with a resolution of 0.086 mm. As flow increases, the distance sensor detects the rise in water height behind the weir face and adjusts its output voltage. The flow meters were designed to fit into existing rooftop drains and accommodate roughly 50 mm $hr^{-1}$ of rainfall in saturated substrate conditions based on watershed area. Above this flow rate, water overflows into the roof drain to prevent backup and ponding of water on the roofs. The flow meters function between 0 and 70 °C. Each flow meter was calibrated at flow rates up to maximum capacity in a chamber designed to mimic water flow conditions in roof drains. Once calibrated, weirs were installed in rooftop drains and connected to the logger for data recording. Further description of flow meter design, construction, and calibration is provided in Appendix B.

Flow meter voltage readings were sampled every second. Five minute rainfall totals and five minute flow meter averages were recorded by the data logger and wirelessly uploaded the to the Onset Hobolink data service. Continuous data were collected at all rooftop sites from June 2011 to April 2013, except during several intermittent offline periods due to hurricane safety

measures, power loss, or equipment failure. Data were imported into MATLAB and the unique calibration equation for each flow meter was then applied to the voltage records. Flow rates were normalized by the monitored watershed area to calculate runoff depth per unit time at each interval. Further data manipulation, analysis, visualization, and statistics were performed with the MATLAB software package and Statistics Toolbox.

## 4.4 Results

### *4.4.1 Determination of storm events and characteristics*

A modified version of the National Oceanic and Atmospheric Administration (NOAA) definition of a 6-hour "no rainfall" period required to separate storm events was used in this analysis. An event begins when rainfall is first recorded and ends when no rainfall or runoff has been observed for six hours. Once individual events were determined in this manner, events considered unsuitable for analyses were removed based on the following four exclusion criteria: (1) peak runoff rate exceeded 90% of the flow meter's voltage output range, as turbulence at flows above this rate distort depth readings (36 Events); (2) rainfall or runoff measurements resulted from snowfall, since the time scale of snowmelt prevents reliable event separation (29 Events); (3) total event runoff was in excess of rainfall, the result of partial blockage of the flow meter outlet weir by debris and sediment (40 Events); and (4) sensor errors, due to power loss or equipment failure (25 Events). Following data removal based on the discussed exclusion criteria, 501 storm events from 631-recorded events across all monitored roofs were used for analysis (Table 5). From this point forward, all discussion and analysis of monitored storm events is limited to the 501 suitable events.

In order to analyze green roof detention performance, a series of event rainfall and runoff characteristics were determined. For this study, the most important event rainfall and runoff characteristics and their abbreviated names are described in Table 6. To determine maximum hourly peak rain and peak runoff; at each five-minute measurement interval, rainfall and runoff depth over the following hour were summed. The peak hourly rainfall and runoff were defined as the maximum of these values. The 1-hour duration for peak rain was used for analysis due to the availability of hourly historic rainfall data in New York City (Central Park, NY). Unless otherwise specified, all discussion of peak rain or peak runoff refers to the maximum event 1-hr peak rates. All other statistics are based on 5-minute data collected during each storm event.

Table 6: Event rainfall, runoff (normalized by area), and reduction characteristics for analysis

| Characteristic | | Unit | Description |
|---|---|---|---|
| Rainfall | Rain Depth | mm | Total event rainfall depth |
| | Peak Rain | mm $hr^{-1}$ | Peak hourly rainfall rate |
| | 5-min Peak Rain | mm $min^{-1}$ | Peak 5-minute rainfall rate |
| | Time to Peak | min | Time between event start and Peak Rain |
| | Rain Depth to Peak | mm | Rainfall depth before Peak Rain |
| | Rain Duration | hr | Time between initial and final event rainfall records |
| | Average Rain | mm $hr^{-1}$ | Average rainfall rate (Rain Depth/Rain Duration) |
| Runoff | Runoff Depth | mm | Total event runoff depth |
| | Peak Runoff | mm $hr^{-1}$ | Peak hourly runoff rate |
| | 5-min Peak Runoff | mm $min^{-1}$ | Peak 5-minute runoff rate |
| | Runoff Delay | min | Time from event start to initial runoff |
| | Rain Depth to Runoff | mm | Rain Depth before initial runoff |
| | Runoff Duration | hr | Time between initial and final event runoff records |
| | Average Runoff | mm $hr^{-1}$ | Average runoff rate (Runoff Depth/Runoff Duration) |
| Reduction | Peak Reduction | % | (1- (Peak Runoff/Peak Rain))×100 |
| | 5-min Peak Reduction | % | (1- (5-min Peak Runoff/5-min Peak Rain))×100 |
| | Average Rate Reduction | % | (1- (Average Runoff/Average Rain))×100 |

*4.4.2 Rainfall peak analysis and distribution*

In order to compare monitored peaks to historic data, hourly precipitation data recorded at the Belvedere Castle weather station in Central Park, NY were downloaded from the NOAA National Climatic Data Center website (ncdc.noaa.gov) for the years 1971-2010. Events were separated based on the NOAA standard 6-hour dry weather period. Peak rain and rain depth were determined for each of the 4,291 precipitation events from the 40-year historic period. As actual 1-hour peak rainfall rates do not necessarily occur at clock-hour intervals; in order to correct for differences between clock-hour and 1-hour values, the National Weather Service correction factor, 1.13, was applied to event hourly peak rainfall rates from historic data for events longer than 1 hour (Hershfield 1963, Fredrick *et al* 1977).

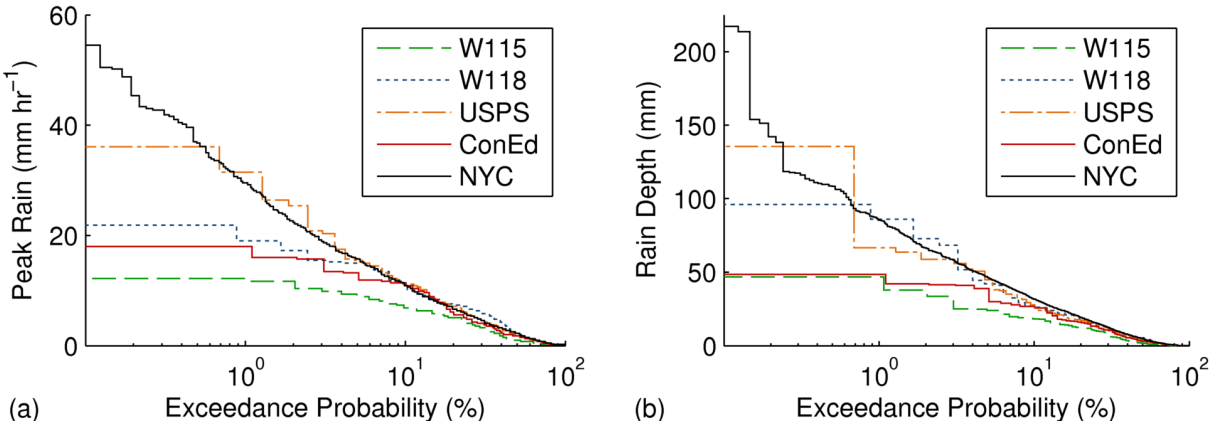


Figure 18: (a) Peak rain and (b) rain depth frequency analysis of monitored events compared to historic data (Central Park, NY 1971-2010). Exceedance probabilities from 0.1-100% displayed. Exceedance probability is defined as the probability that a single storm event will have a peak rain rate or rain depth above the corresponding value.

Figure 18 displays the exceedance probability of monitored 1-hour event peak rainfall rate and event rainfall depth compared to historic events. Exceedance probability is defined as the probability that a given storm event will have a peak rain rate or rain depth above the

corresponding value. For smaller event peak rain rates, with an exceedance probability greater than 10%, W118, USPS, and ConEd events have a similar frequency distribution to historic data (Figure 18(a)), with events on W118 showing slightly higher peak rainfall rates. Below 10% exceedance probability, peak rain rates are lower for W118 and ConEd, while USPS maintains a similar distribution to historic data. Monitored events on W115 have smaller peaks than the other roofs, as well as the historic data as a result of shading by adjacent buildings. The maximum monitored peak rain rate is 14.5 mm $hr^{-1}$ for W115, 24.1 mm $hr^{-1}$ for W118, 38.6 mm $hr^{-1}$ for USPS, and 21.1 mm $hr^{-1}$ for ConEd, compared to 49.5 mm $hr^{-1}$ for the historic data. Rain depth distributions vary similarly (Figure 18(b)), with W118, USPS, and ConEd showing differences below 10% exceedance probability compared to historic data. The maximum monitored event rain depth is 61.7 mm for W115, 180.3 mm for W118, 162.8 mm for USPS, and 74.7 mm for ConEd, compared to 233.4 mm for the historic data. Reduced frequency of events with large rain depth on ConEd is the result of removal of certain large events due to overflows and sensor malfunctions, as discussed in section 4.4.1.

*4.4.3 Peak rainfall rate and rainfall depth cumulative probabilities*

In order to evaluate and compare extensive green roof performance based on event magnitude and frequency, storm events were classified by cumulative probability (the complement of exceedance probability) and probability intervals for rain depth and peak rain based on the distribution of historic data. Cumulative probability describes the likelihood that peak rain or rain depth will be less than the specified values. Probability intervals categorize storms within the bounds of two specified cumulative probabilities. Due to limited data corresponding to higher cumulative probabilities from the historic data, cumulative probabilities and probability intervals

were restricted to events below 99 and 95% cumulative probability, respectively. The cumulative probabilities of 90, 95, and 99%, together with probability intervals of 0-25%, 25-50%, 50-75%, and 75-95%, were used to evaluate each green roof's peak reduction performance. Cumulative probabilities and probability intervals were assigned to each event based on rain depth or peak rain, whichever had a greater cumulative probability (Table 7).

Table 7: Rain depth and peak rain values associated with cumulative probability.

| Event Characteristic | Cumulative Probability (%) | | | | | |
|---|---|---|---|---|---|---|
| | 25 | 50 | 75 | 90 | 95 | 99 |
| Rain Depth (mm) | 1.02 | 4.83 | 15.49 | 31.75 | 46.23 | 83.57 |
| Peak Rain (mm $hr^{-1}$) | 0.76 | 2.30 | 5.45 | 10.91 | 15.75 | 28.70 |

*4.4.4 Runoff detention statistics*

Analysis of variance (ANOVA) (Hogg and Ledolter 1987) of peak and average runoff rates shows distributions from all roofs were significantly lower than corresponding rainfall rates ($p < 0.05$). To compare roofs, performance characteristics were calculated from rainfall and runoff properties. Table 8 displays average rainfall detention statistics for each roof. Zero runoff events represents the percent of events with 100% retention. Rate reductions are defined in Table 6.

Table 8: Green roof average rainfall detention statistics.

| Roof Name | | W115 | W118 | USPS | ConEd |
|---|---|---|---|---|---|
| Zero Runoff Events (%) | | 32.0 | 38.3 | 45.3 | 20.0 |
| All events | 1-hr Peak Reduction (%) | 83.0 | 81.7 | 85.3 | 82.3 |
| | 5-min Peak Reduction (%) | 87.7 | 88.2 | 91.7 | 88.2 |
| | Avg. Rate Reduction (%) | 86.6 | 86.4 | 90.2 | 85.6 |
| Non-zero runoff events | 1-hr Peak Reduction (%) | 75.0 | 70.3 | 73.1 | 77.8 |
| | 5-min Peak Reduction (%) | 81.9 | 80.9 | 84.8 | 85.2 |
| | Average Rate Reduction (%) | 80.3 | 78.0 | 82.1 | 81.9 |
| | Runoff Delay (min) | 44.9 | 96.3 | 125.0 | 57.8 |
| | Rain Depth to Runoff (mm) | 1.28 | 4.02 | 3.85 | 1.57 |

USPS was able to fully retain the highest percent of events, 45.3 %, compared to ConEd, which was only able to fully retain 20.0 % of events. ConEd showed the strongest 1-hr peak rain rate reduction of 77.8 %, compared to W115, W118, and USPS when only considering events with non-zero runoff. USPS had the longest average runoff delay (125 minutes) from the start of event rainfall. Values for runoff delay and rain depth to runoff were highly variable, with an average standard deviation across roofs of 121 min and 1.95 mm, respectively. Considering all events, USPS showed the highest overall reductions in peak and average rainfall rates. Events with peak hourly rain rate greater than or equal to 3 mm $hr^{-1}$ (cumulative probability = 42%), stated by Montalto *et al* (2007) to cause CSO events in NYC had 1-hr peak rain rate reductions of 62.0, 68.2, 68.2, and 65.9 % for W115, W118, USPS, and ConEd, respectively.

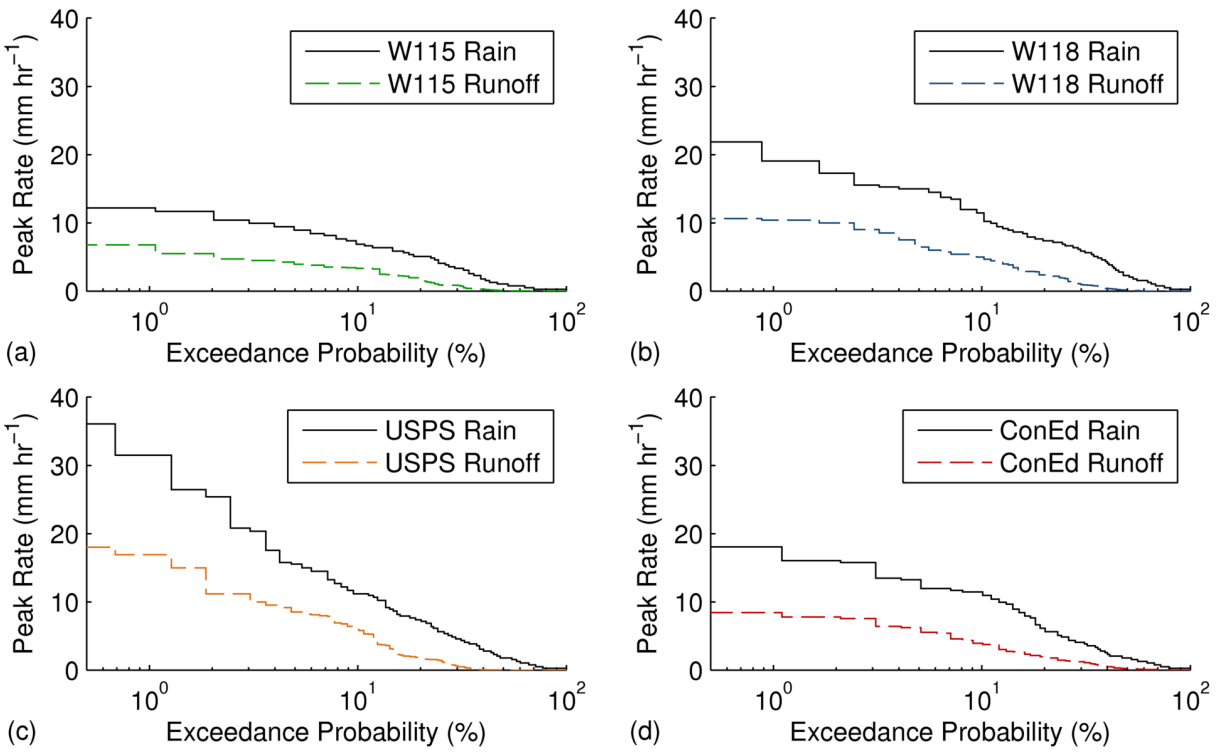


Figure 19: Peak 1-hour rainfall and runoff rate probability of monitored events for (a) W115, (b) W118, (c) USPS, and (d) ConEd. Exceedance probabilities from 0.5-100% displayed.

Exceedance probabilities of peak rain and peak runoff for each roof were analyzed (Figure 19) to compare distributions, normalizing data for variations in site, climate, and rainfall characteristics that affect peak reduction performance. While this analysis cannot be used to forecast performance for individual events, it provides basic understanding of expected flows. Results from the frequency analysis show that, for all roofs, percent difference in peak rain and runoff rates decreases with exceedance probability. Maximum peak runoff rates for the monitored data were 8.3, 17.4, 18.0, and 9.9 mm $hr^{-1}$ for W115, W118, USPS, and ConEd, respectively.

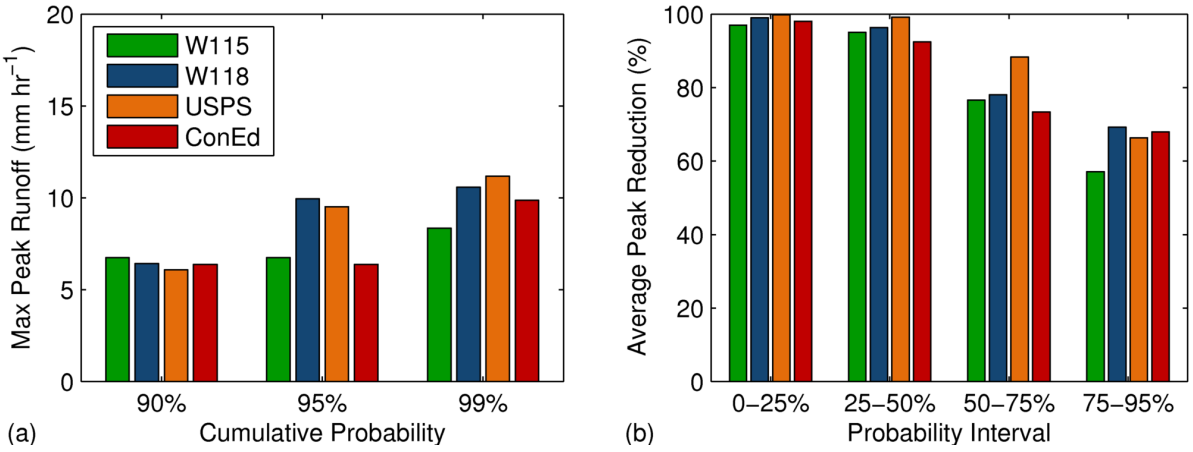


Figure 20: Frequency analysis of peak rain and rain depth from analysis of all historic NYC events (Central Park, 1971-2010); (a) observed maximum peak runoff rate (mm $hr^{-1}$) within 90, 95, and 99% cumulative probabilities, and (b) observed average peak reduction (%) within 0-25, 25-50, 50-75, and 75-95% probability intervals.

To evaluate trends in peak runoff rate and peak reduction, observed events were assigned cumulative probabilities based on the methodology described in section 4.4.3. Figure 20(a) shows the maximum-recorded peak runoff rate (mm $hr^{-1}$) at events within 90, 95, 99% cumulative probabilities. USPS shows the lowest maximum peak runoff rate, 6.1 mm $hr^{-1}$, for 90% of events; however, maximums above 90% cumulative probability are heavily influenced by variance in the size of large storms monitored on each roof. W118 and USPS, where larger

events were recorded, show higher maximum peak runoff rates, 10.6 and 11.2 mm $hr^{-1}$, respectively for events within 99% cumulative probability.

Peak reduction performance decreases with cumulative probability (Figure 20 (b)). USPS shows the highest average peak reduction (96%) for the smaller 75% of events. However, W118 shows highest average peak reduction (69%) for events between 75 and 95% cumulative probabilities.

*4.4.5 Seasonal analysis of rainfall rate and peak reduction*

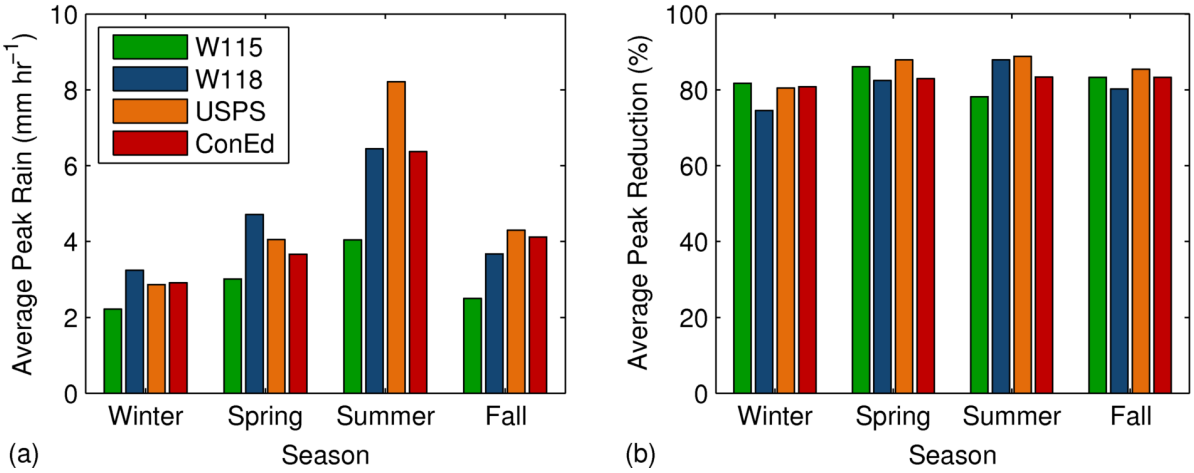


Figure 21: Seasonal variation of average (a) peak rain, and (b) peak reduction for all monitored events.

An analysis of variance (ANOVA) was performed for seasonal peak rain rate and peak reduction (Figure 21). Seasonal variation in event peak rain rate (Figure 21(a)) is significant on W118 and USPS ($p < 0.05$), with higher average rates in the summer, 6.4 and 8.2 mm $hr^{-1}$, compared to the winter, 3.2 and 2.9 mm $hr^{-1}$, for W118 and USPS, respectively. Analysis of peak reduction shows no statistically significant performance variations between winter (Dec-Feb), spring (Mar-May), summer (Jun-Aug), and fall (Sep-Nov) on any roof ($p > 0.05$) (Figure 21 (b)).

*4.4.6 Event based comparative analysis of peak runoff behavior*

It is difficult to directly compare peak reduction performance as the distribution of the event peak rain rate varies between the monitored rooftops (Figure 18). To understand the factors that influence peak runoff and analyze peak reduction performance, an event based regression analysis was performed, based on event rainfall characteristics from each roof specified in section 4.4.1. A single-factor linear regression model to predict peak runoff was undertaken for each event rainfall characteristic. The characteristics with the highest coefficients of determination (r-squared) were rain depth, peak rain, rain depth to peak, time to peak, and rain duration (Table 9). Differences in r-squared values between roofs show variation in the significance of certain variables for prediction of peak runoff. On ConEd, the modular system, peak rain is the strongest predictor for peak runoff (r-squared = 0.84); however, on the continuous systems, event rain depth has equal or more significance (r-squared = 0.85 for W115, 0.86 for W118, and 0.73 for USPS). Rain depth to peak showed limited correlation compared to total event rain depth, as event peak runoff is not necessarily a response to the peak rain, especially when peak rain occurs early in an event. Across all roofs, 70% of event peak runoff rates occurred within 30 minutes of the event peak rain rate.

Table 9: Coefficient of determination (r-squared) for linear regression of 5 strongest rainfall based predictors for peak runoff.

| Roof Name | W115 | W118 | USPS | ConEd |
|---|---|---|---|---|
| Rain Depth (mm) | 0.85 | 0.86 | 0.73 | 0.69 |
| Peak Rain (mm $hr^{-1}$) | 0.64 | 0.60 | 0.73 | 0.84 |
| Rain Depth to Peak (mm) | 0.58 | 0.77 | 0.45 | 0.38 |
| Time to Peak (min) | 0.40 | 0.40 | 0.16 | 0.31 |
| Rain Duration (min) | 0.32 | 0.36 | 0.38 | 0.05 |

A forward selection stepwise regression (Draper and Smith. 1998) was performed to evaluate the combined significance of multiple event rainfall characteristics (Table 6) for prediction of event peak runoff. The analysis first performs a linear regression of peak runoff against each rainfall characteristic individually. The rainfall characteristic that provides the best prediction is then added to the model. Remaining rainfall characteristics are then individually tested in the primary model. The characteristic that most improves the model is then added and the process is repeated until remaining characteristics do not significantly improve the prediction ($p > 0.05$). Rain depth showed the strongest correlation with peak runoff in the final stepwise model for W115 and W118 data, while peak rain showed strongest correlation for USPS and ConEd. Additionally, rain depth to peak showed stronger correlation for USPS and ConEd compared to rain depth only once peak rain was included in the model.

*4.4.7 Roof-specific peak runoff models*

As rain depth and peak rain showed the strongest average coefficient of determination among rainfall characteristics, a generalized linear regression was performed for each roof to predict peak runoff from these values. Squared terms were included in the model for both predictors as they significantly ($p < 0.05$) improved the in the peak runoff model for at least one roof. The regression model equations to calculate peak runoff rate ($R_p$) are of the following form

$$R_p = C(1) + C(2){P_p}^2 + C(3)P_p + C(4){P_t}^2 + C(5)P_t$$

$$where, 0 \leq R_p \leq P_p \qquad (1)$$

where $P_p$ is peak rain, $P_t$ is the total rain depth, and *C(1)-C(5)* are empirical model coefficients listed in Table 10. The final model (Equation (1)) is referred to as a Characteristic Peak Runoff Equation (CPRE).

Table 10: Coefficients for the roof-specific CPRE regression models (Equation (1))

| Roof Name | W115 | W118 | USPS | ConEd |
|---|---|---|---|---|
| *C(1)* | -0.153 | -0.157 | -0.422 | -0.056 |
| *C(2)* | 0.010 | 0.007 | 0.008 | 0.019 |
| *C(3)* | -0.035 | -0.102 | -0.046 | -0.044 |
| *C(4)* | -0.001 | 0.000 | -0.001 | 0.000 |
| *C(5)* | 0.157 | 0.163 | 0.174 | 0.097 |

Only storm events with non-zero runoff were used for analysis in order to prevent overestimation of peak runoff in small events. However, zero runoff events were still applied to calculate r-squared values in the model selection and application process. Excluding zero-runoff events in model creation (and defining negative predictions of peak runoff to be equal to zero) improved CPRE r-squared values for all roofs. Event peak runoff ($R_p$) predictions are constrained between 0 and the event peak rain ($P_p$). While complex rooftop configurations and accumulated rainfall can theoretically cause peak runoff rates in excess of peak rain, this is abnormal, only occurring in 1 monitored event on W115 and 1 event on USPS; the ratios of peak runoff and peak rain for both of these events were outliers compared to the total dataset, 4.1 and 5.6 standard deviations away from the mean ratio for W115 and USPS events, respectively. Figure 22 shows the comparison of observed and modeled peak runoff for each rooftop. The final regression models have r-squared values of 0.87 for W115, 0.90 for W118, 0.88 for USPS, and 0.91 for ConEd.

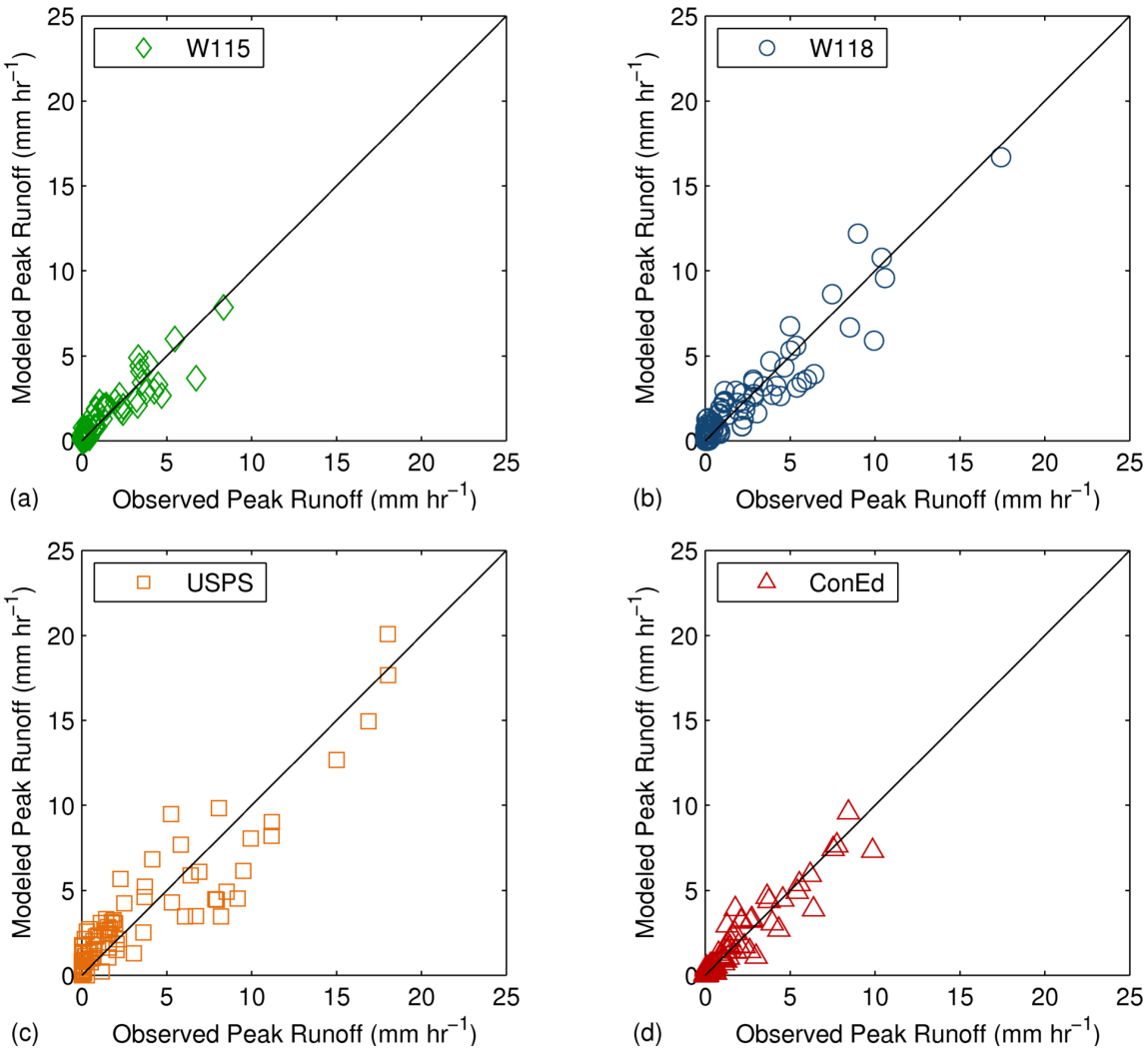


Figure 22: Modeled peak runoff rate compared to observed peak runoff rate (mm hr$^{-1}$) for (a) W115, (b) W118, (c) USPS, and (d) ConEd.

Figure 23 shows the modeled values of peak runoff rate based on the CPRE models. The upper boundary signifies that peak rain rate cannot exceed rain depth. The lower boundary indicates where CPREs predict peak runoff in excess of peak rain. Below this boundary, it is assumed that peak runoff is equal to peak rain.

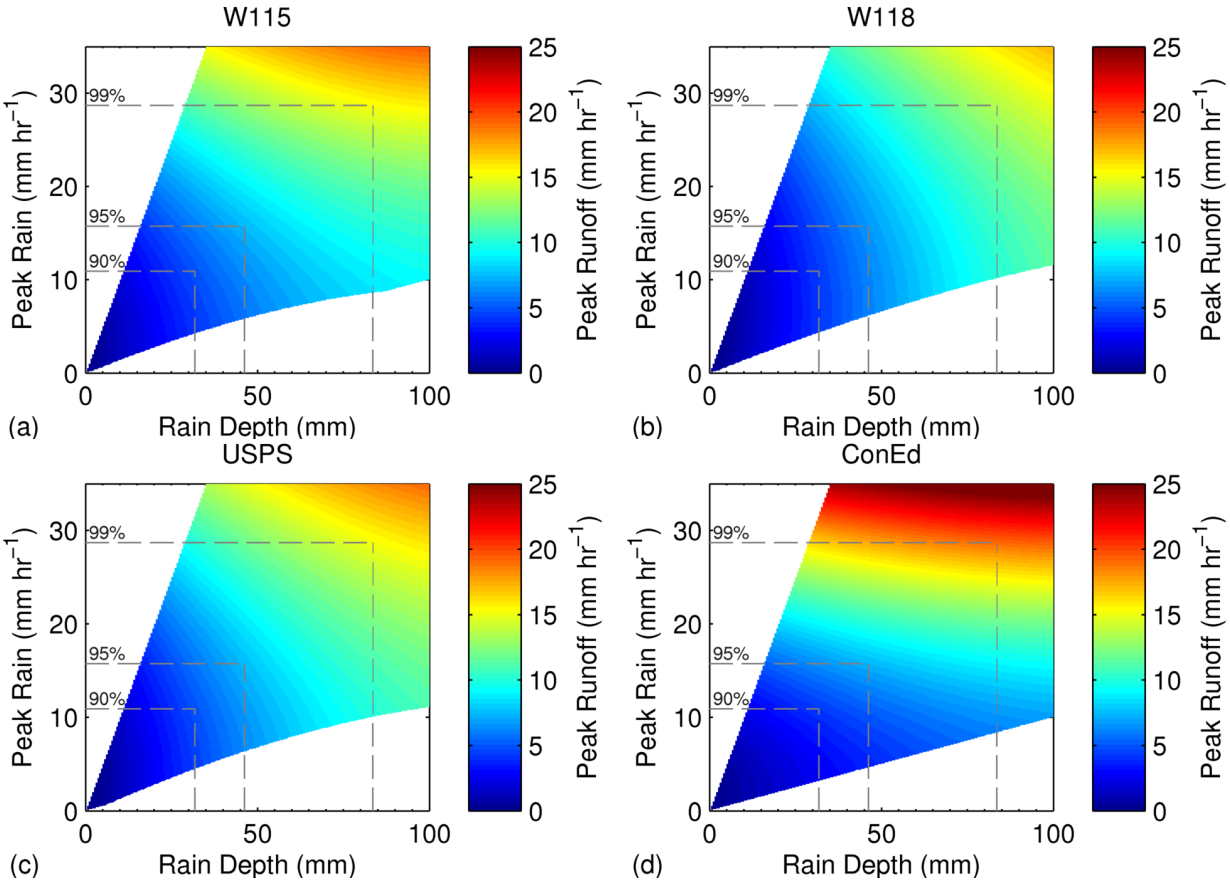


Figure 23: Modeled peak runoff rate (mm hr$^{-1}$) based on rain depth and peak rain rate for (a) W115, (b) W118, (c) USPS, and (d) ConEd. Marked lines represent 90%, 95%, and 99% cumulative probability peak rain rate and rain depth.

The marked lines in Figure 23 represent peak rain rates and rain depths with cumulative probabilities of 90, 95, and 99%, based on the analysis of historic data in section 4.4.3. However due to limited monitored data for events with peak rain greater than 20 mm hr$^{-1}$, CPREs may not properly represent roof behavior for large events, greater than 95% cumulative probability. Based on CPREs, the maximum recorded hourly runoff rate for 90% of all events from the historic period is 4.9 mm hr$^{-1}$ (Figure 23(a)).

Results indicate a difference in comparative influence of peak rain and rain depth for the prediction of peak runoff (Figure 23). The CPRE for W118 shows rain depth is the primary predictor for peak runoff, which corresponds to the strong r-squared (Table 9) for rain depth in the initial linear regression. In contrast, the CPRE for ConEd shows peak rain to be most influential. W115 and USPS CPREs show similar influence of both factors for the prediction of peak runoff.

*4.4.8 Unified model for peak rainfall reduction*

Because the continuous green roof systems (W115, W118, and USPS) showed similar trends, a combined model was developed to predict overall peak rain reduction behavior of green roofs. The combined equation is as follows

$$R_p = -0.2493 + 0.0087{P_p}^2 - 0.0665P_p - 0.0005{P_t}^2 + 0.1631P_t$$

$$where, 0 \leq R_p \leq P_p \qquad (2)$$

The combined model still accurately predicts peak runoff on each roof (r-squared = 0.86 for W115, 0.90 for W118, and 0.87 for USPS) (Figure 24(a)), but does not capture comparative variations in peak reduction behavior between roofs. Equation (2) shows a similar behavior to the individual equations of W115 and USPS (Figure 24(b)) but is still able to approximate peak runoff on W118. While not as effective as the roof-specific equation for the modular ConEd system, the equation can still give an estimation of the peak runoff response (r-squared = 0.81). Additionally, models for each combination of the continuous systems (i.e. W115 and W118, W115 and USPS, W118 and USPS) were validated against the monitored data from the

remaining system. Each model was able to estimate behavior of the remaining roof, with r-squared values between 0.84 and 0.88.

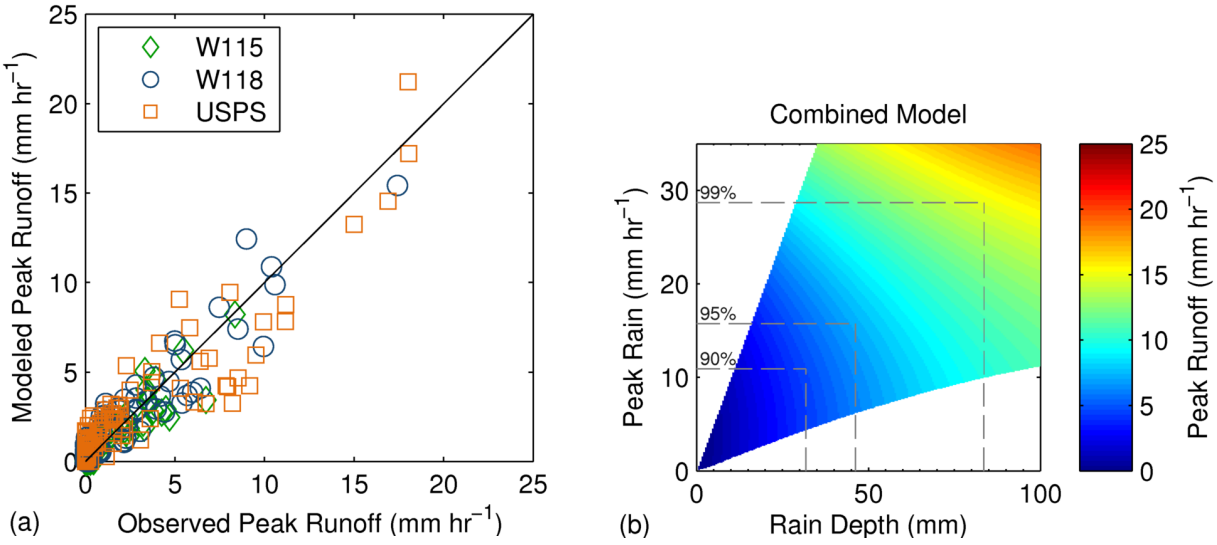


Figure 24: Results from combined runoff model for W115, W118, and USPS; (a) modeled compared to observed peak runoff rate (mm hr$^{-1}$), (b) peak runoff predictions (mm hr$^{-1}$) based on rain depth and peak rain.

*4.4.9 Modeled peak reduction performance*

To determine peak runoff responses on each roof, the roof-specific and combined CPREs were applied to historic rainfall data discussed in section 4.4.2. For the roof-specific CPREs, variances in modeled peak rain reduction and peak runoff distributions between roofs are significant ($p$<0.05). USPS still showed the highest percent of fully retained storms, 39.3% compared to 24.9% for W115, 30.7% for W118, and 18.4% for ConEd. ConEd showed the best performance overall and for events with non-zero runoff (Table 11). For events with peak rain greater than 3 mm, peak rainfall reductions are 53.9, 58.4, 55.2, and 63.7% for W115, W118, USPS, and ConEd, respectively.

Table 11: Green roof model detention statistics.

| Roof Name | W115 | W118 | USPS | ConEd | Combined |
|---|---|---|---|---|---|
| Zero Runoff Events (%) | 24.9 | 30.7 | 39.3 | 18.4 | 33.5 |
| 1-hr Peak Reduction (%) | | | | | |
| -All events | 70.8 | 74.3 | 75.1 | 77.1 | 76.7 |
| -Non-zero runoff events | 61.1 | 63.0 | 58.9 | 72.0 | 65.0 |

W118 had the lowest maximum peak runoff, 13.3 mm $hr^{-1}$ for events less than 99% cumulative probability (Figure 25(a)); however, this was not indicative of overall performance. Figure 25(b) displays average peak reductions at different event probability intervals. USPS has highest average peak reduction (98.6%) for events below 50% cumulative probability, while ConEd shows the highest average reduction (69.2%) for events between 50 and 95% cumulative probability.

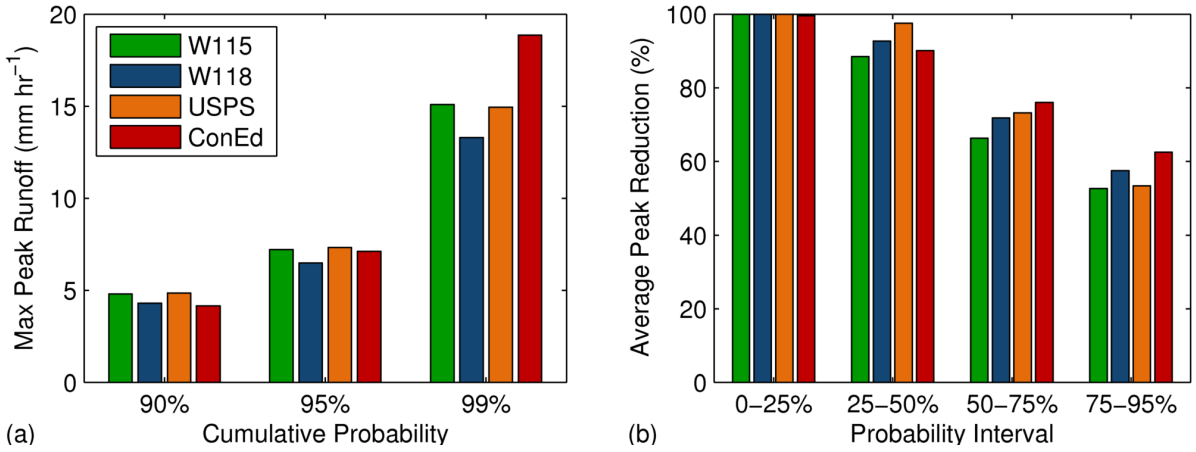


Figure 25: Frequency analysis of peak rain and rain depth from analysis of all historic NYC events (Central Park, 1971-2010); (a) modeled maximum peak runoff (mm $hr^{-1}$) within 90, 95, and 99% cumulative probabilities, and (b) modeled average peak reduction (%) within 0-25, 25-50, 50-75, and 75-95% probability intervals.

The combined model shows slightly improved peak reduction performance than the roof-specific models for W115, W118, and USPS (Table 11). The combined model benefited from W118's better performance in large events and USPS's higher retention performance for small events.

Combination of data permitted the model to be parameterized by both large volume events from W118 and events with higher peak rain rates from USPS (Figure 18).

## 4.5 Discussion and concluding remarks

### *4.5.1 Peak rainfall reduction behavior of green roofs*

The peak rain reductions observed for W115, W118, USPS and ConEd are within the range of performance documented by others, discussed in section 4.2. During the monitoring period, USPS showed the highest observed average peak rain reduction (85%) for all events, due in part to the roof's ability to fully retain 45% of storm events. Because of differences in peak rain distributions between rooftops, W118 showed the highest average reduction in events with higher cumulative probability, especially above 90%.

Modeling of peak runoff rates using historic data allowed better evaluation and comparison of the studied green roofs. Modeled results show that ConEd has the strongest overall average peak rain reduction (77%); however, USPS still shows the best performance for events below 50% cumulative probability, with 98.6% peak rain rate reduction. W118 shows the lowest maximum peak runoff for events below 95 and 99% cumulative probability (Figure 25(a)), but its overall peak reduction performance is lower than ConEd and USPS.

Analysis of peak runoff and rainfall characteristics demonstrates that peak rain and event rain depth can be applied to predict event peak runoff. However, the correlation of these factors with peak runoff varies among roofs (Table 9). It is hypothesized that differences in the relative influence of peak rain rate and rain depth is the result of two main factors: (1) the configuration

of rooftop non-vegetated regions and (2) flow paths through green roof substrate and drainage layers, which vary between the continuous and modular green roof systems.

It is theorized that runoff rates on the modular tray system, ConEd, are dominated by rainfall on non-vegetated areas. On ConEd, a significant section of the non-vegetated area, including a sloped glass skylight, is located adjacent to the watershed drain; as a result, runoff from these sections flows directly to the drain. Additionally, the open space beneath the modular trays is less effective than a drainage course at dampening horizontal water flow. In contrast, the distance from the drain and configuration of non-vegetated areas on W115, W118 and USPS allows increased opportunity for runoff to be delayed and buffered, reducing flow rate before water reaches the roof drain. It is believed that on W118, where peak runoff rate was most correlated with rain depth, flow rate is controlled by the volume of water within roof vegetated areas. As the volume of water in the substrate and drainage layers increases, retention and detention performance is reduced, resulting in higher runoff flow rates in large rainfall events. In contrast, on ConEd, the hydraulic conductivity from the roof substrate is restricted by small outlets at the base of each modular tray, limiting flow from vegetated areas during these larger events.

Rooftop configuration (e.g. size, slope, flow paths) also appears to affect peak rain reduction. Modeled average reduction for the four roofs corresponded with the roof size. Stronger reductions in peak flow were shown for larger roofs with long and irregular flow paths. The rectangular configuration and small comparative size of W115 makes it is most similar to a "pilot-scale" roof, which other studies have shown to have reduced detention performance (Fassman-Beck *et al* 2013). Due to W115's small size and simple configuration, 75% of peak

runoff rates occurred within 30 minutes of the peak rain rate, compared to 69, 63 and 62% for W118, USPS, and ConEd, respectively.

### *4.5.2 Benefits and Limitations of CPRE Models*

Green roof peak reduction performance was predicted by applying roof-specific CPRE models to a standard rainfall dataset. Variations in monitored event peak rain distributions influence overall peak reduction performance. For example, W118 had the highest average rain depth (12.6 mm), and consequently worst average peak rain rate reduction (82%). Application of CPRE model normalized the distribution of events among roofs, improving W118's comparative performance.

Unexplained variance in the CPRE model of peak runoff each roof is believed to be the result of differences in site conditions and event rainfall characteristics. Initial substrate moisture has been shown to influence hydrologic performance of green roofs, especially in small events (Carson *et al* 2013). No significant seasonal variation was found in peak attenuation or peak runoff rates; however, higher peak rain rates may have offset benefits from increased substrate moisture evapotranspiration in warmer months, as discussed in Chapter 2. Empirical models based on a singular variable, similar to the CRE method for event runoff volume discussed by Carson *et al* (2013), were unable to capture the complex peak runoff behavior on all roofs; however, models based on both peak rain and rain depth provide a reasonable approximation. The combined model based on data from W115, W118, and USPS, was still able to predict peak runoff for each roof (r-squared = 0.88), demonstrating its utility for determining the rainfall detention performance of green roofs for stormwater management purposes. When applied to historic data, the model reveals that on average a continuous vegetated mat or built-in-place system can fully capture 33.5% of events and reduce peak rainfall rate 76.7%, compared to a modular system,

which only fully retained 18.4% of events but is able to reduce event peak rainfall by 77.1% on average.

# Chapter 5

# CONTRIBUTIONS

The research presented in this dissertation makes significant theoretical and practical contributions to the areas of environmental measurement methods, urban sustainability, green infrastructure performance, stormwater management, hydrology, and boundary layer climatology. Overall, this composition aims to improve the understanding of the hydrologic performance of green roofs. The processes of evapotranspiration (ET) and peak rainfall rate reduction were analyzed to allow researchers, practitioners, and policymakers to quantify and maximize environmental benefits of green roofs. Specific contributions are described in the following sections.

## 5.1 Theoretical Contributions

*Chapter 2: Quantifying Evapotranspiration from Urban Green Roofs: A Comparison of Chamber Measurements with Commonly Used Predictive Methods*

High-resolution measurement of green roof ET has historically been limited. Measurements have often made indirectly, through a water balance of precipitation, runoff, and moisture storage data measured with an elevated lysimeter system (Ouldboukhitine *et al* 2012, DiGiovanni *et al* 2013, Wadzuk *et al* 2013). Study of the dynamic chamber method discussed in Chapter 2 contributes to existing literature by: providing a methodology for high-resolution measurement of ET; presenting diurnal and seasonal green roof ET behavior; and providing an initial evaluation of predictive methods for calculating green roof ET.

The dynamic chamber technique is valuable for directly measuring ET from green roofs, shallow vegetation, or bare soil at 30 to 60-minute intervals. While sealed chambers have been employed for measurement of ET in arid environments (Arnone and Obrist 2003, Garcia *et al* 2008), they have not been applied for continuous ET measurement in urban environments. The system utilized and described in this PhD dissertation can be rapidly deployed on existing sites, is minimally invasive, and operates autonomously, allowing researchers to conduct continuous measurements over an extended period (as performed in this study), or individual measurements at multiple sites.

While the LI-8100 system is expensive, the measurement, deployment, and calibration methodology discussed in Chapter 2 can also be applied to a low-cost single-measurement system. Custom single-measurement chamber systems have successfully been employed in studies of arid environments (Arnone and Obrist 2003, Garcia *et al* 2008). Thus, it is thought that a low-cost single-measurement chamber system can be developed and calibrated for measurement of ET in urban environments using readily available materials and affordable sensors.

Results of this study allowed an initial evaluation of green roof ET performance and the utility of the Penman-Monteith equation and the energy balance method for estimating ET. Extensive data collected from chamber deployment expands upon the limited number of studies reporting diurnal (Ouldboukhitine *et al* 2012) and seasonal (DiGiovanni *et al* 2013, Wadzuk *et al* 2013) green roof ET trends. With respect to diurnal trends, chamber measurements show that ET increased after sunrise and peaked just after noon. Seasonal trends agreed with ET studies that

state warm weather conditions support higher ET fluxes (Gaffin *et al* 2010, DiGiovanni *et al* 2013, Mentens *et al* 2006, Villarreal *et al* 2004, Sumner and Jacobs 2005, Wever *et al* 2002).

Comparison of measured and predicted fluxes revealed that the Penman-Monteith equation overestimated ET at lower fluxes and underestimated higher fluxes compared to dynamic chamber measurements; similar to results from models employed in certain agricultural (Ali and Mawdsley 1987, Salvucci and Gentine 2013), natural (Kahler and Brutsaert 2006), and other green roof studies (Sherrard and Jacobs 2012, Wadzuk *et al* 2013). The energy balance, as with other energy methods, was shown to underestimate ET (Rosenberg 1969, Blad and Rosenberg 1974, Bertela 1989).

Chapter 2 contributes to the existing literature on green roof ET by presenting a new technique for measuring ET from green roof, which can be employed for high-resolution measurement and analysis. The study further contributes by providing hourly ET results, which revealed important diurnal and seasonal trends in green roof ET. Overall, the work provided an important base for further analysis of green roof ET behavior and evaluation of predictive techniques.

*Chapter 3: Applicability of common predictive models for estimation of evapotranspiration on urban green roofs*

Because the unique properties of green roofs (including the small scale, vegetation heterogeneity, shallow substrate depth, underlying impervious layers, and uncertain moisture availability) can affect the ET flux (Spronken-Smith *et al* 2000, Grimmond and Oke 2002, Jim and Peng 2012, DiGiovanni *et al* 2013); it is important to validate predictive models against measured ET data. In Chapter 3, potential ET and actual ET models parameterized by on-site climate conditions were evaluated against ET measurements from the urban green roofs that were the focus of this

PhD research. This work expands upon comparison studies of predictive ET equations on green roofs by Lazzarin *et al* (2005), Sherrard and Jacobs (2012), and DiGiovanni *et al* (2013), where reduction factors to reduce ET estimates in water-limited conditions were applied with varying levels of success. While Wadzuk *et al* (2013) also compared potential ET estimates from the Hargreaves, Priestley-Taylor, and Penman-Monteith equations to ET measurements, correlation was only evaluated for monthly results. Additionally, concerns arise over the abnormally high potential ET fluxes calculated from the Hargreaves equation and the absence of an under drain on the monitored lysimeter setup.

Furthermore, application of the Savitzky-Golay filter (Vaughan and Ayars 2009, Peters *et al* 2014) to daily data was shown to enhance visualization of ET trends compared to other display methods. Observed vs. predicted scatter plots (Lazzarin *et al* 2005, Sherrard and Jacobs 2012, DiGiovanni *et al* 2013), monthly tables (Wadzuk *et al* 2013), and raw line graphs (DiGiovanni *et al* 2011) employed in other studies did not reveal the complex relationships between ET estimates and measurements. This type of filtering has been used in studies of ET in agricultural and natural environments (Wu 1997, Hargreaves and Allen 2003, Czikowsky and Fitzjarrald 2004, Vaughan and Ayars 2009, Peters *et al* 2014) and can be an important for evaluating ET behavior in green roof studies.

Results of this PhD research component demonstrated that the Priestley-Taylor equation was the most effective potential ET model for predicting ET on the studied green roofs. Furthermore, crop coefficients based on linear regression of Priestley-Taylor and dynamic chamber fluxes were approximately one, meaning the equation gives reasonable estimates of ET without calibration. These results demonstrate the applicability of the Priestley-Taylor equation for both

input in green roof hydrologic models (Sherrard and Jacobs 2012, Stovin *et al* 2013) and energy models (Lazzarin *et al* 2005, Ouldboukhitine *et al* 2011). This analysis also expands on results from other studies that showed estimates from predictive equations were more correlated with measured ET during years with frequent precipitation (Lazzarin *et al* 2005, Wadzuk *et al* 2013) or when considering only non-water-limited days in the analysis (DiGiovanni *et al* 2013).

Analysis of the antecedent precipitation index, originally applied by Mawdsley and Ali (1985) at agricultural sites, revealed that it properly reduced potential ET estimates on green roofs in water-limited conditions. The storage model applied in this study was very sensitive to storage depth, which agrees with findings by DiGiovanni *et al* (2013), and underestimated ET in the summer when energy available for ET was high. Reductions in ET estimates from the storage model occurred before those in dynamic chamber ET, which supports the belief that there is a range of moisture conditions where ET remains energy limited (Allen *et al* 2005a).

Further exploration of trends in dynamic chamber measurements and potential estimates revealed more details about green roof ET behavior. Results showed that green roof ET exceeded potential ET during the in the summer, where elevated surface temperatures and increased precipitation were recorded. Records from this period showed that maximum daily surface temperatures were significantly higher than maximum air temperatures, which resulted in more energy available for ET, as discussed by Jim and Peng (2012). Additionally, increased precipitation during this period is believed to have enhanced *Sedum* transpiration and surface water availability (Allen *et al* 2005a). Potential ET equations overestimated ET in the winter, which is thought to be caused by seasonal variations in crop coefficients and surface reflectance (Allen *et al* 1998).

The analysis in Chapter 3 contributes to current green roof ET literature through evaluation of green roof ET estimates from various predictive methods, including models designed to account for water availability. A secondary contribution is the data visualization methodology, which allowed a thorough analysis ET behavior. In the end, Chapter 3 revealed important ET behavior and the applicability of various ET models for predicting performance and parameterizing hydrologic and energy models.

*Chapter 4: Peak rainfall reduction performance of four extensive green roofs in New York City: hydrologic observations and analysis*

Peak rainfall rate reduction has historically received less attention than rainfall volume retention. While some previous studies have reported the peak rainfall rate reduction of green roofs (Moran *et al* 2005, Carpenter and Kaluvakolanu 2011, Fassman-Beck *et al* 2013), there has been limited research related to predicting peak runoff (Stovin *et al* 2012, Villarreal and Bengtsson 2005). Chapter 4 makes significant contributions to existing literature by presenting an instrumentation method for full scale green roofs, performance data from four green roof installations, an analysis of factors influencing peak reduction, and a model for predicting performance.

Due to limited access and difficulty instrumenting full-scale roof downspouts, many studies of peak rainfall reduction have been conducted on elevated test boxes or miniature "pilot-scale" roofs (Berghage *et al* 2009, Bliss *et al* 2009, Sherrard and Jacobs 2012, Stovin *et al* 2012). The runoff flow meters employed in this study can be installed in existing downspouts without alteration of the rooftop membrane or drainage system, in order to monitor runoff behavior of full-scale green roofs. Due to the success of this monitoring system, similar flow meters have

been deployed on a green roof at the University of Bologna in Bologna, IT and a rooftop farm in Brooklyn, NY.

The analysis techniques used to evaluate peak rainfall rate reduction are valuable tools for exploring green roof hydrologic behavior. The frequency analysis employed by Fassman-Beck *et al* (2013) was expanded to compare measured peak rainfall and runoff rates and classify storm events based on both rainfall depth and peak rainfall rate. Additionally, regression models presented in Chapter 4 are valuable tools for assessing relationships between multiple event rainfall and runoff characteristics.

Chapter 4 contributes to existing literature reporting the reduction in peak rate of stormwater runoff from green roofs. Green roof peak rainfall rate reduction performance has historically received limited attention, especially compared to the volume retention performance (Mentens *et al* 2006, Spolek 2008, Berndtsson 2010, Gregoire and Clausen 2011, Stovin *et al* 2012, Carson *et al* 2013, Fassman-Beck *et al* 2013). Monitored and modeled green roof peak rainfall rate reduction performance reported in Chapter 4 expands on the results from full scale roofs presented by Moran *et al* (2005), Carpenter and Kaluvakolanu (2011), and Fassman-Beck *et al* (2013). Performance variations between the thin vegetated mat systems and deeper systems match findings by Fassman-Beck *et al* (2013) that demonstrated deeper substrates more effectively dampened peak runoff flow. Performance was also correlated with rooftop size. The lowest overall reduction was predicted on the smallest green roof system. The smallest system is most similar to "pilot-scale" roofs, which other studies have shown to have reduced hydrologic performance (Fassman-Beck *et al* 2013).

Expanding upon the findings by Carson *et al* (2013) that showed that rooftop configuration was related to volume retention; results from Chapter 4 revealed that peak rainfall reduction increased with roof size and was affected by rooftop configuration. The influence of the non-vegetated areas adjacent to the downspout on the modular tray system discussed by Carson *et al* (2013) was shown in the development of the empirical peak runoff models. On the modular tray system, peak runoff was most correlated with peak rainfall, which supports the idea that rainfall from non-vegetated areas flows uninhibited to the rooftop drain. This behavior contrasted that of the continuous systems, which showed that peak rainfall rate was more correlated to event rainfall depth. Additionally, the small event detention performance, as with retention (Carson *et al* 2013), for modular tray system was lower than the other roofs.

The influence of rainfall depth on peak runoff supports findings by Bliss *et al* (2009) that showed accumulated rainfall and increased substrate saturation reduced green roof detention performance. The empirical model developed to predict peak rainfall rate improved upon previous models, which resulted in limited correlation (Stovin *et al* 2012), or were applicable to only a handful of storms and required input of initial runoff delay and total runoff depth (Villarreal and Bengtsson 2005, Villarreal 2007).

The peak rainfall rate reduction study presented in Chapter 4 expands on the volume retention study performed by Carson *et al* (2013). Monitoring, statistical analysis, and modeling of performance reveal important details about the effects of rooftop configurations on peak rainfall rate reduction. Overall, Chapter 4 contributes to existing research by providing an extensive analysis of peak rainfall rate reduction behavior together with a useable model for predicting reduction performance from readily available rainfall data.

## 5.2 Practical Contributions

A large number cities in the US and abroad are investing in low impact development (LID) as part of larger stormwater runoff mitigation programs designed to counter the detrimental impacts of sewer overflows. For example, New York City (NYC) has adopted a stormwater management plan incorporating LID techniques. The plan focuses on reducing runoff volume and peak rainfall rates to help mitigate local combined sewer overflow (CSO) pollution (NYC DEP 2010). The predictive models and environmental measurements presented in this dissertation allow governing entities, building owners, and other stakeholders to evaluate the performance and maximize the effectiveness of green roof systems.

The research presented in Chapter 2 and Chapter 3 explored ET behavior of green roofs, which is important for evaluating green roof benefits. While ET is generally estimated in order to determine irrigation requirements for agriculture, green roof ET is correlated with many urban environmental benefits. Quantifying ET can enhance understanding of green roof stormwater retention (Stovin *et al* 2013, Wadzuk *et al* 2013) and detention (Bliss *et al* 2009), urban heat island mitigation (Taha 1997), reduction to building energy usage (Ouldboukhitine *et al* 2011), carbon sequestration (Pataki *et al* 2006), and vegetation vitality (Stovin *et al* 2013). ET measurements or predictions can parameterize green roof hydrologic models (Sherrard and Jacobs 2012, Stovin *et al* 2013) to improve stormwater retention and detention predictions, as well as energy models (Lazzarin *et al* 2005, Ouldboukhitine *et al* 2011) to determine reductions to urban air and building temperatures. Subsequently, accurate quantification of ET can better inform green roof investment, implementation, and design decisions, in order to maximize environmental benefits and minimize cost.

The high-resolution dynamic chamber ET measurement system and daily ET models are important tools for analyzing and optimizing green roof urban heat island mitigation and stormwater management performance. When ET drops below potential due to limited water availability, excess energy availability causes increased soil and air temperatures. ET quantification and the antecedent precipitation index can be used to identify water-limited periods for manual or active control of rainwater irrigation. Green roofs can be irrigated with stored rainwater in water-limited conditions to enhance ET, reduce temperature, improve plant vitality, and increase overall volume retention performance. For effective irrigation control, it is important to have the temporal resolution of the methods discussed in Chapter 2 and 3 of this dissertation.

Because many North American municipalities, including: Philadelphia, PA; Milwaukee, WI; New York, NY; Portland, OR; Syracuse, NY; Washington, D.C.; Aurora, IL; and Toronto, Ontario; are specifying LID solutions in stormwater management plans, developing on-site retention standards, and offering financial incentives for LID implementations (Garrison and Hobbs 2011), it is important to understand rainfall detention behavior and how hydrologic performance can be optimized. The analysis of peak rainfall rate reduction presented in Chapter 4 helps quantify how green roof installations reduce the flow rate of stormwater into the sewer system. Additionally, runoff data from green roofs can be input into a sewer system model to quantify CSO reduction performance. Results showed that stormwater detention varied based on green roof installation method, configuration of non-vegetated areas, and substrate depth. Additionally, results from the combined model for continuous systems showed that a singular

model may be applied to approximate performance of a network of similar continuous green roof systems.

The utility of a green roof is dependent on stormwater management goals. Modeled runoff data showed that, on average, the modular tray system was more effective at reducing peak rainfall rate compared to the three continuous systems. However, considering that even small rainfall rates, as little as 3 mm $hr^{-1}$, can cause CSOs in NYC (Montalto *et al* 2007), a governing body may be more interested in keeping smaller events from causing a CSO. In this case, the built-in-place system might be preferred as it fully captured 45% of all storms. Finally, it is important to note that the vegetated mat system might also be the most constructible on a wider range of existing building stock due to its significantly lower weight. Additionally, if designers are interested in the maximum flow from a certain percent of storms, in order to size drainage systems and determine sewer system loading, Figure 23 and Figure 24(a) are valuable tools for determining peak runoff.

Insights about the effect of configuration on performance are important for maximizing the effectiveness of future green roofs installations. Study of peak rainfall rate reduction in small events demonstrated that on the modular tray system, non-vegetated areas adjacent to the drain resulted in excess runoff in small storms. Relocating non-vegetated areas to locations farther from the drain in future installations would improve hydrologic performance for small events with no increase to cost. Longer flow paths between non-vegetated areas and the rooftop downspouts would improve rainfall detention and allow more opportunities for depression storage.

# Chapter 6

## PROPOSED AVENUES OF FUTURE RESEARCH

The study of green roof evapotranspiration (ET) and peak rainfall rate reduction behavior in this dissertation greatly expands upon the scientific literature exploring the hydrologic monitoring and performance of green roofs. It is thought that future research can be built upon methods and results from this PhD research to further explore these performance metrics. Additionally, it is important to note that the methodologies presented here can be employed with minimal modification for determining the hydrologic performance of other low impact development implementations, specifically, tree pits, bio-swales, and green streets.

*Development of low cost evapotranspiration measurement system*

The measurement, deployment, and calibration methodologies discussed in Chapter 2 are not unique to the LI-8100 system. Similar approaches have been used for custom single-measurement chamber systems (Arnone and Obrist 2003, Garcia *et al* 2008). Future work could explore how a low-cost single-measurement chamber system can be developed.

The chamber can be constructed with readily available materials and affordable sensors. The requirements for the simplified system are: (1) an open-faced container that is otherwise sealed (e.g. a large plastic bin); (2) a relative humidity/temperature sensor that could respond quickly to humidity changes; and (3) a fan or air pump to establish steady mixing. The system can be laboratory calibrated as described in Chapter 2 and deployed for ET measurements on tree pits, bio-swales, green streets, and other green infrastructure implementations. To compare

measurements from different sites at different times, results can be normalized based on potential ET estimates and antecedent rainfall.

*Evapotranspiration estimates from humidity gradients*

During exploratory analysis of dynamic chamber measurements, it was shown that an empirical model for daily ET, based on multi-variate regression of mean temperature (°C), net radiation (MJ $m^{-2}$ $d^{-1}$), saturation vapor pressure (kPa), and air vapor pressure (kPa) could be significantly improved by including the vapor pressure at the rooftop surface, as recorded by the dynamic chamber. Results showed that if surface vapor pressure was near or below air vapor pressure, measured ET was significantly lower. This behavior suggests that if there is energy and water available for ET, there will be increased water vapor in the surface boundary layer (Oke 1987).

Humidity gradients have been employed for ET estimation in previous studies (Berthier *et al* 2006, Salvucci and Gentine 2013). Required relative humidity sensors are very affordable and require minimal setup. If explored, the method could allow for estimation of ET on a large green infrastructure network, especially if the systems are calibrated with the dynamic chamber or another existing ET measurement technique.

*Continuous Runoff Model*

The analysis in Chapter 4 and previous study by Carson *et al* (2013) provide methodologies for estimating two major storm event runoff characteristics, i.e. the peak runoff rate and the runoff volume, respectively. However, attempts to predict high-resolution continuous performance are limited (Berthier *et al* 2011, Stovin *et al* 2013). Development of a model to predict runoff hydrographs, based on inputs of rainfall, site characteristics, and ET estimations can provide

valuable insight into other factors of runoff behavior, including time and rainfall depth before runoff initiation, which were shown to vary greatly among the monitored storm events.

*Green roof performance compared to green roofs and non-vegetated roofs in different climates*

The analysis discussed in Chapter 4 is important for evaluating the effectiveness of green roofs for stormwater management. However, only extensive green roofs in New York City were monitored. There is still limited understanding of the hydrologic performance of green roofs in New York City compared to green roofs and non-vegetated roofs in other climates.

In October 2013, three runoff flow meters, similar to those discussed in Chapter 4, were installed on two vegetated roofs and one non-vegetated roof in Bologna, Italy. Bologna has a sub-Mediterranean climate and receives less precipitation compared to New York, especially in summer months, where potential evapotranspiration is higher (Figure 12) and New York City is subject to higher precipitation intensities (Figure 21(a)). Additionally, precipitation records from Bologna show increased seasonal variations in precipitation depth compared to New York City. Comparison of precipitation and runoff data from Bologna and New York City can enhance the understanding of the effects of climate on green roof hydrologic performance and the performance variations between green roofs and non-vegetated roofs. Additionally, the determined effects of climate on hydrologic performance can be used to refine the peak runoff models and predict performance in other regions.

*Controlled setups to evaluate hydrologic performance*

The analysis presented in Chapter 4 and previous study by Carson *et al* (2013) demonstrated the relationship between green roof hydrologic performance and configuration. However, there are

construction aspects that differ between the roofs, specifically substrate depth, watershed shape, flow path lengths, slope, drainage pathways through substrate, and the locations and type of non-vegetated area on these rooftops. The complex interaction of these construction aspects makes determining their exact influence of on hydrologic performance difficult.

Future research can explore the effect of these variables individually by monitoring a system of test boxes, which include non-vegetated areas. Test boxes have been studied to explore the influence of substrate depth (De Cuyper *et al* 2004, VanWoert *et al* 2005), rooftop slope (Getter *et al* 2007, VanWoert *et al* 2005), areal plant coverage (Berghage *et al* 2009, Morgan *et al* 2013), plant type (Nardini *et al* 2011), and orientation (Mentens *et al* 2003) on hydrologic performance. However, these studies have generally excluded non-vegetated regions in their test box designs. Evaluating performance of test boxes with varying non-vegetated area percentages, constructions, and configurations would provide a better understanding of how these properties affect performance. This experiment would provide a relationship to extrapolate green roof test box performance reported in many studies (Berghage *et al* 2009, De Cuyper *et al* 2004, VanWoert *et al* 2005, Getter *et al* 2007, DiGiovanni *et al* 2010, Morgan *et al* 2013, Nardini *et al* 2011, Schroll *et al* 2011, Stovin *et al* 2012) to predict behavior of full-scale roof, especially if results are related to data from the full-scale green roofs discussed in this dissertation.

# REFERENCES


Ali M F and Mawdsley J A 1987 Comparison of two recent models for estimating actual evapotranspiration using only regularly recorded data *J. Hydrol.* **93** 257–76 Online: http://linkinghub.elsevier.com/retrieve/pii/0022169487900990

Allen R . 2000 Using the FAO-56 dual crop coefficient method over an irrigated region as part of an evapotranspiration intercomparison study *J. Hydrol.* **229** 27–41 Online: http://linkinghub.elsevier.com/retrieve/pii/S0022169499001948

Allen R G, Pereira L S, Raes D and Smith M 1998 *Crop Evapotranspiration - Guidelines for computing crop water requirements - FAO Irrigation and drainage paper 56* (Rome, IT) Online: http://www.fao.org/docrep/x0490e/x0490e00.htm#Contents

Allen R G, Pruitt W O, Businger J A, Fritschen L J, Jensen M E and Quinn F H 1996 Evaporation and Transpiration *Hydrology Handbook* (New York, NY: American Society of Civil Engineers) pp 125–252 Online: http://ascelibrary.org/doi/book/10.1061/9780784401385

Allen R G, Pruitt W O, Raes D, Smith M and Pereira L S 2005a Estimating Evaporation from Bare Soil and the Crop Coefficient for the Initial Period Using Common Soils Information *J. Irrig. Drain. Eng.* **131** 14–23 Online: http://ascelibrary.org/doi/abs/10.1061/%28ASCE%290733-9437%282005%29131%3A1%2814%29

Allen R, Walter I A, Ellior R, Howell T, Itenfisu D and Jensen M 2005b *The ASCE Standardized Reference Evapotranspiration Equation* (Reston, VA) Online: http://books.google.com/books?hl=en&lr=&id=Sq4FEqD0Jc4C&oi=fnd&pg=PA1&dq=THE+ASCE+STANDARDIZED+REFERENCE+Evapotranspiration+Equation&ots=0IWrsB-Kti&sig=u3rTUVjdson55glzh4iLedfjQIM

Arnone J a. and Obrist D 2003 A large daylight geodesic dome for quantification of whole-ecosystem CO2 and water vapour fluxes in arid shrublands *J. Arid Environ.* **55** 629–43 Online: http://www.sciencedirect.com/science/article/pii/S0140196302002914

Arora V K 2002 The use of the aridity index to assess climate change effect on annual runoff *J. Hydrol.* **265** 164–77 Online: http://linkinghub.elsevier.com/retrieve/pii/S0022169402001014

Bengtsson L, Grahn L and Olsson J 2005 Hydrological function of a thin extensive green roof in southern Sweden *Nord. Hydrol.* **36** 259–68 Online: http://www.iwaponline.com/nh/036/0259/0360259.pdf

Berghage R D, Beattie D, Jarrett A R, Thuring C, Razaei F, O'Connor T, Razaci F and O'Connor T P 2009 *Green Roofs for Stormwater Runoff Control* (Cincinnati, OH) Online: http://nepis.epa.gov/Exe/ZyNET.exe/P1003704.TXT

Berghage R D, Miller C, Bass B, Moseley D and Weeks K 2010 Stormwater Runoff From a Large Commercial Roof In Chicago *CitiesAlive!: Eighth Annual Green Roof and Wall Conference* (Vancouver, BC) pp 1–13

Berndtsson J C 2010 Green roof performance towards management of runoff water quantity and quality: A review *Ecol. Eng.* **36** 351–60 Online: http://linkinghub.elsevier.com/retrieve/pii/S0925857410000029

Berndtsson J C, Bengtsson L and Jinno K 2009 Runoff water quality from intensive and extensive vegetated roofs *Ecol. Eng.* **35** 369–80 Online: http://www.sciencedirect.com/science/article/pii/S0925857408002024#

Bertela M 1989 Inconsistent surface flux partitioning by the Bowen ratio method *Boundary-Layer Meteorol.* **49** 149–67 Online: http://link.springer.com/10.1007/BF00116409

Berthier E, Dupont S, Mestayer P G and Andrieu H 2006 Comparison of two evapotranspiration schemes on a sub-urban site *J. Hydrol.* **328** 635–46 Online: http://linkinghub.elsevier.com/retrieve/pii/S0022169406000370

Berthier E, Ramier D and Gouvello B De 2011 Simulation of green roof hydrological behavior with a reservoir model *2nd International Conference on Urban Drainage* (Porto Alegre, Brazil) pp 10–5

Blad B L and Rosenberg N J 1974 Lysimetric Calibration of the Bowen Ratio-Energy Balance Method for Evapotranspiration Estimation in the Central Great Plains *J. Appl. Meteorol.* **13** 227–36 Online: http://journals.ametsoc.org/doi/abs/10.1175/1520-0450%281974%29013%3C0227%3ALCOTBR%3E2.0.CO%3B2

Bliss D J, Neufeld R D and Ries R J 2009 Storm Water Runoff Mitigation Using a Green Roof *Environ. Eng. Sci.* **26** 407–18 Online: http://www.liebertonline.com/doi/abs/10.1089/ees.2007.0186

Bouchet R 1963 Evapotranspiration réelle et potentielle, signification climatique *IAHS Publ* **62** 134–42 Online: http://ks360352.kimsufi.com/redbooks/a062/iahs_062_0134.pdf

Boulet G, Chehbouni a., Gentine P, Duchemin B, Ezzahar J and Hadria R 2007 Monitoring water stress using time series of observed to unstressed surface temperature difference *Agric. For. Meteorol.* **146** 159–72 Online: http://linkinghub.elsevier.com/retrieve/pii/S0168192307001487

Bowen I 1926 The Ratio of Heat Losses by Conduction and by Evaporation from any Water Surface *Phys. Rev.* **27** 779–87 Online: http://link.aps.org/doi/10.1103/PhysRev.27.779

Bricker S, Longstaff B, Dennison W, Jones A, Boicourt K, Wicks C and Woerner J 2007 *Effects of Nutrient Enrichment In the Nation's Estuaries: A Decade of Change. NOAA Coastal Ocean Program Decision Analysis Series No. 26* (Silver Spring, MD)

Brutsaert W 2005 *Hydrology: An Introduction* (Cambridge, UK)

Brutsaert W and Stricker H 1979 An advection-aridity approach to estimate actual regional evapotranspiration *Water Resour. Res.* **15** 443–50 Online: http://doi.wiley.com/10.1029/WR015i002p00443

Calder I R, Harding R J and Rosier P T W 1983 An objective assessment of soil-moisture deficit models *J. Hydrol.* **60** 329–55 Online: http://linkinghub.elsevier.com/retrieve/pii/0022169483900306

Carpenter D D and Kaluvakolanu P 2011 Effect of Roof Surface Type on Storm-Water Runoff from Full-Scale Roofs in a Temperate Climate *J. Irrig. Drain. Eng.* **137** 161–9 Online: http://ascelibrary.org/doi/abs/10.1061/(ASCE)IR.1943-4774.0000185

Carson T B, Keeley M, Marasco D E, McGillis W R and Culligan P J 2014 Assessing methods for predicting green roof rainfall capture: A comparison between full-scale observations and four hydrologic models *Urban Water J.* Under Review

Carson T B, Marasco D E, Culligan P J and McGillis W R 2013 Hydrological performance of extensive green roofs in New York City: observations and multi-year modeling of three full-scale systems *Environ. Res. Lett.* **8** 024036 Online: http://stacks.iop.org/1748-9326/8/i=2/a=024036?key=crossref.73afc90e83a6ffe34cee22872a062492

Choudhury B J and Blanchard B J 1983 SIMULATING SOIL WATER RECESSION COEFFICIENTS FOR AGRICULTURAL WATERSHEDS *J. Am. Water Resour. Assoc.* **19** 241–7 Online: http://doi.wiley.com/10.1111/j.1752-1688.1983.tb05321.x

Christen A and Vogt R 2004 Energy and radiation balance of a central European city *Int. J. Climatol.* **24** 1395–421 Online: http://doi.wiley.com/10.1002/joc.1074

Coffman L 2000 *Low-Impact Development Design Strategies: An Integrated Design Approach* (Prince George's County, MD)

De Cuyper K, Dinne K and Van De Vel L 2004 Rainwater Discharge from Green Roofs *CIB W062 30th International Symposium on Water Supply and Drainage for Buildings* (Rotterdam, Netherlands) p 12 Online: http://www.irb.fraunhofer.de/CIBlibrary/search-quick-result-list.jsp?A&idSuche=CIB+DC10549

Czikowsky M and Fitzjarrald D 2004 Evidence of seasonal changes in evapotranspiration in eastern US hydrological records *J. Hydrometeorol.* 974–88 Online: http://journals.ametsoc.org/doi/abs/10.1175/1525-7541(2004)005%3C0974%3AEOSCIE%3E2.0.CO%3B2

D'Errico J 2005 Surface Fitting using gridfit *MATLAB Cent. File Exch.* Online: http://www.mathworks.com/matlabcentral/fileexchange/8998

DiGiovanni K, Gaffin S R and Montalto F 2010 Green Roof Hydrology: Results from a Small-Scale Lysimeter Setup (Bronx, NY) *Low Impact Development 2010: Redefining Water in the City* (San Francisco, CA: ASCE) pp 1328–41 Online: http://link.aip.org/link/?ASCECP/367/114/1

DiGiovanni K, Gaffin S R, Montalto F and Rosenzweig C 2011 The Applicability of Classical Predictive Equations for the Estimation of Evapotranspiration from Urban Green Spaces: Green Roof Results *World Environmental and Water Resources Congress 2011: Bearing Knowledge for Sustainability* (ASCE) pp 783–92 Online: http://link.aip.org/link/?ASCECP/414/80/1

DiGiovanni K, Montalto F, Gaffin S and Rosenzweig C 2013 Applicability of Classical Predictive Equations for the Estimation of Evapotranspiration from Urban Green Spaces: Green Roof Results *J. Hydrol. Eng.* **18** 99–107 Online: http://ascelibrary.org/doi/abs/10.1061/%28ASCE%29HE.1943-5584.0000572

Draper N R and Smith. H 1998 *Applied Regression Analysis* (Hoboken, NJ: Wiley-Interscience)

Fassman-Beck E, Voyde E, Simcock R and Hong Y S 2013 4 Living roofs in 3 locations: Does configuration affect runoff mitigation? *J. Hydrol.* **490** 11–20 Online: http://dx.doi.org/10.1016/j.jhydrol.2013.03.004

Feller M M 2011 *Quantifying Evapotranspiration in Green Infrastructure: a Green Roof Case Study* (Villanova University) Online: http://www3.villanova.edu/vusp/Outreach/Pdf/Thesis/Feller-Thesis11.pdf

Fredrick R H, Myers V A and Auciello E P 1977 *Five- to 60-Minute Precipitation Frequency for the Eastern and Central United States* (Silver Spring, MD)

Fritschen L J 1965 Accuracy Of Evapotranspiration Determination by the Bowen Ratio Method *Int. Assoc. Sci. Hydrol. Bull.* **10** 38–48 Online: http://www.tandfonline.com/doi/abs/10.1080/02626666509493388

Fuchs M and Tanner C B 1970 Error analysis of bowen ratios measured by differential psychrometry *Agric. Meteorol.* **7** 329–34 Online: http://linkinghub.elsevier.com/retrieve/pii/0002157170900270

Gaffin S R, Rosenzweig C, Khanbilvardi R and Susca T 2010 *A Temperature and Seasonal Energy Analysis of Green, White, and Black Roofs* (New York, NY)

Gaffin S R, Rosenzweig C, Parshall L, Beattie D, Berghage R, O'Keeffe G and Braman D 2005 Energy Balance Modeling Applied to a Comparison of White and Green Roof Cooling Efficiency *Third Annual Greening Rooftops for Sustainable Communities Conference* (Washington. DC) pp 1–11 Online: http://www.buildingreen.net/assets/cms/File/GaffinetalPaperDC-0009.pdf

Garcia C A, Johnson M J, Andraski B J, Halford K J and Mayers C J 2008 *Portable Chamber Measurements of Evapotranspiration at the Amargosa Desert Research Site near Beatty , Nye County , Nevada , 2003 – 06 Scientific Investigations Report 2008 – 5135* (Reston)

Garrison N and Hobbs K 2011 *Rooftops to Rivers II: Green Strategies for Controlling Stormwater and Combined Sewer Overflows* (New York, NY) Online: http://www.nrdc.org/water/pollution/rooftopsii/

Getter K L, Rowe D B and Andresen J A 2007 Quantifying the effect of slope on extensive green roof stormwater retention *Ecol. Eng.* **31** 225–31

Getter K L, Rowe D B, Robertson G P, Cregg B M and Andresen J A 2009 Carbon sequestration potential of extensive green roofs. *Environ. Sci. Technol.* **43** 7564–70

Graham P, Maclean L and Medina D 2004 The role of water balance modelling in the transition to low impact development *Water Qual. Res. ...* **39** 331–42 Online: http://www.cawq.ca/journal/temp/journal/68.pdf#page=22

GreenRoofs.com 2014 The International Greenroof & Greenwall Projects Database!

Gregoire B G and Clausen J C 2011 Effect of a modular extensive green roof on stormwater runoff and water quality *Ecol. Eng.* **37** 963–9 Online: http://dx.doi.org/10.1016/j.ecoleng.2011.02.004

Grimmond C S B and Oke T R 1991 An evapotranspiration-interception model for urban areas *Water Resour. Res.* **27** 1739–55 Online: http://doi.wiley.com/10.1029/91WR00557

Grimmond C S B and Oke T R 2002 Turbulent Heat Fluxes in Urban Areas: Observations and a Local-Scale Urban Meteorological Parameterization Scheme (LUMPS) *J. Appl. Meteorol.* **41** 792–810 Online: http://search.ebscohost.com/login.aspx?direct=true&profile=ehost&scope=site&authtype=crawler&jrnl=08948763&AN=6806588&h=nHK1cHRlIjmGmb5Yg%2BXpuo72Y96tHke8Ym1w9y4kwbzYNQ73tWVCRNnMSBB4JaudrczW6zqenDEfBWIwcUa%2BRQ%3D%3D&crl=c

Grindley J 1970 Estimation and mapping of evaporation *World Water Balanc.* 200–13 Online: http://ks360352.kimsufi.com/redbooks/a092/092030.pdf

Hargreaves G H and Allen R G 2003 History and Evaluation of Hargreaves Evapotranspiration Equation *J. Irrig. Drain. Eng.* **129** 53–63 Online: http://ascelibrary.org/doi/abs/10.1061/%28ASCE%290733-9437%282003%29129%3A1%2853%29

Hathaway A M, Hunt W F and Jennings G D 2008 A Field Study of Green Roof Hydrologic and Water Quality Performance *Am. Soc. Agric. Biol. Eng.* **51** 37–44

Henderson-Sellers B 1984 A new formula for latent heat of vaporization of water as a function of temperature *Q. J. R. Meteorol. Soc.* **110** 1186–90 Online: http://doi.wiley.com/10.1002/qj.49711046626

Hershfield D M 1963 *Rainfall Frequency Atlas of the United States for Durations from 30 Minutes to 24 Hours and Return Periods from I to 100 Years* (Washington D.C.)

Hillel D 1998 Water Balance And Energy Balance In The Field *Environmental Soil Physics* (Academic Press, San Diego, CA) pp 589 – 613

Hogg R V. and Ledolter J 1987 *Engineering Statistics* (New York, NY: MacMillan)

Howell T A, Schneider A D and Jensen M E 1991 History of Lysimeter Design and Use for Evapotranspiration Measurements *The International Symposium on Lysimeters for Evapotranspiration and Environmental Measurements* (New York, NY: American Society of Civil Engineers) p 9

Hutchinson D, Abrams P, Retzlaff R and Liptan T 2003 Stormwater monitoring two ecoroofs in Portland, Oregon, USA *Greening Rooftops for Sustainable Communities* (Chicago, IL) pp 1–18

Jim C Y and Chen W Y 2009 Ecosystem services and valuation of urban forests in China *Cities* **26** 187–94 Online: http://linkinghub.elsevier.com/retrieve/pii/S0264275109000456

Jim C Y and Peng L L H 2012 Substrate moisture effect on water balance and thermal regime of a tropical extensive green roof *Ecol. Eng.* **47** 9–23

Jones J A and Grant G E 1996 Peak Flow Responses to Clear-Cutting and Roads in Small and Large Basins, Western Cascades, Oregon *Water Resour. Res.* **32** 959–74 Online: http://doi.wiley.com/10.1029/95WR03493

Jordan C F 1968 A Simple Tension-Free Lysimeter *Soil Sci.* **105** 81–6 Online: http://content.wkhealth.com/linkback/openurl?sid=WKPTLP:landingpage&an=00010694-196802000-00003

Kahler D M and Brutsaert W 2006 Complementary relationship between daily evaporation in the environment and pan evaporation *Water Resour. Res.* **42** n/a–n/a Online: http://doi.wiley.com/10.1029/2005WR004541

Kohler M A and Linsley R K 1951 *Research Paper No. 34 - Predicting the runoff from storm rainfall* (Washington, DC)

Köhler M and Keeley M 2005 The Green Roof Tradition in Germany: the Example of Berlin *EarthPledge, Green Roofs: Ecological Design and Construction* (New York, New York: Schiffer Publishing)

Kurtz T 2008 Flow Monitoring of Three Ecoroofs in Portland, Oregon *2008 Low Impact Development Conference* (Seattle, WA: ASCE)

Lazzarin R, Castellotti F and Busato F 2005 Experimental measurements and numerical modelling of a green roof *Energy Build.* **37** 1260–7 Online: http://linkinghub.elsevier.com/retrieve/pii/S0378778805000514

Liss P 1973 Processes of gas exchange across an air-water interface *Deep Sea Res. Oceanogr. Abstr.* **20** 221–38 Online: http://linkinghub.elsevier.com/retrieve/pii/0011747173900132

Liu C, Zhang X and Zhang Y 2002 Determination of daily evaporation and evapotranspiration of winter wheat and maize by large-scale weighing lysimeter and micro-lysimeter *Agric. For. Meteorol.* **111** 109–20 Online: http://linkinghub.elsevier.com/retrieve/pii/S0168192302000151

Liu K and Minor J 2005 Performance evaluation of an extensive green roof *Greening Rooftops for Sustainable Communities* (Washington, DC) pp 1–11

Loague K M and Freeze R A 1985 A Comparison of Rainfall-Runoff Modeling Techniques on Small Upland Catchments *Water Resour. Res.* **21** 229–48 Online: http://doi.wiley.com/10.1029/WR021i002p00229

Marasco D E, Hunter B N, Culligan P J, Gaffin S R and McGillis W R 2014 Quantifying Evapotranspiration from Urban Green Roofs: A Comparison of Chamber Measurements with Commonly Used Predictive Methods *Environ. Sci. Technol.* Under Review

Martens R, Bass B and Alcazar S S 2008 Roof–envelope ratio impact on green roof energy performance *Urban Ecosyst.* **11** 399–408 Online: http://www.springerlink.com/index/10.1007/s11252-008-0053-z

Mawdsley J A and Ali M F 1985 Estimating Nonpotential Evapotranspiration by Means of the Equilibrium Evaporation Concept *Water Resour. Res.* **21** 383–91 Online: http://doi.wiley.com/10.1029/WR021i003p00383

Mayor's Office of Long-Term Planning and Sustainability 2008 *Sustainable Stormwater Management Plan* (New York) Online: www.nyc.gove/PlaNYC2030

Mentens J, Raes D and Hermy M 2003 Effect of Orientation on the Water Balance of Greenroofs *Greening Rooftops for Sustainable Communities* (Chicago, IL) pp 1–9

Mentens J, Raes D and Hermy M 2006 Green roofs as a tool for solving the rainwater runoff problem in the urbanized 21st century? *Landsc. Urban Plan.* **77** 217–26 Online: http://linkinghub.elsevier.com/retrieve/pii/S0169204605000496

Montalto F, Behr C, Alfredo K, Wolf M, Arye M and Walsh M 2007 Rapid assessment of the cost-effectiveness of low impact development for CSO control *Landsc. Urban Plan.* **82** 117–31 Online: http://linkinghub.elsevier.com/retrieve/pii/S0169204607000515

Monteith J L 1965 Evaporation and environment. *Symp. Soc. Exp. Biol.* **19** 205–34 Online: http://www.ncbi.nlm.nih.gov/pubmed/5321565

Moran A C, Hunt W F and Smith J T 2005 Green Roof Hydrologic and Water Quality Performance from Two Field Sites in North Carolina *Managing Watersheds for Human and Natural Impacts* (Reston, VA: American Society of Civil Engineers) pp 1–12 Online: http://dx.doi.org/10.1061/40763(178)99

Moran M, Clarke T, Inoue Y and Vidal A 1994 Estimating crop water deficit using the relation between surface-air temperature and spectral vegetation index *Remote Sens. Environ.* **49** 246–63 Online: http://www.sciencedirect.com/science/article/pii/0034425794900205

Morgan S, Celik S and Retzlaff W 2013 Green Roof Storm-Water Runoff Quantity and Quality *J. Environ. Eng.* **139** 471–8 Online: http://ascelibrary.org/doi/abs/10.1061/(ASCE)EE.1943-7870.0000589

Nardini A, Andri S and Crasso M 2011 Influence of substrate depth and vegetation type on temperature and water runoff mitigation by extensive green roofs: shrubs versus herbaceous plants *Urban Ecosyst.* **15** 697–708

NYC DEP 2010 *NYC Green Infrastructure Plan* (New York, NY)

Oberndorfer E, Lundholm J, Bass B, Coffman R R, Doshi H, Dunnett N, Gaffin S, Köhler M, Liu K K Y and Rowe B 2007 Green Roofs as Urban Ecosystems: Ecological Structures, Functions, and Services *Bioscience* **57** 823–33

Oke T R 1987 *Boundary Layer Climates* (New York: Methuen) Online: http://books.google.com/books?hl=en&lr=&id=K_2dW7crfVIC&oi=fnd&pg=PP1&dq=Boundary+Layer+Climates&ots=103_wvMz9U&sig=7duQ1PV8bXGUlyVW0AfgRqlkEyE

Olejnik J, Eulenstein F, Kedziora A and Werner A 2001 Evaluation of a water balance model using data for bare soil and crop surfaces in Middle Europe *Agric. For. Meteorol.* **106** 105–16

Ouldboukhitine S-E, Belarbi R and Djedjig R 2012 Characterization of green roof components: Measurements of thermal and hydrological properties *Build. Environ.* **56** 78–85 Online: http://linkinghub.elsevier.com/retrieve/pii/S0360132312000698

Ouldboukhitine S-E, Belarbi R, Jaffal I and Trabelsi A 2011 Assessment of green roof thermal behavior: A coupled heat and mass transfer model *Build. Environ.* **46** 2624–31 Online: http://linkinghub.elsevier.com/retrieve/pii/S0360132311002010

Palla a., Sansalone J J, Gnecco I and Lanza L G 2011 Storm water infiltration in a monitored green roof for hydrologic restoration *Water Sci. Technol.* **64** 766 Online: http://www.iwaponline.com/wst/06403/wst064030766.htm

Pataki D E, Alig R J, Fung a. S, Golubiewski N E, Kennedy C a., Mcpherson E G, Nowak D J, Pouyat R V. and Romero Lankao P 2006 Urban ecosystems and the North American carbon cycle *Glob. Chang. Biol.* **12** 2092–102 Online: http://doi.wiley.com/10.1111/j.1365-2486.2006.01242.x

Penman H L 1948 Natural Evaporation from Open Water, Bare Soil and Grass *Proc. R. Soc. A Math. Phys. Eng. Sci.* **193** 120–45 Online: http://rspa.royalsocietypublishing.org/content/193/1032/120.short

Perez P J, Castellvi F, Ibañez M and Rosell J I 1999 Assessment of reliability of Bowen ratio method for partitioning fluxes *Agric. For. Meteorol.* **97** 141–50 Online: http://linkinghub.elsevier.com/retrieve/pii/S0168192399000805

Peters A, Nehls T, Schonsky H and Wessolek G 2014 Separating precipitation and evapotranspiration from noise – a new filter routine for high-resolution lysimeter data *Hydrol. Earth Syst. Sci.* **18** 1189–98 Online: http://www.hydrol-earth-syst-sci.net/18/1189/2014/

Priestley C and Taylor R 1972 On the assessment of surface heat flux and evaporation using large-scale parameters *Mon. Weather Rev.* 81–92 Online: http://journals.ametsoc.org/doi/abs/10.1175/1520-0493(1972)100%3C0081:OTAOSH%3E2.3.CO;2

Rada J 2006 *LI-8100 Automated Soil CO2 Flux System & LI-8150 Multiplexer Instruction Manual* (Lincoln, NE: Licor Biosciences) Online: ftp://ftp.licor.com/perm/env/LI-8100/Manual/LI8100_8150_Manual.pdf

Rosenberg N J 1969 Seasonal Patterns in Evapotranspiration by Irrigated Alfalfa in the Central Great Plains *Agron. J.* **61** 879 Online: https://www.agronomy.org/publications/aj/abstracts/61/6/AJ0610060879

Sailor D J and Hagos M 2011 An updated and expanded set of thermal property data for green roof growing media *Energy Build.* **43** 2298–303

Salvucci G D and Gentine P 2013 Emergent relation between surface vapor conductance and relative humidity profiles yields evaporation rates from weather data. *Proc. Natl. Acad. Sci. U. S. A.* **110** 6287–91 Online: http://www.pubmedcentral.nih.gov/articlerender.fcgi?artid=3631684&tool=pmcentrez&rendertype=abstract

Schroll E, Lambrinos J, Righetti T and Sandrock D 2011 The role of vegetation in regulating stormwater runoff from green roofs in a winter rainfall climate *Ecol. Eng.* **37** 595–600

She N and Pang J 2010 Physically Based Green Roof Model *J. Hydrol. Eng.* **15** 458–64 Online: http://link.aip.org/link/JHYEFF/v15/i6/p458/s1&Agg=doi

Sherrard J A and Jacobs J M 2012 Vegetated Roof Water-Balance Model: Experimental and Model Results *J. Hydrol. Eng.* **17** 858–68 Online: http://ascelibrary.org/doi/abs/10.1061/%28ASCE%29HE.1943-5584.0000531

Singh K P 1976 Unit Hydrographs- A Comparative Study *J. Am. Water Resour. Assoc.* **12** 381–92 Online: http://doi.wiley.com/10.1111/j.1752-1688.1976.tb02686.x

Slatyer R O and McIlroy I C 1961 *Practical Microclimatology* (Australia: UNESCO)

Spolek G 2008 Performance monitoring of three ecoroofs in Portland, Oregon *Urban Ecosyst.* **11** 349–59

Spronken-Smith R A, Oke T R and Lowry W P 2000 Advection and the surface energy balance across an irrigated urban park *Int. J. Climatol.* **20** 1033–47 Online: http://doi.wiley.com/10.1002/1097-0088%28200007%2920%3A9%3C1033%3A%3AAID-JOC508%3E3.0.CO%3B2-U

Stovin V, Poë S and Berretta C 2013 A modelling study of long term green roof retention performance. *J. Environ. Manage.* **131** 206–15 Online: http://www.ncbi.nlm.nih.gov/pubmed/24178313

Stovin V, Vesuviano G and Kasmin H 2012 The hydrological performance of a green roof test bed under UK climatic conditions *J. Hydrol.* **414-415** 148–61 Online: http://dx.doi.org/10.1016/j.jhydrol.2011.10.022

Sumner D M and Jacobs J M 2005 Utility of Penman–Monteith, Priestley–Taylor, reference evapotranspiration, and pan evaporation methods to estimate pasture evapotranspiration *J. Hydrol.* **308** 81–104 Online: http://www.sciencedirect.com/science/article/pii/S0022169404005244

Tabares-Velasco P C and Srebric J 2012 A heat transfer model for assessment of plant based roofing systems in summer conditions *Build. Environ.* **49** 310–23 Online: http://linkinghub.elsevier.com/retrieve/pii/S0360132311002332

Tabares-Velasco P C and Srebric J 2011 Experimental quantification of heat and mass transfer process through vegetated roof samples in a new laboratory setup *Int. J. Heat Mass Transf.* **54** 5149–62 Online: http://linkinghub.elsevier.com/retrieve/pii/S0017931011004790

Taha H 1997 Urban climates and heat islands: albedo, evapotranspiration, and anthropogenic heat *Energy Build.* **25** 99–103 Online: http://linkinghub.elsevier.com/retrieve/pii/S0378778896009991

Taha H, Akbari H and Rosenfeld A 1991 Heat Island and Oasis Effects of Vegetative Canopies: Micro-Meterological Field-Measurements *Theor. Appl. Climatol.* **44** 123–38

Taha H, Akbari H and Rosenfeld A 1989 *Vegetation Microclimate Measurements: The Davis Project* (Berkeley, CA)

Tasker G D and Stedinger J R 1989 An operational GLS model for hydrologic regression *J. Hydrol.* **111** 361–75 Online: http://linkinghub.elsevier.com/retrieve/pii/0022169489902680

Thornthwaite C W and Mather J R 1955 The Water Balance *Publications in Climatology* (Centerton, NJ: Drexel Institute of Climatology) pp 1–104

Toronto and Region Conservation Authority 2006 *Evaluation of an Extensive Greenroof* (Toronto, ON)

Tyagi N K, Sharma D K and Luthra S K 2000 Determination of evapotranspiration and crop coeffients of rice and sunflower with lysimeter *Agric. Water Manag.* **45** 41–54

US EPA 2004 *Report to Congress: Impacts and Control of CSOs and SSOs* (Washington, DC) Online: http://cfpub.epa.gov/npdes/cso/cpolicy_report2004.cfm

VanWoert N D, Rowe D B, Andresen J a, Rugh C L, Fernandez R T and Xiao L 2005 Green roof stormwater retention: effects of roof surface, slope, and media depth. *J. Environ. Qual.* **34** 1036–44 Online: http://www.ncbi.nlm.nih.gov/pubmed/15888889

Vaughan P J and Ayars J E 2009 Noise Reduction Methods for Weighing Lysimeters *J. Irrig. Drain. Eng.* **135** 235–40 Online: http://ascelibrary.org/doi/abs/10.1061/%28ASCE%290733-9437%282009%29135%3A2%28235%29

Villarreal E L 2007 Runoff detention effect of a sedum green-roof *Nord. Hydrol.* **38** 99 Online: http://www.iwaponline.com/nh/038/nh0380099.htm

Villarreal E L and Bengtsson L 2005 Response of a Sedum green-roof to individual rain events *Ecol. Eng.* **25** 1–7 Online: http://linkinghub.elsevier.com/retrieve/pii/S0925857404001740

Villarreal E L, Semadeni-Davies A and Bengtsson L 2004 Inner city stormwater control using a combination of best management practices *Ecol. Eng.* **22** 279–98 Online: http://www.sciencedirect.com/science/article/pii/S0925857404000680

Voyde E, Fassman E and Simcock R 2010a Hydrology of an extensive living roof under sub-tropical climate conditions in Auckland, New Zealand *J. Hydrol.* **394** 384–95 Online: http://linkinghub.elsevier.com/retrieve/pii/S0022169410005937

Voyde E, Fassman E, Simcock R and Wells J 2010b Quantifying Evapotranspiration Rates for New Zealand Green Roofs *J. Hydrol. Eng.* **15** 395–403 Online: http://www.scopus.com/inward/record.url?eid=2-s2.0-77953997845&partnerID=40&md5=016f727a43b0037d0e3fc31e45bf8180

Wadzuk B M, Schneider D, Feller M and Traver R G 2013 Evapotranspiration from a Green-Roof Storm-Water Control Measure *J. Irrig. Drain. Eng.* **139** 995–1003 Online: http://ascelibrary.org/doi/abs/10.1061/%28ASCE%29IR.1943-4774.0000643

Wang Z-H, Bou-Zeid E and Smith J a. 2013 A coupled energy transport and hydrological model for urban canopies evaluated using a wireless sensor network *Q. J. R. Meteorol. Soc.* **139** 1643–57 Online: http://doi.wiley.com/10.1002/qj.2032

Westenbroek S, Kelson V and Dripps W 2010 *SWB — A Modified Thornthwaite-Mather Soil-Water- Balance Code for Estimating Groundwater Recharge* (Reston, VA) Online: http://pubs.usgs.gov/tm/tm6-a31/

Wever L A, Flanagan L B and Carlson P J 2002 Seasonal and interannual variation in evapotranspiration, energy balance and surface conductance in a northern temperate grassland *Agric. For. Meteorol.* **112** 31–49 Online: http://www.sciencedirect.com/science/article/pii/S0168192302000412

Wu I 1997 A simple evapotranspiration model for Hawaii: the Hargreaves model Online: http://scholarspace.manoa.hawaii.edu/handle/10125/12218

Yang J, Yu Q and Gong P 2008 Quantifying air pollution removal by green roofs in Chicago *Atmos. Environ.* **42** 7266–73

Zhao L, Xia J, Xu C, Wang Z, Sobkowiak L and Long C 2013 Evapotranspiration estimation methods in hydrological models *J. Geogr. Sci.* **23** 359–69 Online: http://link.springer.com/10.1007/s11442-013-1015-9

# APPENDIX A: SITE DESCRIPTIONS

## A.1 Green Roofs and Monitoring Equipment

The following table provides a summary of the green roof installations that were monitored as part of this PhD dissertation. The installations span a variety of commercially available green roofs. The green roof components in each case were all provided and installed by various and independent green roofing companies (Table A-1). Figure A-1 illustrates the locations of the green roof sites, which are distributed throughout New York City.

Table A-1: Summary of monitored green roof sites

| **Roof Name** | **W115** | **W118** | **USPS** | **ConEd** |
|---|---|---|---|---|
| Construction Type | Vegetated mat | Vegetated mat | Built-in-place | Modular tray |
| Manufacturer | Xero Flor America | Xero Flor America | Tecta Green | GreenGrid Roofs |
| Year Built | 2007 | 2007 | 2009 | 2008 |
| Substrate Depth (mm) | 32 | 32 | 100 (200 berms) | 100 |
| Vegetation Type | Sedum mix | Sedum mix | Sedum mix & natives | Sedum mix |
| Monitored Watershed Area ($m^2$) | 99 | 310 | 390 | 940 |
| Watershed Vegetated (%) | 58 | 53 | 67 | 52 |

Weather stations installed on each roof to monitor environment conditions, specifically, precipitation, runoff, temperature, radiation, humidity, and wind speed and direction. Monitoring equipment budgets varied for each roof and thus sensor selection was not identical everywhere.

## A.2 Green Roof Site Descriptions

The following paragraphs provide images and descriptions of the study's monitored rooftops. Figure A-2 through to Figure A-5 consist of: (a) Satellite images of each roof (Courtesy Google Maps), with locations of green roof water quantity measurements ($VG_{\#}$), as well as, green roof dynamic chamber measurements (DC). Drainage areas monitored for green roof water quantity are denoted by the dotted lines. (b) Photographs of the flow meters used to measure green roof water quantity. (c) Photographs of the roof taken on-site.

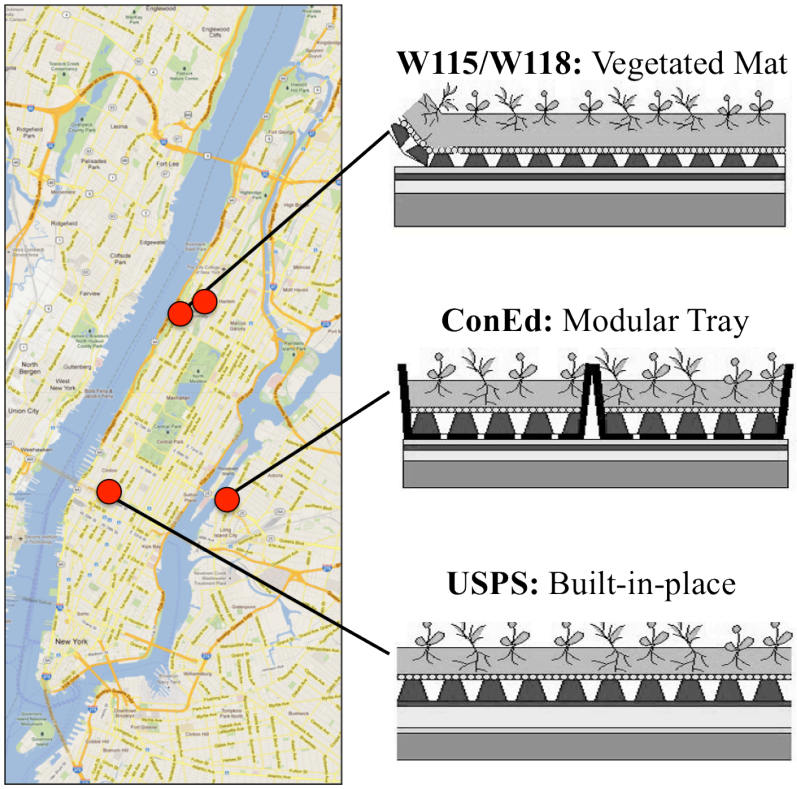


Figure A-1: Monitored green roof locations in New York City and construction diagrams.

*W115 and W118:*

The 635 West 115$^{th}$ Street building (W115) houses the Columbia University Office of Environmental Stewardship, while the 423 West 118th Street building (W118) is a Columbia University graduate student residence. In 2007, a pre-vegetated mat, Xero Flor America's XF301+2FL green roof system, was retrofitted on both buildings. This system consists of a 32 mm thick pre-vegetated mat, supported by two 6 mm thick water retention fleeces created from recycled synthetic fibers, a 19 mm non-woven polymer drainage mat, and an 0.5 mm polyethylene root barrier. A variety of sedums species, such as: *Saxifraga granulata, Sedum acre, Sedum album, Sedum ellacombianum, Sedum hybridum 'Czars Gold', Sedum oregonum, Sedum pulchellum, Sedum reflexum, Sedum sexangulare, Sedum spurium var. coccineum, Sedum stenopetalum*, are present on these roofs. The growing substrate on these roofs has a water-saturated density of 1.37 g cm$^{-3}$, water storage capacity of 37.1%, and a saturated hydraulic conductivity of 0.021 cm s$^{-1}$, as reported by Hummel and Co Inc in April 2007. The W115 green roof has a single 99 m$^2$, 58% vegetated watershed connected to an exterior parapet downspout. The 600 m$^2$ W118 total roof area consists of two watersheds connected to exterior parapet downspouts, of which the 310 m$^2$, 53% vegetated drainage area of the Southeast watershed was monitored for rainfall and runoff. Gravel walkways, parapets, and the raised rooftop above the elevator shaft comprise the non-vegetated areas of both rooftops.


Figure A-2: W115 roof; (a) satellite photograph, (b) weir device, and (c) roof photograph

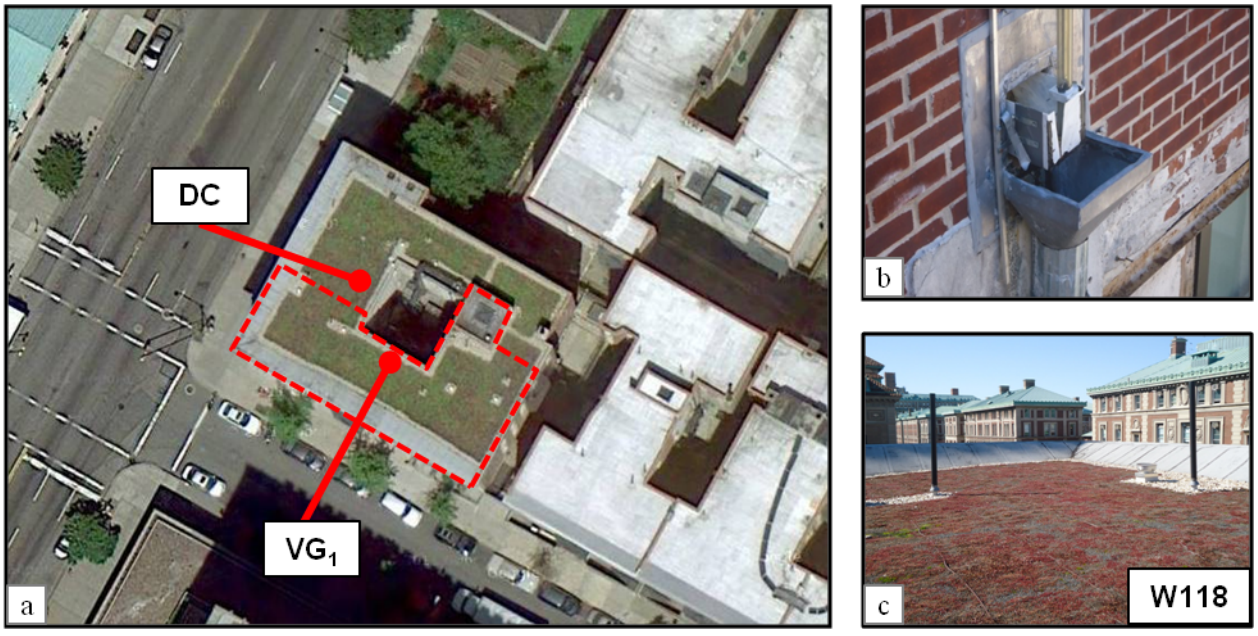


Figure A-3: W118 roof; (a) satellite photograph, (b) weir device, and (c) roof photograph.

*USPS:*

The 10,000 $m^2$ US Post Office Morgan Processing and Distribution Center green roof (USPS) in mid-Manhattan, NY was installed in 2009 by TectaGreen of Tecta America. The roof was built-in-place. Roof edges were established with 100 mm tall metal brackets, and an expanded shale based substrate of varying depth was placed in the bounded area. A majority of the green roof is comprised of 100 mm of substrate depth and was planted with sedum types, including: *Sedum acre, Sedum album 'Coral Carpet', Sedum album murale, Sedum reflexum, Sedum sexangulare, Sedum reflexum 'Blue Spruce', Sedum grisebachii, Sedum kamtschaticum, Sedum 'Matrona', Sedum pluricaule 'Rosenteppich', Sedum spurium 'Roseum', Sedum telephium 'Autumn Joy'*. 200mm thick berms throughout the roof, usually about 2 m wide, have the following larger plant species: *Achilea filipendula 'Moonshine', Alium schoenoprasum, Coreopsis vert 'Moonbeam', Silenecaroliniana ssp. wherryi, Talinum calycinum, Tradescantia ohiensis*. The growing substrate has a water-saturated density between 1.15-1.35 g $cm^{-3}$, water storage capacity between 35-65%, and a saturated hydraulic conductivity between 0.001-0.120 cm $s^{-1}$, as reported by Skyland USA LLC in March 2011. Monitoring equipment was installed in a 390 $m^2$ watershed in the Northwest corner of the roof. The watershed has one 6 m long berm and a single internal downspout. The watershed is 67% vegetated with the remaining area consisting of gravel ballast.

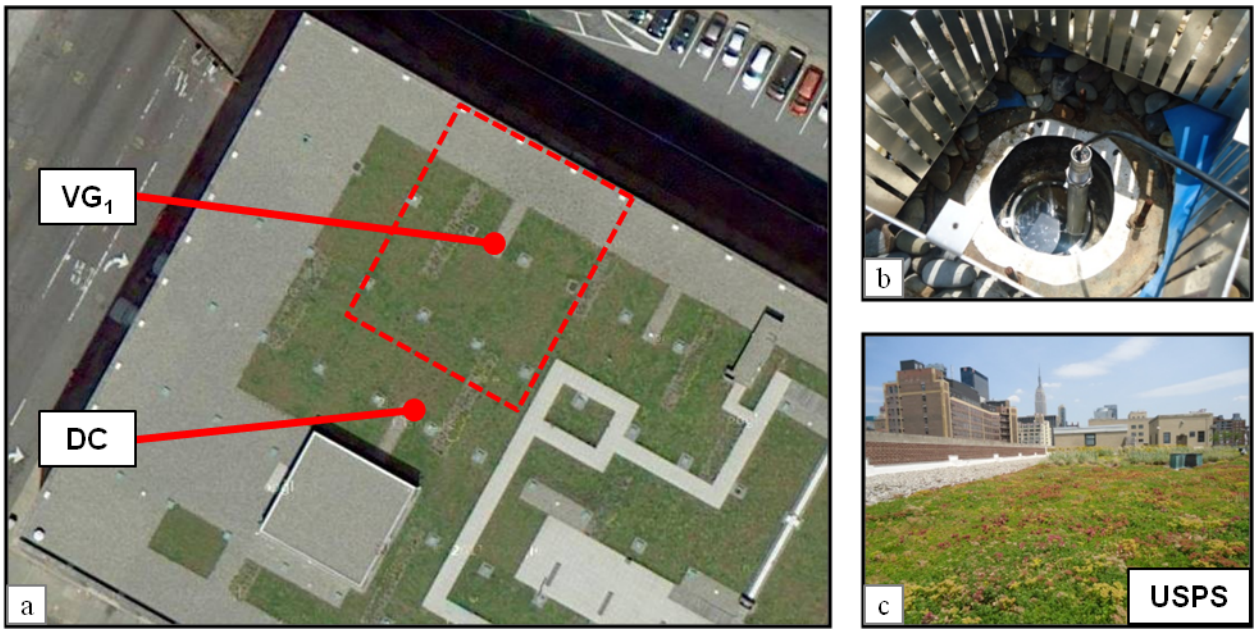

Figure A-4: USPS roof; (a) satellite photograph, (b) weir device, and (c) roof photograph.

*ConEd:*

ConEdison Learning Center (ConEd) green roof in Queens, which was installed in 2008, consists of GreenGrid-G2 modular trays with dimensions 61 cm × 122 cm × 10 cm. The trays were packed with a proprietary expanded shale substrate and then placed in adjacent rows on the 2,700 $m^2$ roof area. The growing substrate has a water-saturated density of 1.18 g $cm^{-3}$, water storage capacity of 31.8%, and a saturated hydraulic conductivity of 0.326 cm $s^{-1}$, as reported by Penn State University's Agricultural Analytical Services Laboratory in July 2008. Plugs and cuttings used to plant the were comprised of the following 15 sedum varieties: *Sedum oreganum, Sedum kamtschaticum 'Weihenstephaner Gold', Sedum kamtschaticum, Sedum ternatum, Sedum 'John Creech', Sedum spurium 'Album Superbum', Sedum spurium 'Fulda Glow', Sedum spurium 'Dragons Blood', Sedum spurium 'Bronze Carpet', Sedum angelina, Sedum sexangulare, Sedum 'Ruby Glow', Sedum 'pachclados', Sedum 'Bertram Anderson', Sedum 'Vera Jameson'.*

Monitoring equipment was installed in the 52% vegetated, 940 $m^2$ Eastern watershed. Both of the watershed's internal downspouts were monitored for runoff. The non-vegetated sections of this roof are comprised of rubber mat walkways, gravel ballast transitions and raised glass skylights.

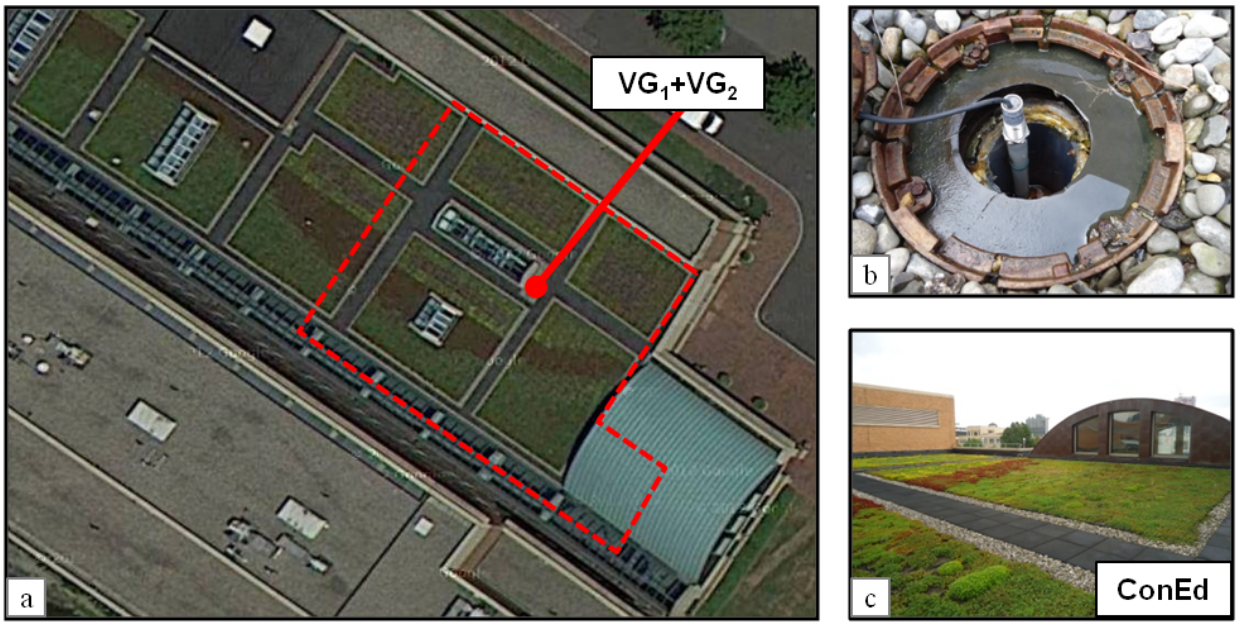


Figure A-5: ConEd roof; (a) satellite photograph, (b) weir device, and (c) roof photograph.

# APPENDIX B: FLOW METER DESCRIPTION

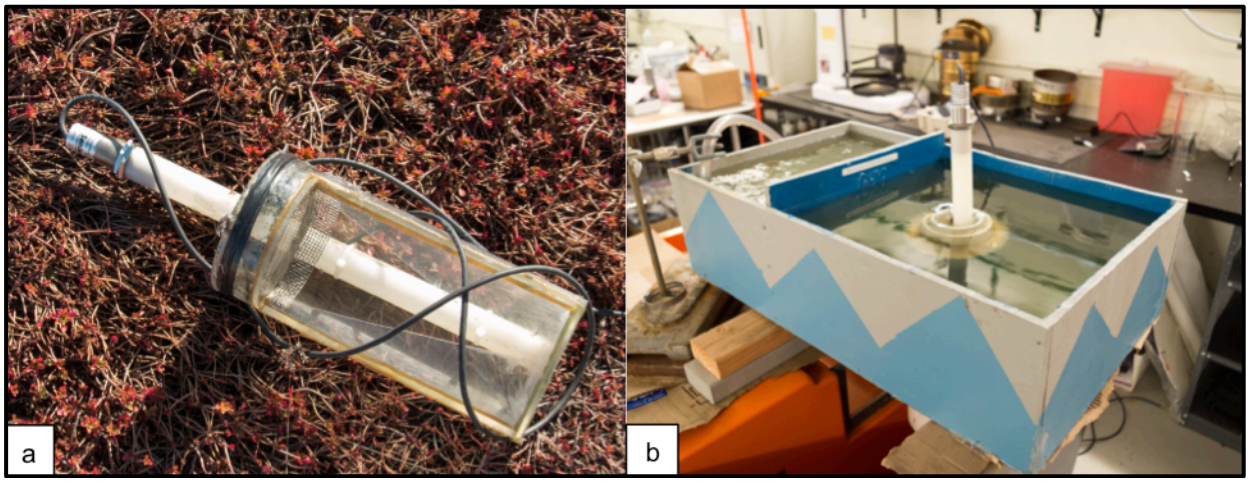


Figure B-1: (a) Runoff monitoring weir device (b) Calibration chamber used to simulate rooftop runoff.

The flow meters for runoff measurement consist of a runoff chamber with an outlet weir and a Senix TSPC-30S1 ultrasonic sensor (Figure B-1(a)).The ultrasonic depth sensor measures the depth of water behind the weir face with a resolution of 0.086 mm. As flow increases the water level behind the weir's face rises. The ultrasonic sensor detects the rise in water height and adjusts its output voltage accordingly. The flow meters were sized to fit into existing rooftop drains and accommodate roughly 50 mm $hr^{-1}$ of rainfall in saturated substrate conditions based on the drainage area. Above this flow rate, water overflows the weir into the roof drain to prevent backup and ponding of water on the roofs. Each flow meter was constructed by cutting acrylic parts and joining them with Scotch-Weld DP-810NS acrylic epoxy. The weir face was cut from flat piece of acrylic and attached to a vertical cutout on the side of the weir cylinder. A baffle was installed at the top of the device and rubber based sealant was applied on all edges to minimize turbulence and eliminate leaks without restricting water flow. The flow meters

function between 0 and 70 °C. To calibrate each flow meter, a box was built that effectively simulates water flow conditions into roof drains (Figure B-1(b)). Weirs were sealed into the simulation box, as they would be under field conditions, and calibrated up to their designated maximum capacity. Water was pumped into the simulation box, flowed under the baffle, then rose up to enter the flow meter from all directions. Repeat measurements were taken at incrementally increasing flow rates using an Armfield F1-10 hydraulic bench, which was supplemented with a 6 L $s^{-1}$ pump at high flow rates. The corresponding voltage output was recorded from the Senix ultrasonic sensor. The resulting data points were used to derive a calibration curve that related sensor output voltage and flow rate. This calibration method significantly reduces errors compared to other techniques that rely on, for example, a combination of measurements at low flow rates and reported weir equations. Once calibrated, flow meters were sealed into the rooftop drains to prevent water loss prior to measurement. Finally, the voltage output of the Senix ultrasonic sensor was connected to the rooftop data logger for recording.